UNIVERSITÀ DEGLI STUDI DI PADOVA

UNIVERSITÀ DEGLI STUDI DI PADOVA

Dipartimento di Salute della Donna e del Bambino

SCUOLA DI DOTTORATO DI RICERCA IN MEDICINA DELLO SVILUPPO E SCIENZE DELLA PROGRAMMAZIONE SANITARIA

Indirizzo: Emato-Oncologia, Genetica, Malattie Rare E Medicina Predittiva

Ciclo XXXVIII

TRANSCRIPTION FACTOR IKAROS: FROM LEUKAEMIA GENETICS TO LYMPHOCYTE DEVELOPMENT

Direttore della Scuola : Ch.mo Prof. Giuseppe Basso

Coordinatore d'indirizzo: Ch.mo Prof. Giuseppe Basso

Supervisore : Dott.ssa Geertruy te Kronnie

Dottorando : Tobia Lana

SUMMARY

Haematopoiesis is a cell differentiation process, starting from multipotent haematopoietic stem cells (HSC) to increasingly more fate-restricted blood cell progenitors. Each step during this process is strictly regulated by key transcription factors, activating or repressing stemness and lineage-specific genes. Not surprisingly, mutations or translocations involving transcription factors are often associated with leukaemia. IKAROS is the founding member of a zinc finger transcription factor family primarily involved in haematopoietic fate-decision. IKAROS protein is characterized by 2 domains: one at the N-terminus, with 4 zinc fingers, necessary for the DNA binding, and one at the C-terminus, with 2 zinc fingers, necessary for the homo- hetero-dimerization of the protein and its consequent activation. IKAROS is expressed in HSC and during lymphoid commitment expression increases, silencing stemness and myelo-erythroid priming genes and enhancing lymphoid specific factors. In *Ikzf1*-knockout mice models, lymphopoiesis is severely impaired, with a retardation of T cell development and a block in B, NK and dendritic cell differentiation due to a failure of HSC to differentiate into common lymphoid progenitors (CLP). *Ikzf1* mutant mice developed T-cell leukaemia or lymphoma with a penetrance of ~95% within 6-8 weeks after birth, and died soon after. In human, *IKZF1* alterations are rarely associated with T-cell leukaemias, but surprisingly *IKZF1* deletions were found to occur in 15% of paediatric B cell precursors ALL (BCP-ALL) and in more than 70% of paediatric Philadelphia positive BCP-ALL.
In this thesis, we evaluate the impact of IKAROS in paediatric leukaemia and during the B-cell lineage specification.

In Chapter 3, we studied the incidence of *IKZF1* point mutations and indels in a European cohort of Ph+ BCP-ALL paediatric patients. In particular, we screened, using next generation amplicon deep sequencing (NGS), the 7 coding exons of *IKZF1* in 98 *IKZF1* non deleted and 61 *IKZF1* deleted patients. Seven missense point mutations and 7 frameshift small indels were identified in *IKZF1*-non deleted and 3 point mutations were detected in *IKZF1*-deleted patients, all of them with a predicted deleterious effect on IKAROS function. Mutations were mainly located in exons 5 and 8, encoding the DNA-binding and dimerization domains respectively. In *IKZF1*-non deleted patients, mutations seem to indicate the same prognosis as macrodeletions, with a higher incidence of adverse

events in patients treated before TKI introduction compared to patients treated with a combination therapy including TKIs.

Among the mutated patients identified in our mutation screening, one patient had the same single nucleotide deletion both at diagnosis and complete remission, suggesting a constitutional status of the mutation. In Chapter 4 we further investigated the constitutional status of the *IKZF1* mutation in the proband and his family, finding in 3 generations the same mutation in the mother and 3 other carriers, as well as a second leukaemia case in the family that had occurred more than 45 years ago. The *IKZF1* single nucleotide deletion gave rise to a truncated protein with loss of the last part of the DNA binding domain and the C-terminal dimerization domain, resulting in DNA-binding deficiency and a diffuse nuclear localization. The mutant allele was transcribed in proband's bone marrow at complete remission, as well as in peripheral blood (PB) cells of his sister, an unaffected mutation carrier. Finally, the truncated protein was identified in the PB cells of the proband's sister, in a lower amount compare to the wt-IKAROS isoforms.

In Chapter 5, a model to study Ikaros-mediated gene expression regulation is described and characterized. Ikaros expression is enhanced during B-cell development, and pilots B cell-progenitors out of cell cycle allowing the Ig light chain recombination. To better comprehend the kinetics and mechanisms of Ikaros-gene expression regulation, we knocked-out endogenous Ikaros from a murine cycling preB cell line, using the CRISPR-Cas9 technique, and subsequently transduced cells with an inducible Ikaros cassette, that allowed to precisely regulating Ikaros translocation in the nuclei. Inducible Ikaros efficiently translocated to the nuclei and bound to target gene promoter, but its gene expression regulation appeared impaired. Indeed, inducible Ikaros was able to up-regulate well known target genes, but failed to down-regulate 3 selected target genes, know to be down-regulate after Ikaros induction in an endogenous Ikaros wt model.

In Chapter 6 we took advantage of the Ikaros inducible system to study the metabolic changes that occur during B-cell lymphocyte development in a cycling to resting preB cell model. Three FRET-sensors specifically designed to evaluate the cellular levels of ATP, glucose and AMPK activation status were transduced in our cell model, and preliminary measurements were performed using at fluorescent microscopy and FACS after 16 hours of Ikaros induction.

RIASSUNTO

L'ematopoiesi è un processo differenziativo che, a partire da cellule staminali ematopoietiche multipotenti, da origine a tutte le cellule del sangue. Ogni step differenziativo durante questo processo è finemente regolato da un insieme di fattori di trascrizione che agiscono in concerto bloccando la trascrizione di geni legati alla staminalità ed attivando geni essenziali per la specificazione ed il differenziamento delle diverse linee maturative ematopoetiche: linfoide, mieloide, eritroide e magacariocitoide. Non è quindi sorprendente che mutazioni o traslocazioni che interessano questi fattori di trascrizione siano spesso associate con l'insorgenza di leucemie. IKAROS fa parte di una famiglia di fattori di trascrizione principalmente coinvolta nella specificazione in senso linfoide delle cellule ematopoietiche. IKAROS è caratterizzato da due domini funzionali: un dominio N-terminale, composto da 4 zinc-finger, necessario per il legame della proteina al DNA, ed un domino C-terminale, formato da 2 zinc-finger, indispensabile per la omo-etero-dimerizzazione della proteina e la sua conseguente attivazione. IKAROS è espresso a livello delle cellule staminali ematopoietiche, e la sua espressione aumenta durante il differenziamento linfoide, silenziando geni legati alla staminalità ed allo sviluppo eritro-mieloide e potenziando l'espressione di geni legati allo sviluppo linfoide. In topi knockout per il gene *Ikzf1* la linfopoiesi è gravemente compromessa, con un ritardo nello sviluppo delle cellule T ed un completo blocco nel differenziamento dei linfociti B, cellule natural killer e delle cellule dendritiche. Questo fenotipo è dovuto all'incapacità delle cellule staminali ematopoietiche di differenziare in cellule progenitrici della linea linfoide in assenza di Ikaros. La mancanza di Ikaros in questi topi porta all'insorgenza di leucemie o linfomi a cellule T nel ~95% dei casi entro sei mesi dalla nascita.
Nell'uomo, aberrazioni associate ad *IKZF1* sono rare nelle leucemie T, ma, al contrario, delezioni di parte del gene sono presenti nel 15% delle leucemie pediatriche a fenotipo B (BCP-ALL), e la percentuale raggiunge circa il 70% se si considera un particolare sottogruppo caratterizzato dalla presenza del cromosoma aberrante Philadelphia.
In questa tesi abbiamo studiato il ruolo di IKAROS nelle leucemie pediatriche e durante il differenziamento dei linfociti B.

Nel terzo capitolo l'incidenza di mutazioni puntiformi e piccole inserzioni/delezioni (indel) del gene *IKZF1* viene studiata in una coorte europea di pazienti pediatrici affetti da BCP-ALL con presenza del cromosoma Philadelphia. Grazie all'utilizzo del sequenziamento di

nuova generazione abbiamo sequenziato i 7 esoni codificanti di *IKZF1* in 98 pazienti *IKZF1*-non deleti ed in 61 pazienti *IKZF1*-deleti. Tra i 98 pazienti non deleti abbiamo riscontrato la presenza di 7 mutazioni puntiformi e 7 indel, mentre 3 mutazioni puntiformi sono state evidenziate nella coorte di pazienti *IKZF1* deleti. Tutte le aberrazioni da noi trovate sono predette avere un effetto deleterio sulla funzionalità della proteina. Queste aberrazioni genetiche sono principalmente localizzate sul quinto e sull'ottavo esone, che codificano per i domini di legame al DNA e di dimerizzazione, rispettivamente. Nei pazienti che non presentavano macrodelezioni di *IKZF1,* le mutazioni da noi identificate sembrano avere lo stesso impatto prognostico delle macro-delezioni, presentando una maggior incidenza di eventi avversi nei pazienti trattati prima dell'introduzione degli inibitori di tirosin-chinasi rispetto a quelli a cui sono stati somministrati in sinergia con la chemioterapia.

Un paziente mutato identificato durante il nostro screening ha mostrato la presenza della stessa delezione di un singolo nucleotide sia nel campione alla diagnosi che in quello in remissione, suggerendo una possible origine costituzionale della mutazione. Nel quarto capitolo è stata indagata la natura costituzionale della mutazione nel paziente e nella sua famiglia. La stessa delezione in eterozigosi è stata identificata nella madre del paziente ed in altri 3 portatori in 3 generazioni; abbiamo inoltre scoperto un secondo caso di leucemia pediatrica all'interno della famiglia verificatasi più di 45 anni fa. La delezione riscontrata nella famiglia dà origine ad una proteina tronca con la perdita della parte terminale del dominio di legame al DNA e la completa perdita del dominio di dimerizzazione al C-terminale. L'assenza di questi domini comporta una ridotta affinità di legame al DNA ed ad una localizzazione nucleare diffusa. L'mRNA dell'allele mutato è stato ritrovato nelle cellule del midollo osseo del paziente in remissione completa, così come in cellule mononucleate del sangue di una delle sorelle, anch'essa portatrice della delezione. Nelle medesime cellule è stata riscontrata anche la presenza della proteina tronca, seppur in minor quantità rispetto alle isoforme wt.

Nel quinto capitolo viene descritto e caratterizzato un nuovo modello cellulare murino per lo studio della regolazione dell'espressione genica mediata da Ikaros. L'espressione di Ikaros aumenta durante il differenziamento dei linfociti B, ad è necessario per arrestare il ciclo cellulare di cellule B progenitrici permettendo il riarrangiamento della catena leggera delle immunoglobuline. Per meglio comprendere la cinetica ed il meccanismo con cui

Ikaros media l'espressione genica, abbiamo creato una linea murina di cellule preB knockout per il gene *Ikzf1* grazie alla tecnica di "gene editing" della CRISPR-Cas9, ed abbiamo quindi trasdotto queste cellule con una cassetta contenente un sistema inducibile di Ikaros, che ci permette di controllare la traslocazione di Ikaros dal citoplasma al nucleo. Ikaros-inducibile è in grado di traslocare efficacemente nel nucleo e di legarsi al promotore di un suo gene target molto noto, ma la sua abilità di regolare l'espressione genica appare parzialmente compromessa. Infatti, Ikaros-inducibile promuove l'aumento di espressione di alcuni suoi geni target, ma non è in grado di silenziare 3 geni da noi selezionati e noti per essere silenziati da Ikaros.

Nel sesto capitolo abbiamo utilizzato il sistema di Ikaros-inducibile per studiare i cambiamenti metabolici che avvengono durante lo sviluppo dei linfociti B, utilizzando un modello cellulare murino di cellule preB. Tre sensori basati sulla tecnica FRET, per quantificare i livelli cellulari di ATP, glucosio e di attivazione della proteina AMPK, sono stati trasdotti nel nostro modello cellulare, e sono quindi state eseguiti esperimenti preliminari utilizzando tecniche di microscopia a fluorescenza e FACS dopo 16 ore di induzione.

INDEX

GLOSSARY

4OHT	-	4-hydroxytamoxifen
ALL	-	Acute lymphoblastic leukaemia
AML	-	Acute myeloid leukaemia
APS	-	Ammonium persulphate
BCP-ALL	-	B cell precursor acute lymphoblastic leukaemia
BCR	-	B cell receptor
bp	-	Base pair
BTK	-	Bruton's tyrosine kinase
C-/-	-	*Ikzf1* homozygous null deletion
CCR	-	Clinical complete remission
cDNA	-	Complementary DNA
CFP	-	Cyan fluorescent protein
ChIP	-	Chromatin immune-precipitation
CIR	-	Cumulative incidence of relapse
CK2	-	Casein kinase 2
CLP	-	Common lymphoid progenitor
CML	-	Chronic myeloid leukaemia
CMP	-	Common myeloid progenitor
COG	-	Children oncology group
DAPI	-	4',6-diamino-2-phenylindole
DFS	-	Disease free survival
DMSO	-	Dimethyl sulfoxide
DN	-	Dominant negative
DN-/-	-	*Ikzf1* homozygous dominant negative mutation
DN+/-	-	*Ikzf1* heterozygous dominant negative mutation
DP	-	Double positive thymocytes
EFS	-	Event free survival
ERt2	-	Ligand-binding domain of the oestrogen receptor
EtOH	-	Ethanol
FACS	-	Fluorescence-activating cell sorting

FRET	-	Förster resonance energy transfer
GFP	-	Green fluorescent protein
GMP	-	Granulocyte-monocyte progenitor
GWAS	-	Genome-wide association study
HA	-	hemagglutinin
HDAC	-	Histone deacetylase complex
HR	-	High risk
HSC	-	Haematopoietic stem cell
HSCT	-	Haematopoietic stem cell transplantation
IF	-	Immune-fluorescence
IgH/L	-	Immunoglobulin heavy/light chain
IKAROS/Ikaros	-	Human/murine ikaros protein
IKZF1/Ikzf1	-	Human/murine ikaros gene
ΔIKZF1	-	*IKZF1* macro-deletions
Kb	-	Kilo-base
LMPP	-	Lymphoid-primed multipotent progenitor
LOH	-	Loss of heterozygosity
MAF	-	Mutant allele frequency
MDa	-	Mega-Dalton
MEP	-	Megakaryocyte-erythrocyte progenitor
MLPA	-	Multiplex ligation-dependent probe amplification
MPP	-	Multipotent progenitor
MRD	-	Minimal residual disease
MSCV	-	Murine stem cell virus
NGS	-	Next generation sequencing
NK	-	Natural killer
NHEJ	-	Non-homologous end joining
NuRD	-	Nucleosome remodeler deacetylase
ON	-	Overnight
OS	-	Overall survival
PBMC	-	Peripheral blood mononuclear cells
PBS	-	Phosphate-buffer saline
PC-HC	-	Pericentromeric heterochromatic region
PEST	-	Proline, glutamic acid, serine and threonine sequence

PFA	-	Paraformaldehyde
PI	-	Propidium iodide
Ph	-	Philadelphia chromosome
PP1	-	Protein phosphatase 1
RFLP	-	Restriction fragment length polymorphism
RQ-PCR	-	Real time quantitative polymerase chain reaction
RT-PCR	-	Retro-transcription polymerase chain reaction
SDS	-	Sodium dodecyl sulphate
siRNA	-	Small interfering
SLC	-	Surrogate light chain
SLE	-	Systemic lupus erythematosus
SNP	-	Single nucleotide polymorphism
SYK	-	Spleen tyrosine kinase
TCR	-	T cell receptor
TEMED	-	N,N,N’tetramethylethylenediamine
TKI	-	Tyrosine kinase inhibitor
Treg	-	Regulatory T cell
TSS	-	Transcription start site
WBC	-	White blood cell count
WGS	-	Whole genome sequencing
wt	-	Wild type
YFP	-	Yellow fluorescent protein
ZF	-	Zinc finger

CHAPTER 1

INTRODUCTION

1.1 TRANSCRIPTION FACTOR IKAROS

1.1.1 IKAROS TRANSCRIPTION FACTOR FAMILY

The *IKZF1* gene is composed of 8 exons spread over 6.2 Kb, located at sub-band p12.2 of chromosome 7 (Figure 1.1 A). Exon1 and the 5' half of exon2 are not translated into protein, but contribute to the regulation of the gene. The other 7 exons encode a 519 amino acid protein[1]. IKAROS belongs to the zinc finger protein superfamily, which totals 5% of protein coding sequences of the eukaryotic genome. Generally speaking the classical zinc finger domain, the Cys2-His2, comprises two antiparallel β-sheets folded on an α-helix. In the core of the domain, 2 cysteines in the β-sheets and 2 histidines in the α-helix coordinate a zinc atom, which confers rigidity to the entire structure. From these four coordination residues there are 3 other hydrophobic residues in the core of the domain important for structural maintenance. Residues in position -1, 3 and 6 contact a triplet of nucleotides on one strand of DNA, and a residue in position 2 interacts with a base next to the triplet on the other strand of DNA. Altogether, these four residues are responsible for the sequence-specific DNA recognition of zinc finger proteins[2–4].

IKAROS structure

IKAROS contains 6 Cys2-His2 zinc finger motifs (ZF) in 2 clusters. The N-terminal domain, encoded by exons 3 to 5, is formed by 4 zinc fingers responsible for the DNA-protein interaction, as demonstrated by gel shift and DNA foot-printing assays[5]. Zinc fingers 2 and 3 are essential for the DNA-protein interaction, since their depletion leads to the complete loss of DNA binding activity[6], while zinc fingers 1 and 4 regulate the interactions to specific genomic sites[7]. Zinc fingers 5 and 6, located at the C-terminal domain, are responsible for IKAROS dimerization, which greatly enhances the binding affinity to DNA. Both zinc fingers are required to gain a stable dimerization[8].

IKAROS isoforms

Alternative splicing of the *IKZF1* gene generates at least 10 different isoforms. These isoforms retain the last exon, encoding the C-terminal dimerization domain, and differ from each other regarding the inclusion of other exons[6,8]. Besides the full-length IK1 isoform, there are at least 9 different isoforms: IK2, IK3, IK4, IK5, IK6, IK7, IK8, IK9 and IKX. IK1 to IK4 are able to interact with DNA, while IK5 to IK9 completely or partially lack the N-terminal domain but retain the dimerization domain (Figure 1.1 B). They are referred to as dominant negative (DN) isoforms, as they are able to interact with longer Ikaros isoforms impairing their DNA-binding (Figure 1B). In haematopoietic cells IK1 and IK2, the longest isoforms, are most abundantly detected. Many of the other isoforms were detected at different stages of haematopoietic development in myeloid (IKX)[9], lymphoid (IK1, IK2 and IK4)[6], and erythropoietic (IK3)[1] cells. Fluorescent microscopy performed on IKAROS transfected-fibroblasts and thymocytes revealed that only DNA-binding isoforms can actively translocate into the nucleus, while DN isoforms remain in the cytoplasm. DN isoforms only display nuclear localisation when co-transfected with DNA binding isoforms, demonstrating that short isoforms can only pass through the nuclear membrane when in complexes with longer isoforms. Remarkably, IK1 loses its ability to activate the transcription of a reporter gene under the control of four copies of IKAROS recognition sites when it is co-expressed with DN isoforms like IK6 and IK7, while when coupled with longer isoforms, such as IK2 or IK3, IK1 can activate transcription[8].

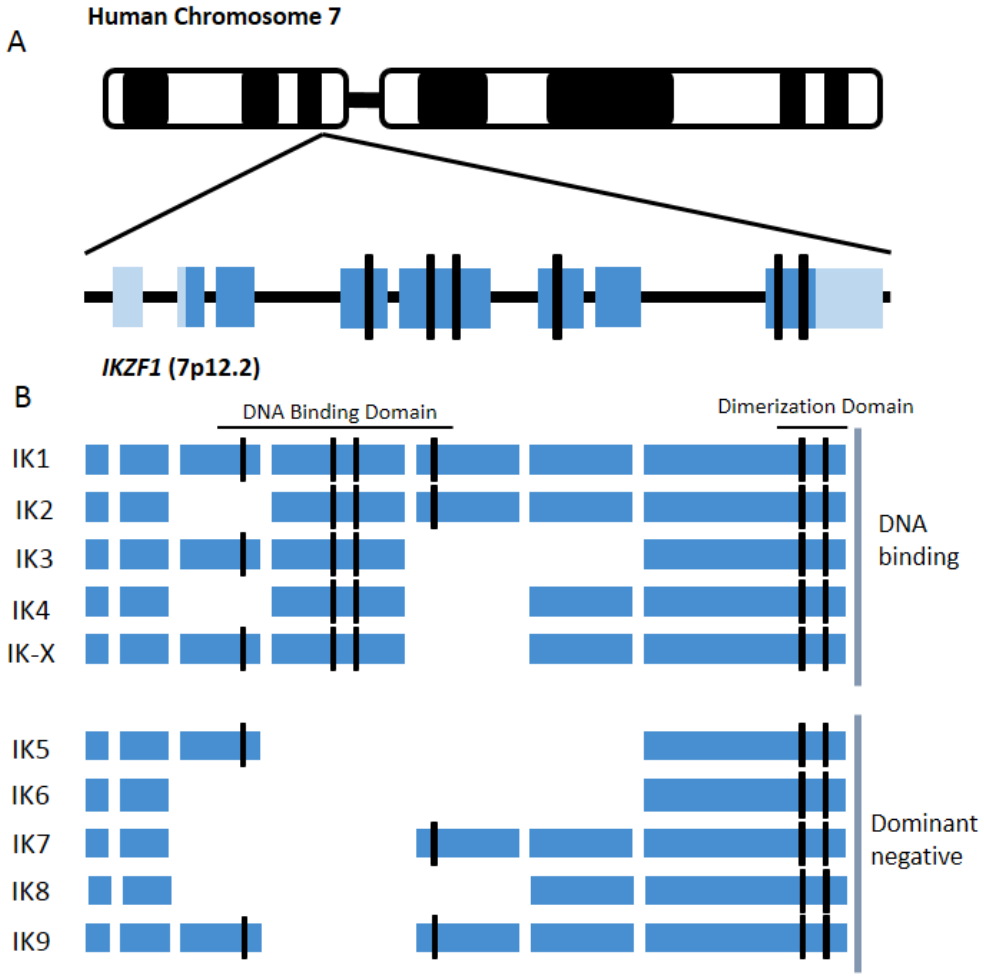

Figure 1.1: Schematic representation of *IKZF1* gene. A) Schematic representation of the *IKZF1* locus and chromosome position. Coding exons are depicted in blue, non-coding exons in light blue. B) The main IKAROS isoforms + indication of ZFs 1-4 DNA binding and 5-6 dimerization. Modified from Olsson et al., 2015

Post-translational modifications of IKAROS

IKAROS function is post-translationally regulated by phosphorylation. Indeed Casein Kinase 2 (CK2) is responsible for IKAROS phosphorylation at multiple sites between amino acids 389 and 398, and in positions 13, 23, 63, 101 and 294[10]. Phosphorylation at these sites affects IKAROS activity, as phospho-mimetic mutants (mutants where phospho-sites are mutated into aspartate to mimic the negative charge of a phosphate residue) at position 13 and 294 show a complete abolishment of IKAROS binding to DNA resulting in a diffuse nuclear localization of the protein and a block of the cell cycle in G1 phase[11,12]. Protein phosphatase 1 (PP1) is responsible for the dephosphorylation of residues at phosphosites. IKAROS interacts with PP1 through a conserved PP1-binding motif located at its C-terminus. Deletions of the PP1-binding motif result in poor DNA affinity, nuclear mislocalization, and a faster rate of IKAROS degradation[13].

Recently, Spleen Tyrosine Kinase (SYK) and Bruton's Tyrosine Kinase (BTK) have been shown to phosphorylate IKAROS. Highresolution confocal microscopy showed that IKAROS partially co-localizes with SYK and BTK, and that these kinases are able to phosphorylate IKAROS at specific, unique sites. DT40 chicken lymphoma cells deficient for SYK or BTK, as well as experiments on single phospho-resistant mutants (mutants where phospho-sites where substituted by alanines, that mimic a non-phosphorylated amino acid) showed an aberrant cytoplasmic localization of IKAROS, indicating a pivotal role of phosphorylation in IKAROS activation and localization. Both SYK and BTK are essential for IKAROS nuclear translocation, as mutations in SYK or BTK target residues impaired IKAROS localization. Finally, SYK and BTK phosphorylation can overrule the inhibitory effects of CK2-phosphorylated residues as phospho-mimetic mutated CK2 sites on the Ikaros protein fail to translocate to the nucleus when either SYK or BTK are depleted by siRNA[14,15] (Figure 1.2).

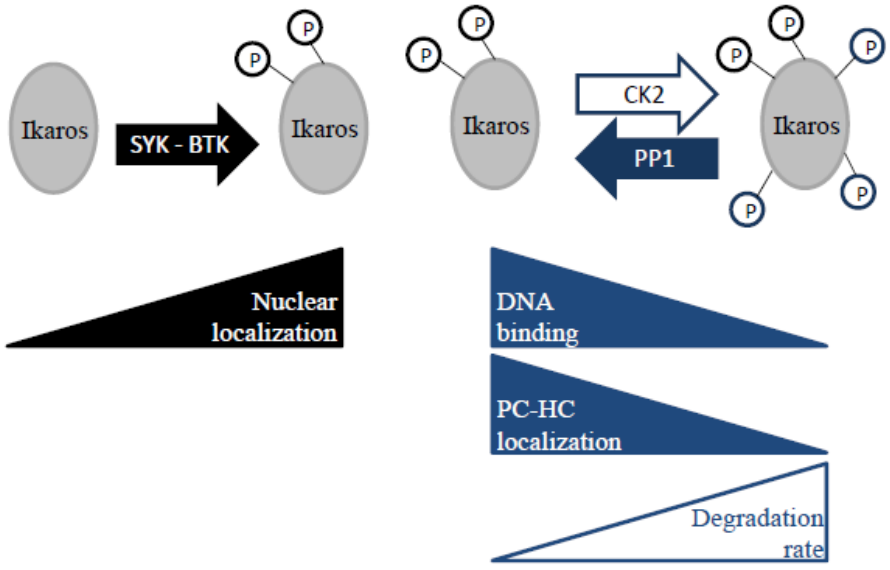

Figure 1.2: Schematic presentation of post-translational modifications that regulate IKAROS activity. Phosphorylation by BTK and SYK kinases promote nuclear translocation of IKAROS, where it binds DNA. CK2 phosphorylation of IKAROS in the nucleus impairs DNA binding, pericentromeric localization and increased its degradation rate, which were restored via de-phosphorylation by PP1.

IKAROS zinc finger family members

Ikaros is the founding member of a family of 5 transcription factor proteins including Helios, Aiolos, Eos and Pegasus[16]. The first 4 components of the family, found by using degenerated primers on the conserved N-terminal and C-terminal regions, display 4 zinc fingers at the DNA-interaction N-terminal domain that recognize the canonical GGAAA sequence, whereas Pegasus, the most divergent of the family members, contains only 3 zinc fingers at the N-terminus and recognizes the atypical GNNNGNNG consensus

sequence[17]. Next to Ikaros itself, Helios and Aiolos are the most studied proteins of the Ikaros family, since they display the highest similarity with Ikaros and are implicated in haematopoiesis.

Aiolos: Aiolos, encoded by *IKZF3*, shows the highest similarity with Ikaros, and can heterodimerize with Ikaros and Helios. Despite high sequence homology, Aiolos is not present in haematopoietic stem cells with Ikaros, but is expressed from the Pro-B cell stage onwards and is upregulated in all later and mature stages of B lymphocyte development[18]. In T cells Aiolos is expressed at the $CD4^-CD8^-$ and the more mature $CD4^+CD8^+$ stage, and has been shown to be required for NK cell maturation[19]. Besides its role in haematopoiesis, Aiolos acts as an anti-apoptotic factor by regulating Bcl-2 expression and by directly binding Bcl-X_L proteins[20]. Aiolos is transcribed in multiple isoforms, differing between each other in the number of N-terminal zinc fingers. Aiolos isoforms have different cellular localization, and are able to change the cellular localization of other Ikaros family members[21].

Helios: The expression of Helios, encoded by *IKZF2*, is restricted to haematopoietic stem cells (HTCs) and a subset of lymphoid cells, in particular early T cells[22]. As a member of the Ikaros protein family, Helios dimerizes with Ikaros and Aiolos and can co-localize *in vivo* with Ikaros long or DN isoforms[22]. Helios was most studied as an important factor in Treg development and function. Helios+ peripheral Treg cells display a higher ability to suppress antigen-specific and TCR specific T cells responses, and are able to down-regulate cytokine expression by T cells in Helios-reporter mice[23].

1.1.2 THE ROLE OF IKAROS AS REGULATOR OF GENE EXPRESSION

Ikaros was initially identified in 1992 by Georgopoulos and colleagues, in their effort to find new transcription factors involved in early T cell commitment. In their first paper, Ikaros was shown to bind one of the enhancer elements of the *CD3δ* gene, promoting its expression. *In vitro* analysis of other B- and T-specific promoter regions and DNase footprinting experiments revealed binding sites at the promoters of *TdT*, *λ5*, and other lymphoid-restricted genes[24,25]; moreover, Ikaros and Aiolos can activate the transcription of reporter genes under control of the Ikaros consensus binding site[6,8]. Further reports from

other groups emphasize a major role of Ikaros as a repressor of gene expression[26], elucidating the dual function of Ikaros as an activator and repressor of gene expression.

The sub-cellular localization of IKAROS

To exert its function, IKAROS needs to localize in apposition to pericentromeric regions in the nucleus. In mature B cells, confocal microscopy experiments highlighted a spotted, toroidal localization in the nucleus, which disappeared during S phase of the cell cycle. Immunofluorescence combined with fluorescent in situ hybridization showed the localization of IKAROS at heterochromatic regions (marked by γ satellite probes). Of note, genes down-regulated by Ikaros were positioned at pericentromeric-heterochromatic (PC-HC) regions and co-localized with Ikaros. Positioning at PC-HC regions is specific for down-regulated genes and is related to developmental stages. For example, *Igll1* (a component of the surrogate light chain) locus was found juxtaposed to Ikaros at the PC-HC region in mature B cells, but not in preB cells[26]. These data were confirmed by a second paper of the same group, showing that Ikaros-regulated genes were dynamically repositioned during the cell cycle. In mature resting B cells, Ikaros is barely detected in the nuclei, but following B cells stimulations Ikaros nuclear signals increased and after 3 days the typical Ikaros-PC-HC foci were observed. In concomitance, *Igll1*, *CD8α* and *Rag* genes (all direct targets of Ikaros) were repositioned at the PC-HC regions. This spatial redistribution clearly parallels Ikaros repositioning[27]. *Rag* and *TdT* were also dynamically repositioned in the transition from resting to cycling immature T cells, and invariably, this re-localization led to the significant down-regulation of gene expression. Quite surprisingly, Koipally and colleagues demonstrated that also the activation of Ikaros target gene expression required PC-HC localization, as reporter vectors containing Ikaros binding sites were shown to be activated only by Ikaros isoforms that are able to localize at PC-HC in NIH-3T3 transfected cells[28]. Two interpretations of this phenomenon are proposed: Ikaros localization at PC-HC regions repositioned NuRD complexes at these regions, decreasing their concentration as well as their inhibitory effects in other portions of the genome; or Ikaros target genes present at PC-HC regions are bound by Ikaros and the NuRD component Mi-2β, that remodelled chromatin in the proximity of its binding sites, enhancing the promoter accessibility to activators.

Ikaros localizes to PC-HC regions by direct binding to γ satellite sequences present at these sites[2], and this binding is preserved during cell cycle progression, when Ikaros DNA binding affinity to its target genes is decreased[29]. A model of Ikaros function was proposed, to link its ability to independently bind promoters and pericentromeric

heterochromatin with the Ikaros-mediated repositioning of its target genes to PC-HC: according to this model, Ikaros dimers contact the promoters of target genes, and subsequently interact with other multimeric Ikaros complexes located at the PC-HC region, thereby recruiting these genes to PC-HC sites[2,30].

IKAROS in the regulation of gene expression and chromatin remodelling

The regulation of gene expression by Ikaros may either be direct or mediated through chromatin modifier complexes. The putative bipartite activation domain of Ikaros, originally identified in a double-hybrid assay[8], was shown to be not essential for the regulation of gene expression, as its mutation does not impair the transcriptional activation of reporter genes[28].

Evidence for a direct regulation of gene expression came initially from the analysis of the *TdT* promoter in $CD4^+$ $CD8^+$ double positive thymocytes. An Ikaros binding site was identified within the core Ets recognition sequence. Gel-shift assays displayed competition between Ikaros and Ets binding at this locus, as increasing the concentration of one led to a progressive decrease in the binding of the other[30]. Down-regulation of *TdT* coincided with the appearance of inhibitory chromatin marks that preceded pericentromeric re-localization, suggesting different temporal mechanisms of gene expression control by Ikaros.

Similar competitive binding inhibition was observed by the analysis of *Igll1 and VpreB* promoters in mature and immature B cells. In these cells Ikaros competes with the transcription factor EBF to bind at these loci (Figure 1.3 A) and down-regulate these genes during B lymphoid development[31,32].

The most studied mechanism of transcription regulation by Ikaros is through the recruitment of chromatin modifier complexes. Ikaros and Aiolos localize with a 2 MDa complex containing the ATPase Mi-2 nucleosome remodeler of the NuRD (nucleosome remodeler deacetylase) complex, histone deacetylase complexes (HDACs) and Sin3A and Sin3B proteins[33,34].

The NuRD complex co-localized with the typical toroidal structures formed by Ikaros and Aiolos at PC-HC regions and their pointed localization disappear in Ikaros-deficient cells, indicating a primary role of Ikaros in the localization of the complex to heterochromatin[33] (Figure 1.3B).

Ikaros-mediated transcriptional repression is mainly exploited through deacetylation of target gene promoters by HDACs[34,35]. However HDAC-independent transcriptional repression by Ikaros has been reported. Ikaros has been shown to interact with the co-

repressor ctBP and ct-interacting protein (ctIP), and the Ikaros-ctBP/ctIP complexes can repress transcription of reporter genes without HDAC recruitment[36,37]. *In vitro* experiments show how Ikaros-ctBP and Ikaros-ctIP can interact with basic components of the transcriptional machine like TFIIB and TBP, implicating the transcription pre-initiation complex as an interesting target for Ikaros' HDAC-independent transcriptional repression[37].

Ikaros has been suggested to act as an activator of transcription by recruiting Brg1-SWI/SNF to upstream regions of its target genes resulting in nucleosome remodelling and activation of transcription[38]. Ikaros-Brg-1 complexes display a diffuse distribution in active T cells, potentially overlapping with euchromatin regions, and never co-localize with the NuRD complex, as revealed by immune-precipitation assays[33] (Figure 1.3 C). Even the Ikaros-NuRD interaction, typically considered as transcriptionally repressive, could lead to different regulatory outcomes. Indeed a recent genome-wide study of Ikaros and Mi-2β binding in double positive (DP) thymocytes revealed that Ikaros can localize the NuRD complex to active chromatin sites involved in T-cell development[39]. Furthermore, an antagonistic interplay between Ikaros and Mi-2β at the CD4 locus was highlighted in DP thymocytes: Mi-2β helps to recruit acetyl transferases at the silencer region of the CD4 locus, possibly antagonizing Ikaros and its associated repressive activity[35].

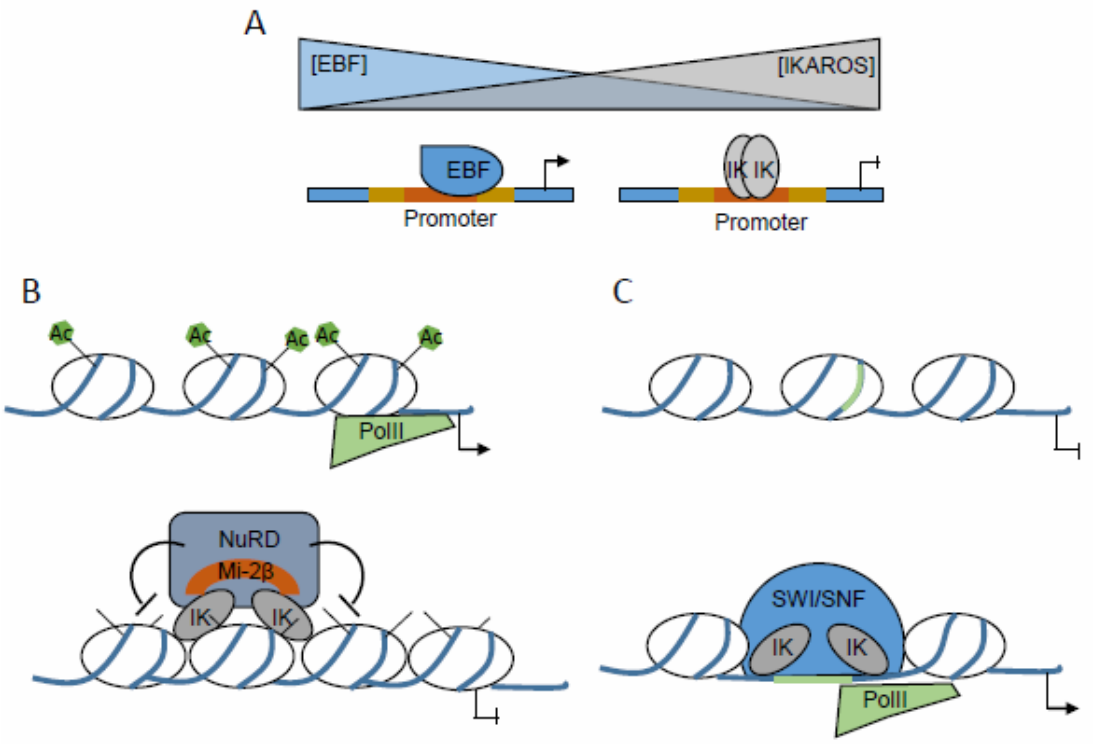

Figure 1.3: Examples of IKAROS function as transcription factor. A) Concentration-dependent competitive binding of IKAROS and EBF transcription factors at the promoter region of *Igll1*. B) Recruitment of the de-acetylase NuRD-Mi-2β complex by IKAROS to promoters leads to down-regulation of transcription. C) Nucleosome-remodeler SWI/SNF is recruited by IKAROS up-stream of target genes and result in target gene activation.

Associations between Ikaros and the transcription elongation process were recently determined. Ikaros associates with NuRD and the positive transcription elongation factor b (P-TEFb) in haematopoietic cells, as revealed by tandem immune-affinity mass spectrometry. The building of this complex depends on Ikaros expression, as low levels of Ikaros lead to an association with the NuRD complex only, inhibiting the recruitment of P-TEFb and Ikaros-NuRD at promoter regions of well-established Ikaros target genes[40].

The experiments discussed above describe the dual function of Ikaros as both an activator and repressor of gene expression. Ikaros-mediated regulation of gene expression is dependent on cell type, developmental and cell cycle stage.

1.1.3 IKAROS AND HAEMATOPOIESIS

Haematopoiesis is a hierarchical process in which multipotent progenitors undergo a restriction in developmental potential culminating in the production of the lineage-committed blood cells. Haematopoiesis occurs in the foetal liver during embryonic development, and in the bone marrow and the thymus of the adult[41,42]. All blood cells derive from multipotent haematopoietic stem cells (HSC), the only haematopoietic cell type that preserves self-renewal potential and multipotency, which reflects the ability to differentiate into lineage-specific cells[42,43]. Characterization of differentially expressed cell

surface markers or surrogate markers activated by lineage-specific cassettes have helped to isolate and characterize haematopoietic stem cells as well as lineage restricted progenitors. HSC initially give rise to multipotent progenitors (MPP), that maintain the lineage-differentiation potential of HSCs but lack self-renewal properties. MPPs can then give rise to 3 lineage specific progenitors: lymphoid-primed multipotent progenitor cells (LMPP) that preserve the lymphoid and myeloid potential but are no longer committed to the erythro-megakaryocyte lineage; megakaryocyte-erythrocyte progenitors (MEPs) that exclusively preserve the potential to differentiate into erythro-megakaryocytes; and common myeloid progenitors (CMPs) that possess erythro-megakaryocyte as well as myeloid differentiation potential[44]. LMPPs can subsequently differentiate into granulocyte-monocyte progenitors (GMPs) and the common lymphoid progenitors (CLPs), which give rise to B and T lymphocytes and natural killer (NK) cells[45] (Figure 1.4).

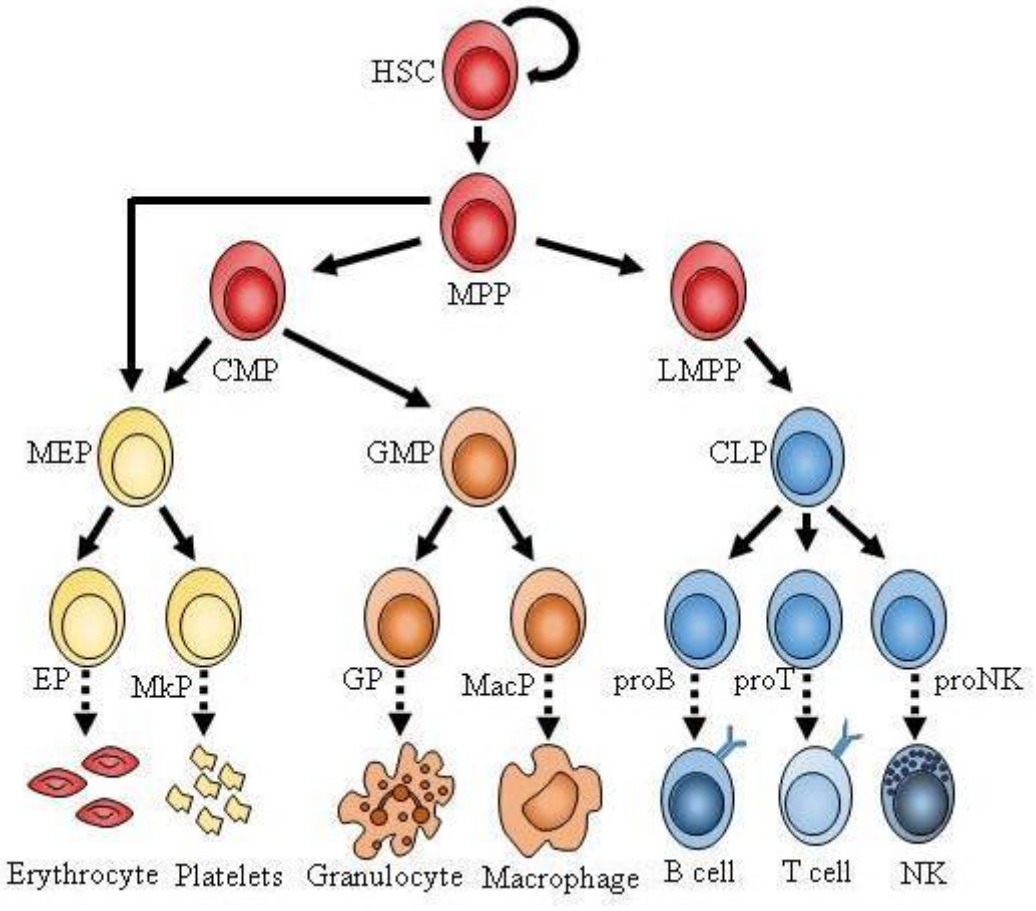

Figure 1.4: Hierarchical model of haematopoiesis differentiation. HSC, haematopoietic stem cell; MPP, multipotent progenitor; LMPP, lymphoid-primed multipotent progenitor; CLP, common lymphoid progenitor; CMP, common myeloid progenitor; MEP, megakaryocyte-erythrocyte progenitor; EP, erythrocyte progenitor; MkP, megakaryocyte progenitor; GP, granulocyte progenitor, MacP, macrophage progenitor; NK, natural killer. Modified from Cedar & Bergman 2011

Focusing on the B lymphoid restricted lineage, B cell development progresses through a series of developmental stages characterized by the expression of different molecular markers, and show oscillation between cell cycle progression and cell cycle arrest. This alternation between proliferation and quiescence is necessary for the somatic rearrangement of the heavy and light immunoglobulin chains, as Rag 1 and 2 activity is restricted to G1 phase to avoid genomic instability[46,47]. CLPs give rise to the first committed B cell progenitor, pre-pro-B cells, which transit through other lineage-commitment stages termed pro-B, cycling pre-B, resting pre-B, and immature B cell. RAG-mediated immunoglobulin rearrangement at the Ig heavy chain (IgH) locus begins at the early pre-pro-B stages. The rearranged IgH locus encodes the Igμ chain, which is expressed at the pre-B stage together with the surrogate light chain (SLC). The SLC is composed of the 2 invariant proteins λ5 and $V_{pre}B$ (encoded by *Igll1* and *$V_{pre}B1$* genes). Together, Igμ and SLC form the pre-BCR complex. Pre-BCR signalling is an important feedback signal in B cell development, as only cells with productive Igμ rearrangements can proceed to the next maturation steps. Pre-BCR signalling induces a burst of proliferation and a simultaneous down-regulation of λ5, inhibiting SLC expression. SLC inhibition and the subsequent termination of pre-BCR signalling pilots cycling pre-B cells out of the cell cycle towards commencing IgL chain rearrangements. This is a critical step in the B-lymphocyte development, as cycling pre-B cells have virtually unlimited proliferative potential. Successful IgL recombination gives rise to an immature B cell expressing the BCR complex on its surface. Immature B cells are then selected for their ability to crosslink with self-antigens, and only non-autoreactive cells are selected to become mature B cells and migrate outside the bone marrow[31,47].

The role of IKAROS in haematopoiesis

Each haematological cell type is specified by a series of signalling networks headed by different transcription factors in a hierarchical as well as combinatorial manner[45]. Multipotent HSCs and MPPs show low levels of lineage-specific gene expression patterns, while during cell specification distinct lineage determinants enhance their expression and/or activity, antagonizing other lineage-specific factor and thereby establishing cell fate. In the last decades, knockout animal models have depicted the network of interactions needed for B-cell specification. The most relevant transcription factors that orchestrate the B-cell development include PU.1 (for HSC to LMPP specification), E2A and EBF (for the control of gene expression in pro-B cells during Ig chain rearrangement), PAX5 (that

restricts the developmental options to the B cell lineage repressing other gene specification cassettes), and Ikaros[41].

During embryogenesis, Ikaros mRNA was detected at primitive and definitive sites of haematopoiesis. The longest IK1 and IK2 isoforms are expressed in the yolk sack, as well as in foetal liver, early thymus and post-natal spleen. The shorter IK4 isoform is detected in the maturing thymus, but its expression declines during mid gestation, while the longest isoforms remain detectable after birth. Ikaros isoforms IK1, IK2 IK3 IK4 and IK5 were detected in the early stages of brain development, but the expression dropped during late development and at day 1 after birth, suggesting a restriction in Ikaros expression to a specific brain cell population[48]. Ikaros' role and importance in haematopoiesis is well depicted by genetic ablation studies in mice. Homozygous deletion of the C-terminal dimerization domain resulted in the generation of Ikaros null mice (C-/-)[49]. C-/- mice present a complete absence of B cells and their precursors, dendritic APC and NK cells, both in foetal and post-natal stages. T cell precursors were not detectable in the thymus during foetal life, but appeared 3–6 days after birth at a hundredfold lower abundance compared to WT mice. Furthermore, these lymphocytes showed an impaired development skewed to the $CD4^+$ lineage, and hyper-proliferated when stimulated through their TCR. The erythro-myeloid lineage seems not to be affected by the Ikaros null mutation, as both erythro- and myeloid precursors and mature cells were found in bone marrow and spleen (Figure 1.5 A). A more severe phenotype was displayed by homozygous Ikaros dominant negative (DN-/-) mice, where the N-terminal zinc fingers 1, 2 and 3 were deleted, leading to the production of a protein that no longer binds to DNA but is still capable of dimerization with other Ikaros family members. Phenotypically, post-natal DN-/- mice displayed a rudimentary, nearly invisible embryonic thymus, and a complete absence of peripheral lymph nodes. Cytometric analysis of the bone marrow and rudimentary thymus revealed complete ablation of B, NK, dendritic and T cell precursors as well as mature cells. Only a small population of $Thy\text{-}1^{lo}$ cells were detected in the bone marrow, probably representing early arrested B and T lymphoid progenitors. Like in the C-/- mice, the erythro-myeloid compartment did not show developmental impairment in $DN^{-/-}$ mice, as erythrocytes and granulocytes were detected in both bone marrow and spleen[50]. However, extending the analysis up to 6 weeks, the DN-/- mice' haematocrit dropped to <50% compared to WT mice[51] (Figure 1.5 B).

Analysis of the bone marrow of heterozygous DN+/- mice displayed a normal phenotype, with T and B cell precursor abundance comparable to WT controls, until 2-3 months after

birth. At that point intermediate precursors of T cells started to accumulate in the thymus and spleen, and soon after mice developed T cell leukaemia or lymphomas with a very high degree of penetrance (95-100%)[52] (Figure 1.5 C).

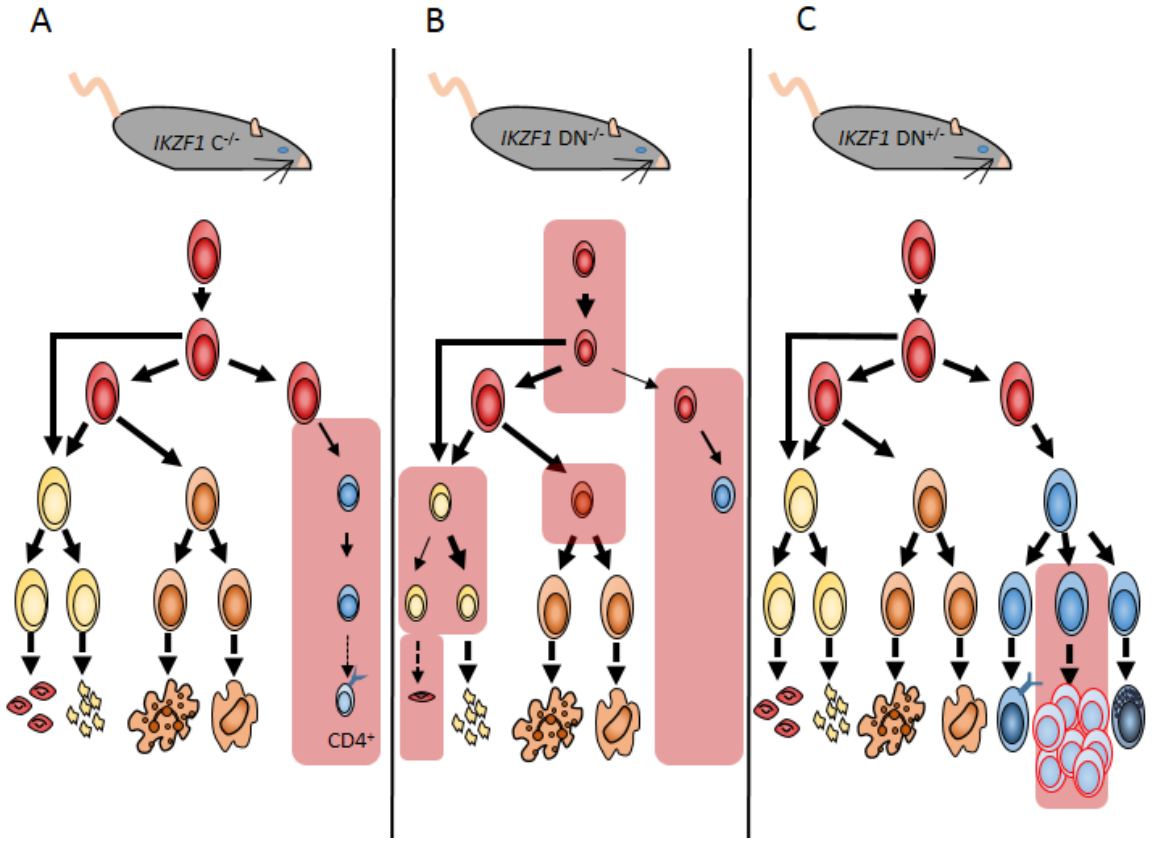

Figure 1.5: Schematic representation of haematological deficiencies in Ikaros mutated mice. *IKZF1* null C-/- mice (A), homozygous Ikaros dominant negative DN-/- mice (B) and heterozygous Ikaros dominant negative DN+/- mice (C). Haematological deficiencies are highlighted in red. Impaired production of a certain progenitor is reported as a smaller picture compare to the other lineages. Leukemic cells are drawn with red edges.

Taken together, these data depict a pivotal role for Ikaros in lymphopoiesis. The more severe phenotype shown by DN-/- mice compared to the null-mutated C-/- mice suggests aninterplay between Ikaros and other Ikaros family members during lymphoid commitment. Indeed, Aiolos and Helios are shown to heterodimerise with Ikaros and to have a role in T and B cell development[19,53], supporting this hypothesis.

The homozygous DN-/- mouse model, with the complete depletion of all lymphoid-related lineages, tells us that Ikaros plays an important role at the very beginning of the lymphoid commitment, at the level of HSC or LMPP progenitors. To elucidate this point, further analysis on DN-/- and C-/- mice were conducted, that revealed a 30-40% HSC long term repopulation rate reduction, indicating a role of Ikaros in self-renewal[51]. In the same study, molecular analysis of mRNA in HSC cells established a lack of expression of *Flt3* and *c-*

Kit tyrosine kinase receptors, implicated in B cell specification and HSC viability, respectively.

The contribution of Ikaros to haematopoietic ontogeny was recently elucidated in a very elegant way by using a GFP reporter cassette under the control of the *Ikzf1* promoter enhancer. By the analysis of bone marrow cells from transgenic mice, a GFP signal was detected in HSC progenitors and in the LMPP fraction, which maintain lymphoid and myeloid potential albeit with limited erythro-megakaryocyte potential. The same experiment repeated in Ikaros null cells showed the presence of LMPP progenitor cells that didn't express the Flt3 marker. These progenitors were unable to differentiate into the B cell lineage even in the presence of B cell specification factors in culture media, but preserved their ability to generate T lymphocytes (this observation could explain the origin of postnatal T lymphocytes in C-/- mice). However, these cells showed a skewed differentiation potential towards the myeloid lineage. Dissection of the role of Ikaros in erythro-myeloid development showed that during myeloid development Ikaros expression is restricted to the granulocyte-macrophage progenitors (GMP) branch, and is poorly expressed in megakaryocyte-erythrocyte progenitor cells (MEP). In Ikaros null cells, MEP cells numbers increased, whereas the GMP cell population decreased. Moreover, MEP cells displayed a skewed differentiation towards the megakaryocyte lineage, indicating that Ikaros is required for cell-fate decision during myelopoiesis, promoting GMP progenitors and erythroid differentiation[54].

The same authors conducted a microarray study on the same cell populations to clarify the mechanisms underlying Ikaros control on haematopoietic differentiation. In Ikaros$^{+/+}$ GFP reporter mice, HSCs show expression of all haematopoietic lineages: erythroid, myeloid and lymphoid, in addition to self-renewal and stem cell related genes. Lineage-restricted progenitors were then analysed. MEP cells expressed only erythroid transcripts while LMPPs displayed a strong lymphoid and myeloid signature with a down-regulation of HSC and erythroid related genes. In GMP cells genes related to myeloid commitment were up-regulated, but surprisingly retain a low level of expression of lymphoid specific genes (Figure 1.6). The same analyses were then performed on Ikaros-null C-/- HSC, LMPP and GMP cells. In the absence of Ikaros, lymphoid-related genes were strongly down-regulated in HSCs and all the other haematopoietic precursors. On the contrary, stemness-related genes were up-regulated in all progenitors' compartment, as well as myeloid priming genes

(Figure 1.6). Taken together, these data confirm the pivotal role of Ikaros in lymphoid commitment from the very first stages of haematopoiesis. They also indicate the importance of Ikaros in extinguishing the expression of stem cell and erythroid genes and in preventing the premature induction of myeloid genes[55].

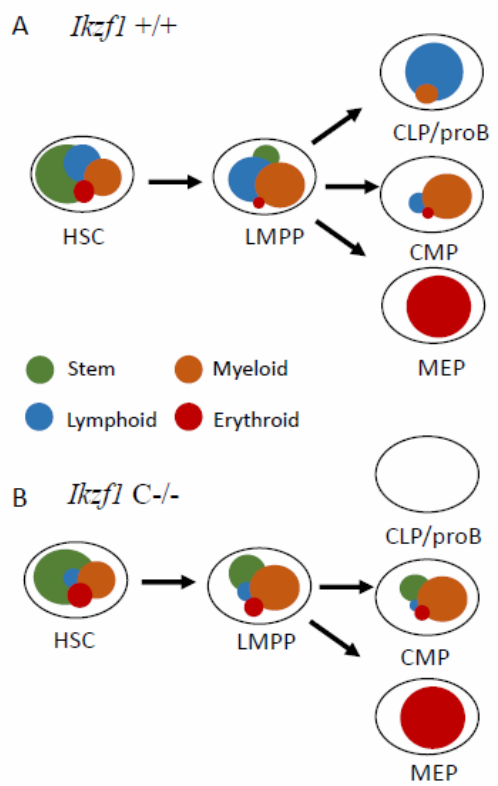

Figure 1.6: A model of multilineage transcriptional priming and IKAROS contribution. Lineage-specific transcriptional programs are all activated in HSC. Subsequent lineage restrictions are marked by changes in lineage-specific transcripts. A) The multilineage restriction process in Ikaros WT cells and B) in Ikaros null mice. Modified from Ng et al. 2009.

1.2 IKAROS AND LEUKAEMIA

1.2.1 ACUTE LYMPHOBLASTIC LEUKAEMIA

Acute lymphoblastic leukaemia (ALL) is a malignant clonal disease of the bone marrow in which lymphoblastic progenitors blocked at an early developmental stage (blasts) abnormally proliferate replacing the normal haematopoietic cells in the marrow. ALL is the most common childhood cancer, representing 80% of all leukaemias and 25% of all cancers that occur in children and adolescents, and can originate both from B cell (85%) and T cell (15%) lineages[56]. Leukemic cells arise from pre-leukemic clones as a result of accumulation of somatic genetic aberrations during life, often already starting *in utero*[57,58]. Nowadays leukaemia is considered a heterogeneous disease, characterized by different genetic alterations such as chromosomal translocations, aneuploidy, mutations in proto-oncogenes or tumour suppressors, and focal deletions (Figure 1.7)[59,60]. Diagnosis of ALL is carried out by light microscopy inspection of bone marrow aspirate and immunophenotypic profiling using flow cytometry. Clinical studies during the past 70 years identified a set of clinical and laboratory parameters that correlate with the patients' response to therapy[60–62]. Adverse prognostic markers include high leukocyte counts at diagnosis (WBC), age <1 year or >9 years, and adverse cytogenetic aberrations like the t(9;22) or MLL rearranged translocations, or acquired hypodiploid status. A combination of these markers is used in treatment protocols to stratify patients in groups based on risk of treatment failure. Patients with favourable markers are treated with less toxic regiments, while those showing high-risk factors attend more aggressive regiments. The patients' response to treatment is evaluated by detecting residual leukemic cells commonly indicated as minimal residual disease (MRD). MRD is typically detected by PCR amplification of the recombined immunoglobulin or T cell receptor gene rearrangement, and it has been shown to be a powerful independent prognostic marker in both paediatric and adult patients[63]. The introduction of risk-stratified treatment and multi-drug combination therapies result in a cure rate of more than 85% (or event free survival EFS) for ALL paediatric patients[64]. Nevertheless, in spite of great improvements in ALL treatment, 15% of patients still experience relapses or die and these patients now represent the new frontier of clinical and biomedical research in ALL.

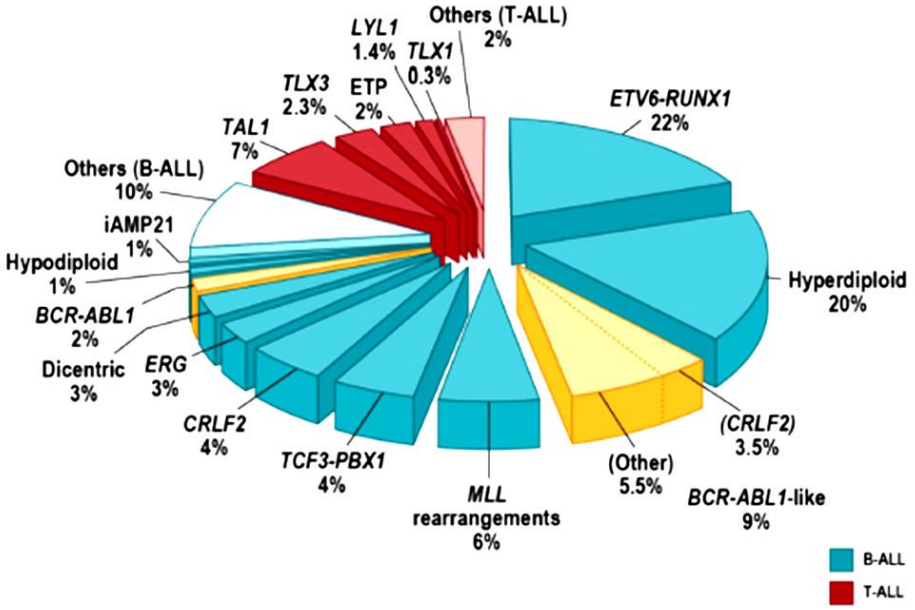

Figure 1.7: Frequency of genetic subtypes in paediatric ALL. From Mullighan 2012**.**

1.2.2 PHILADELPHIA POSITIVE B CELL ACUTE LYMPHOBLASTIC LEUKAEMIA

The Philadelphia chromosome (Ph) was the first chromosomal aberration discovered in association with a human disease. In 1960 Nowell and Hungerford observed in adults with chronic myeloid leukaemia (CML) a chromosomal translocation, t(9;22) resulting in a reduced size of chromosome 22[65]. Later on, the translocation has been more precisely described as a reciprocal balanced translocation between chromosomes 9 and 22 t(9;22)(q34;q11)[66]. The direct consequence of this translocation is the juxtaposition of the *ABL1* gene on chromosome 9 and the *BCR* gene on chromosome 22, forming the chimeric gene *BCR-ABL1*. Wild-type ABL1 is a non-receptor tyrosine kinase expressed during haematopoiesis that shuttles between the cytoplasm and the nucleus. The N-terminus of ABL1 negatively regulates its kinase activity, and its loss as a consequence of the translocation results in a constitutive activation of the kinase activity[67]. The physiological function of the BCR protein is still unclear, but its major contribution in the chimeric protein seems to be related to its coiled-coil domain that facilitates dimerization and autophosphorylation, increasing the kinase activity of the fusion protein[68]. The autoactivation and autophosphorylation of BCR-ABL1 leads to a direct and indirect activation of multiple pathways including AMP, MTOR, PI3K, MAPK and a common downstream target of most of them, STAT5. The aforementioned pathways all converge

ultimately into a unique point: loss of control of proliferation and protection from apoptosis[69].

In addition to being the major cytogenetic aberration in CML *BCR-ABL1* translocations are also detected in 2 to 3% of paediatric B cell precursor (BCP) ALL and in 20% of adult patients with ALL[60]. Despite its low incidence in children, Ph+ BCP ALL is still a major concern for clinicians as the presence of the Ph chromosome correlates with a very adverse prognosis. International efforts to help improve outcome of rare subgroups of ALL patients (Ponte di Legno childhood ALL consortium) reported a 7-years event free survival (EFS) and overall survival (OS) rates of 25 and 36% for 326 Ph+ ALL patients diagnosed between 1985 and 1996, and 32 and 45% for 610 Ph+ patients between 1995 and 2005. Relapse was the main cause of treatment failure, and haematopoietic stem cell transplantation (HSCT) in first remission was considered the best treatment option, although EFS and OS remained below 50% even with HSCT from a matched donor[70,71]. The development of tyrosine kinase inhibitor (TKI) based drugs initiated a new era in the treatment of Ph+ malignancies. Imatinib was the first small molecule developed to selectively target the BCR-ABL1 tyrosine kinase activity, by blocking the binding site for ATP[72]. The introduction of imatinib in the clinical protocols revolutionised the therapy for patients affected by CML, increasing the EFS at 5 years from 35% to over 80%[73]. In 2009, the Children Oncology Group (COG) published the results of the first paediatric clinical trial to evaluate the efficacy of imatinib in the treatment of Ph+ ALL. The 3-years EFS rate from the initial study was 80% compared to 35% in the pre TKI era, and the data was confirmed stable over time by new analysis showing a 7-years EFS rate of 71% compare to the 21.4% of the historical pre TKI group. The same study showed no additional benefit of HSCT on the outcome of patients, reassessing its importance for patients that respond poorly to the chemotherapy plus TKI[74,75]. A parallel study was conducted mainly in Europe to evaluate the efficacy of imatinib, the EsPhALL phase 3. In this study patients were classified as good or poor responders on the basis of the initial response to induction therapy, and then the study randomized the good-risk patients' chemotherapy with or without imatinib, while all poor-risk patients were ascribed to chemotherapy plus imatinib. The 4-years disease free survival (DFS) for good risk patients treated with imatinib was 75.2% and 55.9% for those who received chemotherapy only. The EFS of the poor-risk population was 53.5%, still much higher than the classical EFS of patients in the pre-TKI era[76].

Although the encouraging results obtained by the introduction of imatinib in treatment of pediatric Ph+ ALL, 20-25% of patients still experience treatment failure or resistance to chemotherapy. Mechanisms of resistance of Ph+ ALL cells include duplications and increased BCR-ABL protein signalling, up-regulation of parallel pathways such as the Src-family kinase pathway, and mutations occurring at the kinase domain that impair the efficient binding of imatinib[69,77]. To overcome these issues, second generation TKIs like nilotinib and dasatinib were developed[78,79]. These second generation drugs are more potent inhibitors of BCR-ABL1 *in vitro*, are generally active on the imatinib-resistant TKI mutations with the relevant exception of T315I mutation, and can trigger other kinase signal pathways, such as the Src-family pathway[80,81].

1.2.3 THE ROLE OF IKAROS IN ACUTE LYMPHOBLASTIC LEUKAEMIA

The first link between IKAROS and leukaemia was established with the help of mice models.

Mice heterozygous for a dominant negative mutation on Ikaros (DN+/-) developed aggressive forms of lymphoma or leukaemia with a high degree of penetrance. The blasts clonally developed in the thymus from T cell precursors, and showed a loss of the WT *Ikzf1* allele in most of the cases[52]. A second breed of transgenic mice carrying a point mutation in the DNA-binding domain displayed an even more severe phenotype. T-cell leukaemia/lymphoma evolved in >65% of Ikaros$^{plstc/+}$ mice, while in homozygosity the mutation caused foetal mortality with severe anaemia, block of granulocyte differentiation, excessive macrophage formation and impaired lymphopoiesis[82]. A third mutated mouse was developed by Kirstetter et al. inserting, in frame, the LacZ gene in the second exon of *Ikzf1*. This hypomorphic allele produced a very low amount of truncated Ikaros protein (lacking the protein part encoded by exon2). All these mice developed T cell leukaemia/lymphoma in the thymus in an average of 20 weeks[83].

Several teams, driven by these results, investigated the putative role of *IKZF1* in human T malignancies. Surprisingly, *IKZF1* aberrations are rare in human T-ALL. A multi-parameter study of 25 T-ALL investigating the IKAROS status at DNA (by array CGH), RNA (by RQ-PCR) and protein level (by western blot and immunofluorescence) reported only one case with defective IKAROS[84]. Whole genome sequencing (WGS) and transcriptome sequencing identified *IKZF1* deletions/mutations in 9 out of 106 (8%) cases of paediatric early T-cell precursors (ETP) ALL[85].

IKAROS aberrations in leukaemias: from IK6 to the deletions' era

Most of the initial studies that addressed the impact of IKAROS in human leukaemia focused on the expression pattern of *IKZF1* isoforms. An analysis by RT-Q-PCR on 17 bone marrow samples of CML in blast crisis revealed the presence of the dominant negative isoform IK6 in 5 out of 15 samples[86]. The absence of IK6 in chronic phase CML, as well as in normal granulocyte/macrophage and erythrocyte colonies, led to the suggestion of a pathogenic role of IK6 in human haematological malignancies, and in particular, on the progression to a blast crisis in CML[86,87]. By using the same approach, IK6 was detected in 14 out of 41 patients with B-cell ALL[88]. In the following years, studies demonstrated the presence of IK6 in paediatric and adult B-ALL, paediatric AML and more rarely, in T-ALL[87,89–91]. Interestingly, IK6 was more frequently detected in Ph+ paediatric ALL[88,92,93]. Inducing BCR-ABL1 expression in human or murine preB cells caused the appearance of IK6, and treatment with imatinib partially restored the aberrant expression of IK6[94]. In 2008, Iacobucci and colleagues showed the presence of IK6 in 91% of adult Ph+ ALL patients, and in 49% of the entire patient cohort IK6 was the predominant isoform. IK6 correlated with a higher percentage of blast cells at diagnosis (suggesting that expression of IK6 is associated only with blasts), and its percentage was higher in relapsed samples compared to diagnosis, indicating a role of IK6 in resistance to multidrug and TKI chemotherapy[89]. At that time, the production of the IK6 variant was thought to be caused by aberrant splicing, but analysis of the exon splice junction regions failed to reveal recurrent aberrations related to anomalous splicing[89,93,95].

The advent of the comparative genomic hybridization (CGH) technology shed new light on the *IKZF1* status in BCP-ALL. In 2008, Mullighan and colleagues reported various *IKZF1* deletions (*ΔIKZF1*) in 76.2% of paediatric Ph+ BCP-ALL. The deletions were predominantly monoallelic and confined to a subset of *IKZF1* exons, most frequently Δ4-7 exons. The Δ4-7 deletion was reported to be the main cause of IK6 generation, as all patients with IK6 expression carried the Δ4-7 deletion. Moreover, other intragenic deletions, such as Δ3-7 and Δ2-7, were presented when dominant negative isoforms IK9 and IK10 were observed, corroborating the observation that *ΔIKZF1s* are at the basis of dominant negative isoforms in human leukaemias[96]. *ΔIKZF1* can be subdivided in 3 different categories:dominant negative, haploinsufficient, and null deletions. Deletions spanning exons 4 to 7 (Δ4-7) and exons 3 to 7 (Δ3-7) are the most common in paediatric Ph+ ALL, occurring in 30% and 3.5% of patients respectively[97]. The RAG protein very likely causes these deletions, as the breakpoints in introns juxtaposed exons 3, 4 and 8 are

highly conserved and are flanked by recombination signal sequences. Other monosomic intragenic deletions occur in 22% of cases[96]. These deletions, depleting the DNA binding domain, give rise to dominant negative proteins. Monoallelic null deletions gathered focal deletions of exon 2 (containing the ATG start codon) or exon 8, which encode for the dimerization domain, and invariantly result in a reduced level of IKAROS, i.e. haploinsufficiency. Moreover, Chromosome 7 monosomy or large deletions of its short arm were classified as haploinsufficient deletions as well. Finally, biallelic deletions occur in about 13% of BCP ALL. These deletions are frequently null deletions, leading to a complete loss of IKAROS protein in the cell; these are named as null deletions[98]. Of note, some recent studies have revealed the presence of IK6 in the absence of the Δ4-7 deletion in a few cases of BCP ALL, suggesting that aberrant splicing can generate IKAROS dominant negative isoforms in leukaemia, but deletions remain the main cause of IK6 production[99,100].

After 2008, subsequent studies have depicted the occurrence of *ΔIKZF1* in paediatric and adult ALL: *IKZF1* deletions are now known to occur in 70% of Ph+ BCP ALL[96,101], 30% of high-risk paediatric BCP ALL[102], 15% of general B cell ALL[96,103], and in more than 60% of adult CML in blast crisis[86,96]. These high incidences in leukaemias of distinct lineage origin provides strong evidence of a principal role for IKAROS in leukemogenesis.

The leukemogenic role of IKAROS

Despite the link between IKAROS and leukaemia being well established, the mechanisms underlying its leukemogenic effect are still elusive. Studies on transgenic murine models depicted Ikaros as a master regulator of early B lymphocyte development. Ikaros has been shown to negatively regulate pre-BCR signalling[31] and positively regulate the recombinase activating genes *Rag1* and *Rag2*[104]; thus promoting maturation of preB lymphocytes. Furthermore, in preB cells Ikaros binds and suppresses c-Myc expression, guiding cells from a potentially indefinite proliferation state to the resting and maturation stage[105]. Down-regulation of Ikaros, or expression of dominant negative variants, results in a block of differentiation at the early preB stage and a predisposition to leukaemia/lymphoma.

From a clinical point of view, *IKZF1* deletions seem to be associated with treatment resistance to glucocorticoids, leading to a decrease in apoptosis and increased proliferation compared to WT *IKZF1* BPC ALL cells[106].

In order to elucidate the impact of *ΔIKZF1* in ALL, a gene expression study on adult BCP-ALL was set up. From the analysis of 31 *ΔIKZF1* versus 20 *IKZF1* WT patients, several pathways were down-regulated, such as B-cell differentiation, apoptosis and DNA repair,

while JAK-STAT signalling and haematopoietic stem cell affiliated genes were found to be up-regulated[101]. The up-regulation of HSC genes in Ikaros deficient mice was already known, and very recently this observation was corroborated by data from Churchman and colleagues demonstrating the efficacy of retinoic acid compounds in reversing the HSC-like phenotype and increasing the response of murine Ph+ *ΔIKZF1* BCP-ALL cells to TKIs[97].

Clinical impact of ΔIKZF1

Clinical studies in the last decade linked IKAROS aberrations with prognosis in BCP-ALL. The presence of *ΔIKZF1s* in paediatric patients is associated with a higher WBC, older age, and high MRD at day 29, all general markers of poor prognosis. Moreover, *ΔIKZF1s* are significantly more frequent in high risk patients, both stratified by MRD or by other clinical data according to national protocols. In separate cohorts with different treatment strategies IKAROS deletions, both focal and non-focal, confer poor prognosis in terms of overall survival (OS) and EFS, particularly due to an increased cumulative incidence of relapse (CIR) in *ΔIKZF1* patients (Table 1.1)[107–112]. Indeed, *IKZF1* deletions were the only sub microscopic genetic aberration that is detected at diagnosis and preserved at relapses in BPC-ALL, and can predict relapses[112]. Multivariate analysis identified *ΔIKZF1s* as an independent prognostic factor, in respect to gender, age, WBC, MRD and presence of cytogenetic abnormalities[102,113,114]. Of note, all these studies were conducted before the introduction of TKIs in the clinical practice; it would be interesting to investigate if these observations are still valid in the TKI era.

Considering the high percentage of *IKZF1* deletions in paediatric Ph+ BCP-ALL patients, a recent study estimated their impact before and after the TKI introduction in the clinical practice. In the pre TKI era, *ΔIKZF1s* conferred a worse disease free survival (DFS) rate compare to *IKZF1* WT patients, mainly because of a higher incidence of relapse. In the imatinib era, *IKZF1* deleted patients showed a trend of inferior DFS rate, without reaching significance. Interestingly, when the post-TKI group was subdivided in accordance with the early clinical response, *IKZF1* deletions were predicative of a worse DFS rate in good-risk stratified patients[103].

	IK WT	IK del	p value	Study
WBC				
(mean)	8.1	20.3	NR	Öfverholm et al. 2013
(mean)	8.8	25.5	0.009	Olsson et al. 2014
(>10x(10^{10}/L))	6%	18%	0.02	Yamashita et al. 2013
(>10x(10^{10}/L))	11.1%	19%	0.01	Dörge et al. 2013
(>10x(10^{10}/L))	19.0%	42.0%	0.06	van der Veer et al. 2014
AGE (>10 years)				
	15%	50%	<0.001	Yamashita et al. 2013
	22%	53%	0.009	Asai et al. 2013
	13.8%	27.8%	0.02	Palmi et al. 2013
MRD				
	24%	6.6%	0.001	Mullighan et al. 2009
MRD high risk stratification				
	0.7%	7.9%	0.001	Palmi et al. 2013
	5.2%	17.9%	0.01	Dörge et al. 2013
HR stratification				
	30%	55%	0.02	Yamashita et al. 2013
	18%	46%	<0.001	Olsson et al. 2014
	16.9%	25%	0.03	Dörge et al. 2013
EFS				
	73%*	25%*	<0.001	Mullighan et al. 2009
	85%*	69%*	<0.001	Dörge et al. 2013
	85%†	68%†	0.04	Yamashita et al. 2013
	89%*	63% *	0.001	Asai et al. 2013
	85%*	70%*	0.007	Palmi et al. 2013
	80%‡	45%‡	0.001	Olsson et al. 2014
CIR				
	14%*	55%*	<0.001	Mullighan et al. 2009
	11%§	61%§	<0.001	Kuiper et al. 2010
	10%*	21%*	0.001	Dörge et al. 2013
	13%*	24%*	0.049	Palmi et al. 2013

Table 1.1: Clinical features of different cohorts of paediatric patients in relation to IKZF1 status. Adapted from Olsson & Johansson 2015. EFS, event free survival; CIR, cumulative incidence of relapse; MRD, minimal residual disease; HR, high risk; NR, not reported; del, deleted; WT, wild type; WBC, white blood cell count. * 5 years probability; † 4 years probability; ‡ 10 years probability; § 8 years probability

ΔIKZF1s are repeatedly reported to identify patients with a higher incidence of relapse and, overall, a lower incidence of EFS in different BCP-ALL sub-categories, including Ph+ ALL and the so called "B-other" patients that do not show any cytogenetic aberration at diagnosis[102,113]. For those reasons, some groups proposed to include *IKZF1* status screening in clinical routine as a predictor of treatment failure in paediatric ALL. In this regard, some groups published results on the integration of *IKZF1* status and MRD in paediatric patients classified as B-others and normally stratified as intermediate risk in clinical protocols[115,116]. In all these studies, *IKZF1* was shown as an independent predictor of relapse, and its integration with MRD allows the prediction of 79% of relapses, more than based on MRD data alone[117].

IKZF1 SNPs and predisposition to leukaemia

A first genome-wide association study (GWAS) on 907 British paediatric ALL cases compared to 2398 controls identified 10 SNPs mapping at *IKZF1, ARID5B* and *CEBPE* loci that were significantly enriched in the ALL population[118]. In particular, *IKZF1* rs4132601 SNP (that maps to the 3' region) showed the strongest correlation with ALL and its presence correlated with a significant reduction of *IKZF1* mRNA. The same SNP was subsequently identified in another GWA study on a French cohort(441 ALL samples compared to 570 controls)[119], and was confirmed as a risk variant in a German-British validation study[120]. Interestingly, a validation study of the impact of rs4132601 in a Chinese paediatric ALL cohort (570 ALL cases compared to 673 controls) did not find any significant correlation. The authors underlined that, in the European and in the Chinese populations, the SNP is present in different linkage-disequilibrium blocks, suggesting that this could be the cause of the different results obtained. Rs4132601 positively correlates with the age at diagnosis in a Polish study on 508 paediatric ALL patients, as homozygous carriers of the variant are significantly younger at the time of diagnosis than heterozygous and non-carriers[121]. The same SNP was shown to inversely correlate with AML diagnosis in a French cohort[122].

Another SNP, the rs11978267, was originally described to distinguish T-ALL from B-other and B-hyperdiploid ALL in an European cohort of paediatric ALL, but the result was not confirmed in the validation cohort[123]. Interestingly, rs11978267 was then identified in the children oncology group's (COG) paediatric ALL cohort GWA study[124] as positively correlated with B-ALL and infant ALL[125].

De novo IKZF1-germline mutation: a case report

An *IKZF1* germline mutation was described in a newborn child affected by severe haematological condition soon after birth, with a severe anaemia and a general pancytopenia. The bone marrow aspiration at five days of age revealed a marked hypoplasia, with few erythroid precursors, absence of myeloid precursors, and abundance of lymphocytes. Immunophenotyping highlighted the absence of B- and NK cells, and an abundance of T cells with a normal CD4:CD8 ratio, skewed to the TCR-αβ expression. Because of the severe pancytopenia, the newborn underwent an allogeneic bone marrow transplant following a reduced intensity myeloablative treatment and followed by a cyclosporine plus methotrexate treatment to prevent graft versus host disease. Even if the neutrophil count increased after the bone marrow transplant, 40 days after the clinical condition of the patient kept deteriorating and died of multiorgan failure. As the bone marrow analysis revealed a phenotype similar to *Ikzf1* knock-out mice models, the *IKZF1* status was evaluated by Sanger sequencing, identifying a heterozygous missense point mutation (p.Tyr210Cys) within the zinc finger 4 coding sequence. Immunofluorescence analysis performed on the newborn's peripheral blood mononuclear cells (PBMC) using an α-IKAROS antibody revealed a diffuse nuclear staining of the protein, indicating that the harboured-mutation caused a DNA-binding affinity impairment. Both child's parents were negative for the mutation, pointing out a *de novo* germline origin of the mutation that arose in the parent's gametes.

Post-translational modifications of IKAROS and leukaemia

IKAROS activity is controlled by several mechanisms, and could be impaired in leukemic cells even in the absence of genetic aberrations. The role of post translational modifications on IKAROS tumour suppressor activity has emerged in the last few years. Gene expression analysis of paediatric B-ALL cases expressing low levels of SKY or BTK kinases displayed deregulation of well-known IKAROS target genes, such as *MEF2C*, *RAG1* and *FLT3*[14,15]. The inhibition of these two kinases in B-ALL results in down-regulation of IKAROS activity and its sequestration in the cytoplasm. CK2 kinase, another regulator of IKAROS, has been shown to be up-regulated in high-risk paediatric B-ALL. The up-regulation of CK2 activity leads to inactivation of IKAROS and activation of cell-cycle related genes and the PI3K pathway. CK2 inhibition restored IKAROS activity in high-risk B-ALL cells heterozygous for *ΔIKZF1*, promoting cell-cycle arrest. The efficacy of pharmacological inhibition of CK2 was demonstrated in human leukemic xenograft mice,

where the subsequent restoration of IKAROS activity led to a reduction of blast cell proliferation and a prolonged survival of mice[126].

1.2.4 IKAROS IN OTHER MALIGNANCES

Genome-wide association studies have linked IKZF1 to systemic lupus erythematosus (SLE), a complex autoimmune disease characterized by auto-antibody production and a complex phenotype. IKAROS SNPs rs10911362 and rs2362293, and the upstream SNP rs4917014 have been shown to confer susceptibility to SLE, with a higher risk of nephritis and decreased risk of facial rash[127–129]. IKAROS mRNA is significantly lower in SLE peripheral blood mononuclear cells (PBMC) compared to healthy controls, potentially due to the SNPs, even if a clear correlation is lacking[130]. The lower amount of IKAROS leads to an impairment of interferon signalling and the STAT4 pathway, well known pathways linked to SLE[127,128].

The rs10272724 (T>C) polymorphism correlates with a decreased risk of type I diabetes, another auto-immune disease where auto-antibodies trigger the pancreatic β-cells responsible for insulin production. The T>C allele was also protected in familiar cases of type I diabetes, even if the mechanism is unclear, as the protective allele does not result in expression differences of IKZF1 alleles[131].

The dominant negative isoform IK6 was detected in 36% of pituitary adenomas[132]. The same group previously demonstrated the importance of IKAROS in the regulation of the growth hormone (GH) and prostaglandin production as demonstrated by Ikaros null mice studies, and IKAROS is necessary for the correct development of the pituitary gland[133]. The presence of IK6 mediated cell growth and protection from apoptosis, mediated by up-regulation of the anti-apoptotic protein Bcl-XL[134], and by promoting the expression of the tumorigenic isoform FGFR4, that is transforming both in vitro and in vivo and causes pituitary tumours in mice[135–137].

IKAROS is down-regulated in over 60% of colorectal cancers by epigenetic promoter hypermethylation[138]. Deregulation of IKAROS target genes connected with tumour progression were demonstrated in colorectal primary tumours by its reintroduction in colorectal cells followed by ChIP-ChIP and RQ-PCR analysis.

REFERENCES

1. Olsson L, Johansson B. Ikaros and leukaemia. Br J Haematol. 2015 May;169(4):479–91.

2. Cobb BS, Morales-Alcelay S, Kleiger G, Brown KE, Fisher AG, Smale ST. Targeting of Ikaros to pericentromeric heterochromatin by direct DNA binding. Genes Dev. 2000 Sep 1;14(17):2146–60.

3. Laity JH, Lee BM, Wright PE. Zinc finger proteins: new insights into structural and functional diversity. Curr Opin Struct Biol. 2001 Feb;11(1):39–46.

4. Payne MA. Zinc finger structure-function in Ikaros Marvin A Payne. World J Biol Chem. 2011 Jun 26;2(6):161–6.

5. Ernst P, Hahm K, Smale ST. Both LyF-1 and an Ets protein interact with a critical promoter element in the murine terminal transferase gene. Mol Cell Biol. 1993 May;13(5):2982–92.

6. Molnár A, Georgopoulos K. The Ikaros gene encodes a family of functionally diverse zinc finger DNA-binding proteins. Mol Cell Biol. 1994 Dec;14(12):8292–303.

7. Schjerven H, McLaughlin J, Arenzana TL, Frietze S, Cheng D, Wadsworth SE, et al. Selective regulation of lymphopoiesis and leukemogenesis by individual zinc fingers of Ikaros. Nat Immunol. 2013 Oct;14(10):1073–83.

8. Sun L, Liu A, Georgopoulos K. Zinc finger-mediated protein interactions modulate Ikaros activity, a molecular control of lymphocyte development. EMBO J. 1996 Oct 1;15(19):5358–69.

9. Payne KJ, Huang G, Sahakian E, Zhu JY, Barteneva NS, Barsky LW, et al. Ikaros isoform x is selectively expressed in myeloid differentiation. J Immunol. 2003 Mar 15;170(6):3091–8.

10. Song C, Li Z, Erbe AK, Savic A, Dovat S. Regulation of Ikaros function by casein kinase 2 and protein phosphatase 1. World J Biol Chem. 2011 Jun 26;2(6):126–31.

11. Gurel Z, Ronni T, Ho S, Kuchar J, Payne KJ, Turk CW, et al. Recruitment of ikaros to pericentromeric heterochromatin is regulated by phosphorylation. J Biol Chem. 2008 Mar 28;283(13):8291–300.

12. Gómez-del Arco P, Maki K, Georgopoulos K. Phosphorylation controls Ikaros's ability to negatively regulate the G(1)-S transition. Mol Cell Biol. 2004 Apr;24(7):2797–807.

13. Popescu M, Gurel Z, Ronni T, Song C, Hung KY, Payne KJ, et al. Ikaros stability and pericentromeric localization are regulated by protein phosphatase 1. J Biol Chem. 2009 May 15;284(20):13869–80.

14. Ma H, Qazi S, Ozer Z, Zhang J, Ishkhanian R, Uckun FM. Regulatory phosphorylation of Ikaros by Bruton's tyrosine kinase. PLoS One. 2013 Jan;8(8):e71302.

15. Uckun FM, Ma H, Zhang J, Ozer Z, Dovat S, Mao C, et al. Serine phosphorylation by SYK is critical for nuclear localization and transcription factor function of Ikaros. Proc Natl Acad Sci U S A. 2012 Oct 30;109(44):18072–7.

16. John LB, Ward AC. The Ikaros gene family: transcriptional regulators of hematopoiesis and immunity. Mol Immunol. 2011 May;48(9-10):1272–8.

17. Perdomo J, Holmes M, Chong B, Crossley M. Eos and pegasus, two members of the Ikaros family of proteins with distinct DNA binding activities. J Biol Chem. 2000 Dec 8;275(49):38347–54.

18. Morgan B, Sun L, Avitahl N, Andrikopoulos K, Ikeda T, Gonzales E, et al. Aiolos, a lymphoid restricted transcription factor that interacts with Ikaros to regulate lymphocyte differentiation. EMBO J. 1997 Apr 15;16(8):2004–13.

19. Wang JH, Avitahl N, Cariappa A, Friedrich C, Ikeda T, Renold A, et al. Aiolos regulates B cell activation and maturation to effector state. Immunity. 1998 Oct;9(4):543–53.

20. Rebollo A, Ayllón V, Fleischer A, Martínez CA, Zaballos A. The association of Aiolos transcription factor and Bcl-xL is involved in the control of apoptosis. J Immunol. 2001 Dec 1;167(11):6366–73.

21. Caballero R, Setien F, Lopez-Serra L, Boix-Chornet M, Fraga MF, Ropero S, et al. Combinatorial effects of splice variants modulate function of Aiolos. J Cell Sci. 2007 Aug 1;120(Pt 15):2619–30.

22. Hahm K, Cobb BS, McCarty AS, Brown KE, Klug CA, Lee R, et al. Helios, a T cell-restricted Ikaros family member that quantitatively associates with Ikaros at centromeric heterochromatin. Genes Dev. 1998 Mar 15;12(6):782–96.

23. Sugita K, Hanakawa S, Honda T, Kondoh G, Miyachi Y, Kabashima K, et al. Generation of Helios reporter mice and an evaluation of the suppressive capacity of Helios(+) regulatory T cells in vitro. Exp Dermatol. 2015 Jul;24(7):554–6.

24. Lo K, Landau NR, Smale ST. LyF-1, a transcriptional regulator that interacts with a novel class of promoters for lymphocyte-specific genes. Mol Cell Biol. 1991 Oct;11(10):5229–43.

25. Hahm K, Ernst P, Lo K, Kim GS, Turck C, Smale ST. The lymphoid transcription factor LyF-1 is encoded by specific, alternatively spliced mRNAs derived from the Ikaros gene. Mol Cell Biol. 1994 Nov;14(11):7111–23.

26. Brown KE, Guest SS, Smale ST, Hahm K, Merkenschlager M, Fisher AG. Association of transcriptionally silent genes with Ikaros complexes at centromeric heterochromatin. Cell. 1997 Dec 12;91(6):845–54.

27. Brown KE, Baxter J, Graf D, Merkenschlager M, Fisher AG. Dynamic repositioning of genes in the nucleus of lymphocytes preparing for cell division. Mol Cell. 1999 Feb;3(2):207–17.

28. Koipally J, Heller EJ, Seavitt JR, Georgopoulos K. Unconventional potentiation of gene expression by Ikaros. J Biol Chem. 2002 Apr 12;277(15):13007–15.

29. Li Z, Song C, Ouyang H, Lai L, Payne KJ, Dovat S. Cell cycle-specific function of Ikaros in human leukemia. Pediatr Blood Cancer. 2012 Jul 15;59(1):69–76.

30. Trinh LA, Ferrini R, Cobb BS, Weinmann AS, Hahm K, Ernst P, et al. Down-regulation of TDT transcription in CD4(+)CD8(+) thymocytes by Ikaros proteins in direct competition with an Ets activator. Genes Dev. 2001 Jul 15;15(14):1817–32.

31. Thompson EC, Cobb BS, Sabbattini P, Meixlsperger S, Parelho V, Liberg D, et al. Ikaros DNA-binding proteins as integral components of B cell developmental-stage-specific regulatory circuits. Immunity. 2007 Mar;26(3):335–44.

32. Sabbattini P, Lundgren M, Georgiou A, Chow C, Warnes G, Dillon N. Binding of Ikaros to the lambda5 promoter silences transcription through a mechanism that does not require heterochromatin formation. EMBO J. 2001 Jun 1;20(11):2812–22.

33. Kim J, Sif S, Jones B, Jackson A, Koipally J, Heller E, et al. Ikaros DNA-binding proteins direct formation of chromatin remodeling complexes in lymphocytes. Immunity. 1999 Mar;10(3):345–55.

34. Koipally J, Renold A, Kim J, Georgopoulos K. Repression by Ikaros and Aiolos is

mediated through histone deacetylase complexes. EMBO J. 1999 Jun 1;18(11):3090–100.

35. Naito T, Gómez-Del Arco P, Williams CJ, Georgopoulos K. Antagonistic interactions between Ikaros and the chromatin remodeler Mi-2beta determine silencer activity and Cd4 gene expression. Immunity. 2007 Nov;27(5):723–34.

36. Koipally J, Georgopoulos K. Ikaros interactions with CtBP reveal a repression mechanism that is independent of histone deacetylase activity. J Biol Chem. 2000 Jun 30;275(26):19594–602.

37. Koipally J, Georgopoulos K. A molecular dissection of the repression circuitry of Ikaros. J Biol Chem. 2002 Aug 2;277(31):27697–705.

38. Payne KJ, Dovat S. Ikaros and tumor suppression in acute lymphoblastic leukemia. Crit Rev Oncog. 2011 Jan;16(1-2):3–12.

39. Zhang J, Jackson AF, Naito T, Dose M, Seavitt J, Liu F, et al. Harnessing of the nucleosome-remodeling-deacetylase complex controls lymphocyte development and prevents leukemogenesis. Nat Immunol. 2012 Jan;13(1):86–94.

40. Bottardi S, Mavoungou L, Milot E. IKAROS: a multifunctional regulator of the polymerase II transcription cycle. Trends Genet. 2015 Jul 3;

41. Busslinger M. Transcriptional control of early B cell development. Annu Rev Immunol. 2004 Jan;22:55–79.

42. Cedar H, Bergman Y. Epigenetics of haematopoietic cell development. Nat Rev Immunol. 2011 Jul;11(7):478–88.

43. Morrison SJ, Weissman IL. The long-term repopulating subset of hematopoietic stem cells is deterministic and isolatable by phenotype. Immunity. 1994 Nov;1(8):661–73.

44. Adolfsson J, Månsson R, Buza-Vidas N, Hultquist A, Liuba K, Jensen CT, et al. Identification of Flt3+ lympho-myeloid stem cells lacking erythro-megakaryocytic potential a revised road map for adult blood lineage commitment. Cell. 2005 Apr 22;121(2):295–306.

45. Singh H, Medina KL, Pongubala JMR. Contingent gene regulatory networks and B cell fate specification. Proc Natl Acad Sci U S A. 2005 Apr 5;102(14):4949–53.

46. Zhang L, Reynolds TL, Shan X, Desiderio S. Coupling of V(D)J recombination to the cell cycle suppresses genomic instability and lymphoid tumorigenesis. Immunity. 2011 Feb 25;34(2):163–74.

47. Herzog S, Reth M, Jumaa H. Regulation of B-cell proliferation and differentiation by pre-B-cell receptor signalling. Nat Rev Immunol. 2009 Mar;9(3):195–205.

48. Molnár A, Wu P, Largespada DA, Vortkamp A, Scherer S, Copeland NG, et al. The Ikaros gene encodes a family of lymphocyte-restricted zinc finger DNA binding proteins, highly conserved in human and mouse. J Immunol. 1996 Jan 15;156(2):585–92.

49. Wang JH, Nichogiannopoulou A, Wu L, Sun L, Sharpe AH, Bigby M, et al. Selective defects in the development of the fetal and adult lymphoid system in mice with an Ikaros null mutation. Immunity. 1996 Dec;5(6):537–49.

50. Georgopoulos K, Bigby M, Wang JH, Molnar A, Wu P, Winandy S, et al. The Ikaros gene is required for the development of all lymphoid lineages. Cell. 1994 Oct 7;79(1):143–56.

51. Nichogiannopoulou A, Trevisan M, Neben S, Friedrich C, Georgopoulos K. Defects in hemopoietic stem cell activity in Ikaros mutant mice. J Exp Med. 1999 Nov 1;190(9):1201–14.

52. Winandy S, Wu P, Georgopoulos K. A dominant mutation in the Ikaros gene leads to rapid development of leukemia and lymphoma. Cell. 1995 Oct 20;83(2):289–99.

53. Kelley CM, Ikeda T, Koipally J, Avitahl N, Wu L, Georgopoulos K, et al. Helios, a novel dimerization partner of Ikaros expressed in the earliest hematopoietic progenitors. Curr Biol. 1998 Apr 23;8(9):508–15.

54. Yoshida T, Ng SY-M, Zuniga-Pflucker JC, Georgopoulos K. Early hematopoietic lineage restrictions directed by Ikaros. Nat Immunol. 2006 Apr;7(4):382–91.

55. Ng SY-M, Yoshida T, Zhang J, Georgopoulos K. Genome-wide lineage-specific transcriptional networks underscore Ikaros-dependent lymphoid priming in hematopoietic stem cells. Immunity. 2009 Apr 17;30(4):493–507.

56. Woo JS, Alberti MO, Tirado CA. Childhood B-acute lymphoblastic leukemia: a genetic update. Exp Hematol Oncol. 2014 Jan;3:16.

57. Wiemels JL, Cazzaniga G, Daniotti M, Eden OB, Addison GM, Masera G, et al. Prenatal origin of acute lymphoblastic leukaemia in children. Lancet (London,

England). 1999 Oct 30;354(9189):1499–503.

58. Cazzaniga G, van Delft FW, Lo Nigro L, Ford AM, Score J, Iacobucci I, et al. Developmental origins and impact of BCR-ABL1 fusion and IKZF1 deletions in monozygotic twins with Ph+ acute lymphoblastic leukemia. Blood. 2011 Nov 17;118(20):5559–64.

59. Pui C-H, Robison LL, Look AT. Acute lymphoblastic leukaemia. Lancet. 2008 Mar 22;371(9617):1030–43.

60. Inaba H, Greaves M, Mullighan CG. Acute lymphoblastic leukaemia. Lancet. 2013 Jun 1;381(9881):1943–55.

61. Ghazavi F, Lammens T, Van Roy N, Poppe B, Speleman F, Benoit Y, et al. Molecular basis and clinical significance of genetic aberrations in B-cell precursor acute lymphoblastic leukemia. Exp Hematol. 2015 Aug;43(8):640–53.

62. Roberts KG, Mullighan CG. Genomics in acute lymphoblastic leukaemia: insights and treatment implications. Nat Rev Clin Oncol. 2015 Mar 17;12(6):344–57.

63. Borowitz MJ, Devidas M, Hunger SP, Bowman WP, Carroll AJ, Carroll WL, et al. Clinical significance of minimal residual disease in childhood acute lymphoblastic leukemia and its relationship to other prognostic factors: a Children's Oncology Group study. Blood. 2008 Jun 15;111(12):5477–85.

64. Cooper SL, Brown PA. Treatment of pediatric acute lymphoblastic leukemia. Pediatr Clin North Am. 2015 Feb;62(1):61–73.

65. NOWELL PC, HUNGERFORD DA. Chromosome studies on normal and leukemic human leukocytes. J Natl Cancer Inst. 1960 Jul;25:85–109.

66. Rowley JD. Letter: A new consistent chromosomal abnormality in chronic myelogenous leukaemia identified by quinacrine fluorescence and Giemsa staining. Nature. 1973 Jun 1;243(5405):290–3.

67. Franz WM, Berger P, Wang JY. Deletion of an N-terminal regulatory domain of the c-abl tyrosine kinase activates its oncogenic potential. EMBO J. 1989 Jan;8(1):137–47.

68. Pendergast AM, Muller AJ, Havlik MH, Maru Y, Witte ON. BCR sequences essential for transformation by the BCR-ABL oncogene bind to the ABL SH2 regulatory domain in a non-phosphotyrosine-dependent manner. Cell. 1991 Jul 12;66(1):161–71.

69. Cilloni D, Saglio G. Molecular Pathways: BCR-ABL. Clin Cancer Res. 2011 Dec 8;18(4):930–7.

70. Aricò M, Valsecchi MG, Camitta B, Schrappe M, Chessells J, Baruchel A, et al. Outcome of treatment in children with Philadelphia chromosome-positive acute lymphoblastic leukemia. N Engl J Med. 2000 Apr 6;342(14):998–1006.

71. Arico M, Schrappe M, Hunger SP, Carroll WL, Conter V, Galimberti S, et al. Clinical Outcome of Children With Newly Diagnosed Philadelphia Chromosome-Positive Acute Lymphoblastic Leukemia Treated Between 1995 and 2005. J Clin Oncol. 2010 Sep 27;28(31):4755–61.

72. Druker BJ, Tamura S, Buchdunger E, Ohno S, Segal GM, Fanning S, et al. Effects of a selective inhibitor of the Abl tyrosine kinase on the growth of Bcr–Abl positive cells. Nat Med. 1996 May;2(5):561–6.

73. Druker BJ, Guilhot F, O'Brien SG, Gathmann I, Kantarjian H, Gattermann N, et al. Five-year follow-up of patients receiving imatinib for chronic myeloid leukemia. N Engl J Med. 2006 Dec 7;355(23):2408–17.

74. Schultz KR, Bowman WP, Aledo A, Slayton WB, Sather H, Devidas M, et al. Improved Early Event-Free Survival With Imatinib in Philadelphia Chromosome-Positive Acute Lymphoblastic Leukemia: A Children's Oncology Group Study. J Clin Oncol. 2009 Oct 5;27(31):5175–81.

75. Schultz KR, Carroll A, Heerema NA, Bowman WP, Aledo A, Slayton WB, et al. Long-term follow-up of imatinib in pediatric Philadelphia chromosome-positive acute lymphoblastic leukemia: Children's Oncology Group study AALL0031. Leukemia. 2014 Jul;28(7):1467–71.

76. Biondi A, Schrappe M, De Lorenzo P, Castor A, Lucchini G, Gandemer V, et al. Imatinib after induction for treatment of children and adolescents with Philadelphia-chromosome-positive acute lymphoblastic leukaemia (EsPhALL): a randomised, open-label, intergroup study. Lancet Oncol. 2012 Sep;13(9):936–45.

77. Bernt KM, Hunger SP. Current concepts in pediatric Philadelphia chromosome-positive acute lymphoblastic leukemia. Front Oncol. 2014 Jan;4:54.

78. Kantarjian HM, Shah NP, Cortes JE, Baccarani M, Agarwal MB, Undurraga MS, et al. Dasatinib or imatinib in newly diagnosed chronic-phase chronic myeloid leukemia: 2-year follow-up from a randomized phase 3 trial (DASISION). Blood. 2012 Feb 2;119(5):1123–9.

79. Saglio G, Kim D-W, Issaragrisil S, le Coutre P, Etienne G, Lobo C, et al. Nilotinib versus imatinib for newly diagnosed chronic myeloid leukemia. N Engl J Med. 2010 Jun 17;362(24):2251–9.

80. Chang BH, Willis SG, Stork L, Hunger SP, Carroll WL, Camitta BM, et al. Imatinib resistant BCR-ABL1 mutations at relapse in children with Ph+ ALL: a Children's Oncology Group (COG) study. Br J Haematol. 2012 May;157(4):507–10.

81. O'Hare T. In vitro Activity of Bcr-Abl Inhibitors AMN107 and BMS-354825 against Clinically Relevant Imatinib-Resistant Abl Kinase Domain Mutants. Cancer Res. 2005 Jun 1;65(11):4500–5.

82. Papathanasiou P, Perkins AC, Cobb BS, Ferrini R, Sridharan R, Hoyne GF, et al. Widespread Failure of Hematolymphoid Differentiation Caused by a Recessive Niche-Filling Allele of the Ikaros Transcription Factor. Immunity. Elsevier; 2003 Jul 7;19(1):131–44.

83. Kirstetter P, Thomas M, Dierich A, Kastner P, Chan S. Ikaros is critical for B cell differentiation and function. Eur J Immunol. 2002 Mar;32(3):720–30.

84. Marçais A, Jeannet R, Hernandez L, Soulier J, Sigaux F, Chan S, et al. Genetic inactivation of Ikaros is a rare event in human T-ALL. Leuk Res. 2010 Apr;34(4):426–9.

85. Zhang J, Ding L, Holmfeldt L, Wu G, Heatley SL, Payne-Turner D, et al. The genetic basis of early T-cell precursor acute lymphoblastic leukaemia. Nature. Nature Publishing Group, a division of Macmillan Publishers Limited. All Rights Reserved.; 2012 Jan 12;481(7380):157–63.

86. Nakayama H, Ishimaru F, Avitahl N, Sezaki N, Fujii N, Nakase K, et al. Decreases in Ikaros activity correlate with blast crisis in patients with chronic myelogenous leukemia. Cancer Res. 1999 Aug 15;59(16):3931–4.

87. Nakayama H, Ishimaru F, Katayama Y, Nakase K, Sezaki N, Takenaka K, et al. Ikaros expression in human hematopoietic lineages. Exp Hematol. 2000 Nov;28(11):1232–8.

88. Nakase K, Ishimaru F, Avitahl N, Dansako H, Matsuo K, Fujii K, et al. Dominant negative isoform of the Ikaros gene in patients with adult B-cell acute lymphoblastic leukemia. Cancer Res. 2000 Aug 1;60(15):4062–5.

89. Iacobucci I, Lonetti A, Messa F, Cilloni D, Arruga F, Ottaviani E, et al. Expression of spliced oncogenic Ikaros isoforms in Philadelphia-positive acute lymphoblastic leukemia patients treated with tyrosine kinase inhibitors: implications for a new

mechanism of resistance. Blood. 2008 Nov 1;112(9):3847–55.

90. Nishii K, Katayama N, Miwa H, Shikami M, Usui E, Masuya M, et al. Non-DNA-binding Ikaros isoform gene expressed in adult B-precursor acute lymphoblastic leukemia. Leukemia. 2002 Jul 1;16(7):1285–92.

91. Meleshko AN, Movchan L V., Belevtsev M V., Savitskaja T V. Relative expression of different Ikaros isoforms in childhood acute leukemia. Blood Cells, Mol Dis. 2008 Nov;41(3):278–83.

92. Klein F, Feldhahn N, Harder L, Wang H, Wartenberg M, Hofmann W-K, et al. The BCR-ABL1 kinase bypasses selection for the expression of a pre-B cell receptor in pre-B acute lymphoblastic leukemia cells. J Exp Med. 2004 Mar 1;199(5):673–85.

93. Olivero S, Maroc C, Beillard E, Gabert J, Nietfeld W, Chabannon C, et al. Detection of different Ikaros isoforms in human leukaemias using real-time quantitative polymerase chain reaction. Br J Haematol. 2000 Sep;110(4):826–30.

94. Klein F, Feldhahn N, Herzog S, Sprangers M, Mooster JL, Jumaa H, et al. BCR-ABL1 induces aberrant splicing of IKAROS and lineage infidelity in pre-B lymphoblastic leukemia cells. Oncogene. 2006 Feb 16;25(7):1118–24.

95. Tonnelle C, Imbert M-C, Sainty D, Granjeaud S, N'Guyen C, Chabannon C. Overexpression of dominant-negative Ikaros 6 protein is restricted to a subset of B common adult acute lymphoblastic leukemias that express high levels of the CD34 antigen. Hematol J. 2003 Jan;4(2):104–9.

96. Mullighan CG, Miller CB, Radtke I, Phillips LA, Dalton J, Ma J, et al. BCR-ABL1 lymphoblastic leukaemia is characterized by the deletion of Ikaros. Nature. 2008 May 1;453(7191):110–4.

97. Churchman ML, Low J, Qu C, Paietta EM, Kasper LH, Chang Y, et al. Efficacy of Retinoids in IKZF1-Mutated BCR-ABL1 Acute Lymphoblastic Leukemia. Cancer Cell. 2015 Aug 26;28(3):343–56.

98. Dupuis A, Gaub MP, Legrain M, Drenou B, Mauvieux L, Lutz P, et al. Biclonal and biallelic deletions occur in 20% of B-ALL cases with IKZF1 mutations. Leukemia. 2013 Feb;27(2):503–7.

99. Tokunaga K, Yamaguchi S, Iwanaga E, Nanri T, Shimomura T, Suzushima H, et al. High frequency of IKZF1 genetic alterations in adult patients with B-cell acute lymphoblastic leukemia. Eur J Haematol. 2013 Sep 7;91(3):201–8.

100. Volejnikova J, Mejstrikova E, Dörge P, Meissner B, Zimmermannova O, Svojgr K, et al. Ikaros (IKZF1) alterations and minimal residual disease at day 15 assessed by flow cytometry predict prognosis of childhood BCR/ABL-negative acute lymphoblastic leukemia. Pediatr Blood Cancer. 2013 Mar;60(3):420–7.

101. Iacobucci I, Iraci N, Messina M, Lonetti A, Chiaretti S, Valli E, et al. IKAROS deletions dictate a unique gene expression signature in patients with adult B-cell acute lymphoblastic leukemia. PLoS One. 2012 Jan;7(7):e40934.

102. Mullighan CG, Su X, Zhang J, Radtke I, Phillips LAA, Miller CB, et al. Deletion of IKZF1 and prognosis in acute lymphoblastic leukemia. N Engl J Med. 2009 Jan 29;360(5):470–80.

103. van der Veer A, Waanders E, Pieters R, Willemse ME, Van Reijmersdal S V, Russell LJ, et al. Independent prognostic value of BCR-ABL1-like signature and IKZF1 deletion, but not high CRLF2 expression, in children with B-cell precursor ALL. Blood. American Society of Hematology; 2013 Oct 10;122(15):2622–9.

104. Reynaud D, A Demarco I, L Reddy K, Schjerven H, Bertolino E, Chen Z, et al. Regulation of B cell fate commitment and immunoglobulin heavy-chain gene rearrangements by Ikaros. Nat Immunol. 2008 Jun 22;9(8):927–36.

105. Ma S, Pathak S, Mandal M, Trinh L, Clark MR, Lu R. Ikaros and Aiolos inhibit pre-B-cell proliferation by directly suppressing c-Myc expression. Mol Cell Biol. 2010 Sep;30(17):4149–58.

106. Ruiz A, Jiang J, Kempski H, Brady HJM. Overexpression of the Ikaros 6 isoform is restricted to t(4;11) acute lymphoblastic leukaemia in children and infants and has a role in B-cell survival. Br J Haematol. 2004 Apr;125(1):31–7.

107. Ofverholm I, Tran AN, Heyman M, Zachariadis V, Nordenskjöld M, Nordgren A, et al. Impact of IKZF1 deletions and PAX5 amplifications in pediatric B-cell precursor ALL treated according to NOPHO protocols. Leukemia. 2013 Sep;27(9):1936–9.

108. Olsson L, Castor A, Behrendtz M, Biloglav A, Forestier E, Paulsson K, et al. Deletions of IKZF1 and SPRED1 are associated with poor prognosis in a population-based series of pediatric B-cell precursor acute lymphoblastic leukemia diagnosed between 1992 and 2011. Leukemia. 2013 Jul 4;28(2):302–10.

109. Yamashita Y, Shimada A, Yamada T, Yamaji K, Hori T, Tsurusawa M, et al. IKZF 1 and CRLF 2 gene alterations correlate with poor prognosis in Japanese BCR - ABL 1 -negative high-risk B-cell precursor acute lymphoblastic leukemia. Pediatr Blood Cancer. 2013 Oct 27;60(10):1587–92.

110. Asai D, Imamura T, Suenobu S, Saito A, Hasegawa D, Deguchi T, et al. IKZF1 deletion is associated with a poor outcome in pediatric B-cell precursor acute lymphoblastic leukemia in Japan. Cancer Med. 2013 Jun;2(3):412–9.

111. Palmi C, Valsecchi MG, Longinotti G, Silvestri D, Carrino V, Conter V, et al. What is the relevance of Ikaros gene deletions as a prognostic marker in pediatric Philadelphia-negative B-cell precursor acute lymphoblastic leukemia? Haematologica. 2013 Aug;98(8):1226–31.

112. Kuiper RP, Waanders E, van der Velden VHJ, van Reijmersdal S V, Venkatachalam R, Scheijen B, et al. IKZF1 deletions predict relapse in uniformly treated pediatric precursor B-ALL. Leukemia. 2010 Jul;24(7):1258–64.

113. Den Boer ML, van Slegtenhorst M, De Menezes RX, Cheok MH, Buijs-Gladdines JGCAM, Peters STCJM, et al. A subtype of childhood acute lymphoblastic leukaemia with poor treatment outcome: a genome-wide classification study. Lancet Oncol. 2009 Feb;10(2):125–34.

114. Dörge P, Meissner B, Zimmermann M, Möricke A, Schrauder A, Bouquin J-P, et al. IKZF1 deletion is an independent predictor of outcome in pediatric acute lymphoblastic leukemia treated according to the ALL-BFM 2000 protocol. Haematologica. 2013 Mar;98(3):428–32.

115. Venn NC, van der Velden VHJ, de Bie M, Waanders E, Giles JE, Law T, et al. Highly sensitive MRD tests for ALL based on the IKZF1 Δ3–6 microdeletion. Leukemia. 2011 Dec 9;26(6):1414–6.

116. Caye A, Beldjord K, Mass-Malo K, Drunat S, Soulier J, Gandemer V, et al. Breakpoint-specific multiplex polymerase chain reaction allows the detection of IKZF1 intragenic deletions and minimal residual disease monitoring in B-cell precursor acute lymphoblastic leukemia. Haematologica. 2012 Oct 12;98(4):597–601.

117. Waanders E, van der Velden VHJ, van der Schoot CE, van Leeuwen FN, van Reijmersdal S V, de Haas V, et al. Integrated use of minimal residual disease classification and IKZF1 alteration status accurately predicts 79% of relapses in pediatric acute lymphoblastic leukemia. Leukemia. 2011 Feb;25(2):254–8.

118. Papaemmanuil E, Hosking FJ, Vijayakrishnan J, Price A, Olver B, Sheridan E, et al. Loci on 7p12.2, 10q21.2 and 14q11.2 are associated with risk of childhood acute lymphoblastic leukemia. Nat Genet. 2009 Sep;41(9):1006–10.

119. Orsi L, Rudant J, Bonaventure A, Goujon-Bellec S, Corda E, Evans T-J, et al. Genetic polymorphisms and childhood acute lymphoblastic leukemia: GWAS of the

ESCALE study (SFCE). Leukemia. 2012 Dec;26(12):2561–4.

120. Prasad RB, Hosking FJ, Vijayakrishnan J, Papaemmanuil E, Koehler R, Greaves M, et al. Verification of the susceptibility loci on 7p12.2, 10q21.2, and 14q11.2 in precursor B-cell acute lymphoblastic leukemia of childhood. Blood. 2010 Mar 4;115(9):1765–7.

121. Górniak P, Pastorczak A, Zalewska-Szewczyk B, Lejman M, Trelińska J, Chmielewska M, et al. Polymorphism in IKZF1 gene affects age at onset of childhood acute lymphoblastic leukemia. Leuk Lymphoma. 2014 Sep;55(9):2174–8.

122. Rudant J, Orsi L, Bonaventure A, Goujon-Bellec S, Corda E, Baruchel A, et al. Are ARID5B and IKZF1 polymorphisms also associated with childhood acute myeloblastic leukemia: the ESCALE study (SFCE)? Leukemia. 2012 Aug 27;27(3):746–8.

123. Treviño LR, Yang W, French D, Hunger SP, Carroll WL, Devidas M, et al. Germline genomic variants associated with childhood acute lymphoblastic leukemia. Nat Genet. 2009 Sep;41(9):1001–5.

124. Linabery AM, Blommer CN, Spector LG, Davies SM, Robison LL, Ross JA. ARID5B and IKZF1 variants, selected demographic factors, and childhood acute lymphoblastic leukemia: a report from the Children's Oncology Group. Leuk Res. 2013 Aug;37(8):936–42.

125. Ross JA, Linabery AM, Blommer CN, Langer EK, Spector LG, Hilden JM, et al. Genetic variants modify susceptibility to leukemia in infants: a Children's Oncology Group report. Pediatr Blood Cancer. 2013 Jan;60(1):31–4.

126. Song C, Pan X, Ge Z, Gowda C, Ding Y, Li H, et al. Epigenetic regulation of gene expression by Ikaros, HDAC1 and Casein Kinase II (CK2) in leukemia. Leukemia. Macmillan Publishers Limited; 2015 Dec 7;

127. Cunninghame Graham DS, Morris DL, Bhangale TR, Criswell LA, Syvänen A-C, Rönnblom L, et al. Association of NCF2, IKZF1, IRF8, IFIH1, and TYK2 with systemic lupus erythematosus. PLoS Genet. 2011 Oct;7(10):e1002341.

128. Hu S, Wen L, Hu X, Yin X, Cui Y, Yang S, et al. IKZF1: a critical role in the pathogenesis of systemic lupus erythematosus? Mod Rheumatol. 2013 Mar;23(2):205–9.

129. Leng R-X, Wang W, Cen H, Zhou M, Feng C-C, Zhu Y, et al. Gene-gene and gene-sex epistatic interactions of MiR146a, IRF5, IKZF1, ETS1 and IL21 in systemic lupus erythematosus. PLoS One. 2012 Jan;7(12):e51090.

130. Hu W, Sun L, Gao J, Li Y, Wang P, Cheng Y, et al. Down-regulated expression of IKZF1 mRNA in peripheral blood mononuclear cells from patients with systemic lupus erythematosus. Rheumatol Int. 2011 Jun;31(6):819–22.

131. Swafford AD-E, Howson JMM, Davison LJ, Wallace C, Smyth DJ, Schuilenburg H, et al. An Allele of IKZF1 (Ikaros) Conferring Susceptibility to Childhood Acute Lymphoblastic Leukemia Protects Against Type 1 Diabetes. Diabetes. 2011 Jan 26;60(3):1041–4.

132. Ezzat S, Yu S, Asa SL. Ikaros isoforms in human pituitary tumors: distinct localization, histone acetylation, and activation of the 5' fibroblast growth factor receptor-4 promoter. Am J Pathol. 2003 Sep;163(3):1177–84.

133. Ezzat S, Mader R, Fischer S, Yu S, Ackerley C, Asa SL. An essential role for the hematopoietic transcription factor Ikaros in hypothalamic-pituitary-mediated somatic growth. Proc Natl Acad Sci U S A. 2006 Feb 14;103(7):2214–9.

134. Ezzat S, Zhu X, Loeper S, Fischer S, Asa SL. Tumor-derived Ikaros 6 acetylates the Bcl-XL promoter to up-regulate a survival signal in pituitary cells. Mol Endocrinol. 2006 Nov;20(11):2976–86.

135. Abbass SA, Asa SL, Ezzat S. Altered expression of fibroblast growth factor receptors in human pituitary adenomas. J Clin Endocrinol Metab. 1997 Apr;82(4):1160–6.

136. Ezzat S, Smyth HS, Ramyar L, Asa SL. Heterogenous in vivo and in vitro expression of basic fibroblast growth factor by human pituitary adenomas. J Clin Endocrinol Metab. 1995 Mar;80(3):878–84.

137. Yu S, Asa SL, Ezzat S. Fibroblast growth factor receptor 4 is a target for the zinc-finger transcription factor Ikaros in the pituitary. Mol Endocrinol. 2002 May;16(5):1069–78.

138. Javierre BM, Rodriguez-Ubreva J, Al-Shahrour F, Corominas M, Grana O, Ciudad L, et al. Long-Range Epigenetic Silencing Associates with Deregulation of Ikaros Targets in Colorectal Cancer Cells. Mol Cancer Res. 2011 Jul 7;9(8):1139–51.

CHAPTER 2

AIM OF THE THESIS

The aim of the PhD project was to elucidate the role of the transcription factor IKAROS in leukemogenesis and in normal B-lymphocyte development. In the first part of the thesis we applied next generation amplicon deep sequencing to evaluate the presence and the role of *IKZF1* aberrations in paediatric Ph+ ALL, uncovering a new class of *IKZF1*-aberrant patients, and we discovered the first case of a familial *IKZF1* germline mutation that predisposes to leukaemia. In the second part of this thesis, we characterized 2 inducible Ikaros systems to study Ikaros-mediated gene expression and metabolic changes during cycling- to resting- preB cell stages.

CHAPTER 3

REFINEMENT OF *IKZF1* GENOMIC STATUS IN PAEDIATRIC PHILADELPHIA POSITIVE ALL[1]

Tobia Lana[1], Paola de Lorenzo[2-3], Silvia Bresolin[1], Ilaria Bronzini[1], Monique L. den Boer[4-5], Hélène Cavé[6], Eva Froňková[7], Martin Stanulla[8-9], Marketa Zaliova[7-9], Christine J. Harrison[10], Hester de Groot[5], Maria Grazia Valsecchi[3], Andrea Biondi[2], Giuseppe Basso[1], Giovanni Cazzaniga[2] and Geertruy te Kronnie[1]

[1]Department of Women's and Children's Health, University of Padova, Padova, Italy; [2]Clinica Pediatrica, Centro Ricerca Tettamanti, University of Milano-Bicocca, Monza, Italy; [3]European Study for Philadelphia–Acute Lymphoblastic Leukemia Trial Data Center, Department of Health Sciences, University of Milano-Bicocca, Monza, Italy; [4]Department of Pediatric Oncology, Erasmus University Medical Center-Sophia Children's Hospital, Rotterdam, The Netherlands; [5]Dutch Childhood Oncology Group, The Hague, The Netherlands; [6]Department of Genetics, Assistance Publique Hôpitaux de Paris, Hôspital Robert Debré, University Paris Diderot, Paris, France; [7]Childhood Leukaemia Investigation Prague, Second Faculty of Medicine, Charles University and University Hospital Motol, Prague, Czech Republic; [8]Pediatric Hematology and Oncology, Hannover Medical School, Germany; [9]Department of General Pediatrics, University Hospital Schleswig-Holstein, Kiel; [10]Leukemia Research Cytogenetics Group, Northern Institute for Cancer Research, Newcastle University, Newcastle upon Tyne, United Kingdom

ABSTRACT

IKZF1 deletions are the second most frequent genetic alterations in pediatric Philadelphia-positive B-cell precursor acute lymphoblastic leukaemia (Ph+ BCP-ALL), and are associated with poor outcome. We applied next-generation amplicon deep sequencing technology to investigate single nucleotide variants along the entire coding sequence of *IKZF1* in 98 Ph+ *IKZF1* non-deleted pediatric patients. We identified deleterious mutations in 12 out of 98 patients (12.2%): 5 missense point mutations and 7 frameshift mutations. Eight of 12 patients had aberrations in *IKZF1* Exon4, of which, 6 were within the Zinc Finger 2 (ZF2) domain and 1 within ZF3.

Compared to *IKZF1* wild-type, *IKZF1* status comprising mutations as well as deletions conferred a reduced disease-free survival (DFS) in Ph+ patients not treated with tyrosine kinase inhibitors (TKIs). Prognostic impact of *IKZF1* mutations and deletions was less pronounced in patients treated with imatinib.

[1] This chapter is an extended version of the Letter to the Editor we published on LEUKEMIA, 2015 Oct;29(10):2107-10. The original article is inserted in the Appendix of this thesis.

3.1 INTRODUCTION

Philadelphia-positive B-cell precursor acute lymphoblastic leukaemia (Ph+ BCP-ALL) identifies an unfavourable subgroup of pediatric ALL characterized by the presence of the BCR-ABL1 chimeric protein[1]. However, Ph+ BCP-ALL is a clinically heterogeneous disease and although tyrosine kinase inhibitor (TKI) had improved outcome in pediatric patients, 30% still relapse or die[2].

Recurrent genomic deletions within the IKAROS (*IKZF1*) gene locus have been identified in Ph+ BCP-ALL[3], and since their discovery, the biology and the clinical impact of the *IKZF1* status has been intensively studied[4–6].

IKAROS is a transcription factor composed of two regions: the C terminal, including two zinc finger (ZF) domains, responsible for the homo-hetero dimerization of the protein[7], and a N-terminal domain with four ZFs, responsible for the DNA binding activity: ZF2 and ZF3 ensure a stable DNA binding, while ZF1 and ZF4 regulate the interaction to specific genomic sites[8–10]. Deletions of *IKZF1* can be subdivided into 3 categories: dominant-negative deletions, characterized by loss of the DNA binding domain, deletions causing haploinsufficiency that lack the C-terminal dimerization domain, and null-deletions, that correspond to biallelic C-terminus deletions or loss of the ATG codon[11].

Even though the role of *IKZF1* deletions as a prognostic factor has been extensively investigated, little is known about other genetic alterations[4,12,13]. The aim of this study was to assess the incidence of single-nucleotide mutations and in/del in the coding sequence of *IKZF1* in patients described as *IKZF1* WT with no evidence of deletions.

3.2 MATERIAL AND METHODS

Patients

Leukemic bone marrow samples of 98 Ph+ BCP-ALL pediatric patients at diagnosis were analyzed in this study. The cases were collected from six European centres that participated in the "Ponte di legno" (pre-TKI) cohort and the European study for Ph+ ALL (EsPhALL) cohort, based on a combination of high-risk chemotherapy and imatinib treatment[2]. Sample preparation and *IKZF1* deletion status (checked by MLPA) analysis were performed as described previously[14]. In addition, 61 paediatric Ph+ Ikaros deleted BCP-ALL patients derived from the "Ponte di Legno" and "EsPhALL" cohorts and included in van der Veer et al., 2014 were screened for *IKAROS* mutations. Written informed consent according to the Declaration of Helsinki was obtained from patients and/or parents/guardians.

454 next generation sequencing

Sequence analysis of *IKZF1* transcribed sequences, from Exon2 to Exon8, was performed using amplicon next generation sequencer GS Junior 454 (Roche Applied Science, Penzberg, Germany), using two-step universal-tailed amplicon sequencing. Briefly, during the first PCR the seven *IKZF1* coding exons are amplified using specific primers (Table 3.1) fused with "universal tail" sequences. The PCR products were then purified with agercount AMPure beads (Beckman Coulter Inc) following manufacturer's instructions. Then a second round PCR was carried out using universal primers and adding multiplex identifiers (MID)-labeled primers to barcode the samples. The amplicons were purified again with AMPure beads and quantified using PicoGreen (Invitrogen) following manufacturer's instructions. Amplicons were then diluted to the appropriate concentration and the obtained library was amplified by emulsion PCR and then sequenced by GS Junior 454. The predicted coverage was 250 reads per amplicon (range 102-853 reads), with a minimum coverage of 50 reads in both strands. Sequences obtained were analyzed using Amplicon Variant Analyzed (AVA) Software (Roche Applied Science, Penzberg, Germany) (NCBI RefSeq NM_006060). All variants were compared with published SNPs databases (http://www.ncbi.nlm.nih.gov/projects/SNP/; http://cancer.sanger.ac.uk/cancergenome/projects/cosmic/). To predict the functional impact of identified mutations, SIFT[15] and PolyPhen2[16] bioinformatic tools are applied.

Exon	FW/RV	Sequence	Amplicon Lenght
Ex2	FW	CAAGGTCTGTGCCAGTCTGA	361
	RV	AGGCAAATTCCATCATGGTC	
Ex3	FW	ACTGGCTCCACCCAGTACCT	387
	RV	CCCATCCTGCTGATCTTTGT	
Ex4	FW	ATGACACTGAGTGGCCTCCT	336
	RV	TCTCCAGGCCACTAAAGGAA	
Ex5	FW	AAGGAGCTGGCAGGTTTAGTC	421
	RV	GGTTAGCCAGCAAGGACACA	
Ex6	FW	CTTGGCCACCAACGTTTTTA	392
	RV	CTCTGCTCCTAAGGCTGCAT	
Ex7	FW	GCCTGTCTGGAAGTGTTGCT	379
	RV	CCCTTTCTTCCACCCTCAAC	
Ex8a	FW	CTCACTGTCGCCTGCTTTC	300
	RV	GCAGCAGCAGGTTCTCCAC	
Ex8b	FW	CATCAGCCCGATGTACCAG	266
	RV	GCTCCTCCTTGAGCGACA	
Ex8c	FW	GCGGTCTCATCTACCTGACC	394
	RV	GCAGTCCTTGTGCTTTTCCT	

3.1: Primers used to amplify coding exons2-8 of IKAROS.

Statistical Analysis

DFS was calculated from date of first remission to the date of event, which included relapse, death in complete remission, or second malignancy, whichever occurred first.

Outcome was censored at the date of last patient contact when no events had been observed. Follow-up was carried out on December 31, 2008, for the pre-TKI cohort, and on December 31, 2010, for the EsPhALL cohort, with a median (interquartile range) follow-up of 5.0 years (2.8-6.0) and 2.8 years (1.5-3.7), respectively. The Kaplan-Meier method was used to estimate the probabilities of DFS with standard errors (SE) calculated according to Greenwood's method. Curves were compared using the log-rank test. All tests were two-sided. Analyses were performed using SAS 9.2 (SAS Institute, Cary, NC) at the EsPhALL Trial Center.

Sanger Sequencing

PCR reactions were performed using FastStart High Fidelity Taq Polymerase (Roche Diagnostic, D), using 10ng of patients genomic DNA. Primers used are described in Table 3.1. PCR products were purified using Agercount Ampure XP beads (Beckman coulter, Inc. CA USA). Sequences were carried out using BigDye Terminator Kit (version 3.1, Life technologies) and run on the ABI 310 Analyzer (Life technologies).

3.3 RESULTS

98 samples at diagnosis of patients affected by Ph+ BCP-ALL with no *IKZF1* macrodeletions were collected for this study. The bone marrow samples were collected from 6 European centres: Associazione Italiana di Ematologia Pediatrica (Italy), the German Berlin-Frankfurt-Munster study group (Germany), the Childhood Leukemia Investigation Prague (Czech Republic), the Dutch Childhood Oncology Group (The Netherlands), the European Organization for Research and Treatment of Cancer Children's Leukemia Group, the French Acute Lymphoblastic Leukemia Study Group (France), and the Children's Cancer and Leukemia Group (United Kingdom).

Sequencing analysis of *IKZF1* coding exons, from exon2 to exon8, were performed using an amplicon sequencing strategy on the next generation sequencer GS Junior 454 platform. Today next generation sequencing (NGS)-based sequencing strategies are a well accepted robust substitute for Sanger sequencing[17] that can be applied in a clinical setting. Moreover NGS reliably detects mutations well below the detection rate of Sanger sequencing, provides a precise mutant allele frequency rate (MAF), and allows a robust and sensitive detection of insertions or deletions. Sequences of 882 amplicons were collected with predicted average coverage per amplicon of 250 reads (range 102-853) and a minimum coverage of 50 reads in forward and reverse strands. In total, 313 variants were obtained. To identify predicted deleterious mutations a pipeline (Figure 3.1) was applied that

excluded intronic variants, homopolymeric stretches, known SNPs and silent mutations. In addition, a threshold of 10% of variants detection in both strands was set. Finally, 14 variants were obtained with predicted deleterious effects in the *IKZF1* coding sequence corresponding to 12 distinct mutations in 12 out of 98 patients (12.2%) including three patients from three different centres that were carrying the same mutation (Figure 3.2A and Table 3.2).

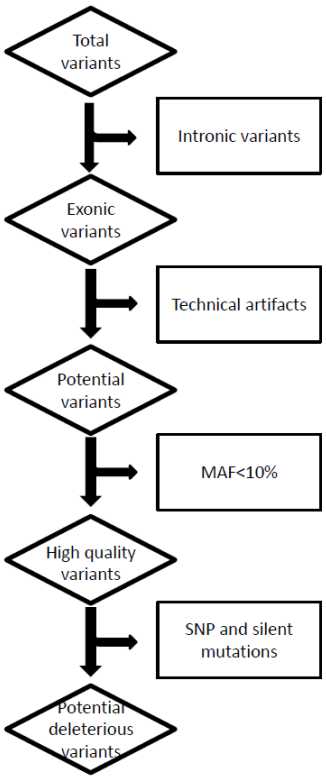

Figure 3.1: Sequence analysis pipeline to retrieve potential deleterious variants. A total of 313 variants were obtained from NGS. From them, we excluded variants presented in intronic regions as well as variants called in homopolymeric sequencing or in overlapping regions between 2 different amplicons but present in one of them only. Finally we excluded variants present in less than 10% of the reads for a quality parameter, and variants already known as SNPs or new silent mutations.

The 12 mutations can be subdivided into 2 categories: mutations localized in the DNA binding domain with a predictive dominant-negative effect (5 missense mutations), and haploinsufficiency aberrations, predicted to affect dimerization of IKAROS indirectly impairing DNA binding (7 frameshift mutations).

The 5 missense mutations were located in exon5, of which 4 were localized within the ZF2 coding sequence, essential for DNA-protein interaction. All missense mutations were predicted to be "probably deleterious" by PolyPhen2[16] (score 0.999) and "damaging" by SIFT[18] (score 0.001) bioinformatic tools.

Regarding the mutated amino acids in the ZF2 domain, Asn159 and Arg162 (Figure 2A) are known to be crucial for the maintenance of the α-helix domain structure, and their substitutions are described to impaired the DNA binding activity of the protein[9]. The

Cys150 (mutated into Arg) is one of the 4 Cys/His residues that coordinate the zinc atom of the domain, and the mutation is predicted to severely impair the function of the domain as well. Of note, the p.Asn159Ser (c.A476>G) substitution is carried by 3 patients (3% in our study cohort). Altogether 6 patients carried point mutations in the ZF2 coding sequence with a predicted deleterious impact.

The 7 frameshift mutations (2 deletions, 4 insertions and 1 Indel) were identified at different positions within the *IKZF1* locus, 2 in exon5, 1 in exon7 and 4 in exon8. These mutations cause shifts in the reading frame that predict formation of premature stop codons and consequent depletion the C-terminal dimerization domain of the protein.

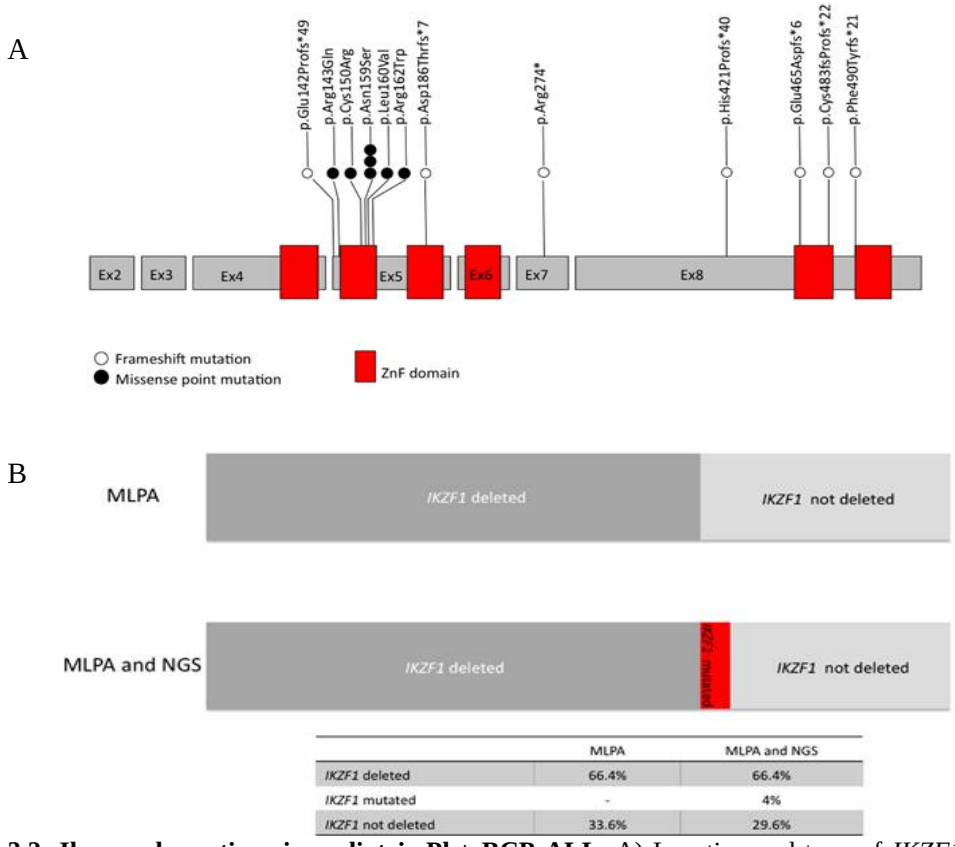

	MLPA	MLPA and NGS
IKZF1 deleted	66.4%	66.4%
IKZF1 mutated	-	4%
IKZF1 not deleted	33.6%	29.6%

Figure 3.2: Ikaros aberrations in pediatric Ph+ BCP-ALL. A) Location and type of *IKZF1* mutations: grey squares define the coding exons of *IKZF1*; red squares represent the zinc-finger domains. Each circle represents a detected mutation. B) Overview of IKZF1 in Ph+ BCP-ALL pediatric patients. Distributions were calculated for each group on the basis of the number of IKZF1-mutated patients detected by amplicon NGS in 98 patients. NGS, next-generation sequencing.

The Mutant Allele Frequency (MAF) of *IKZF1* mutations compared to the blast cells count was in most cases consistent with heterozygous mutation in the entire blast population; only in three cases (MRC-UK-12, BFM-G-1 and AIEOP-24) MAF suggested a *IKZF1* mutated subpopulation. Two patients carried double mutations: in one case, the 2 mutations in exon5 were reciprocally exclusive (p.Glu142Profs*49 and p.Arg143Gln), whereas in the second case mutations were located in different exons (p.Leu160Val in Exon5 and p.Arg274* in Exon7). In both cases one of the two mutations was present at a

higher MAF (63% for p.Glu142Profs* vs. 22% for p.Arg143Gln, and 58% for p.Leu160Val vs. 36% for p.Arg274*), indicating the presence of leukemic sub-populations characterized by different *IKZF1* mutations. For six of 12 mutated patients the remission samples were available, and Sanger sequencing was applied to screen for possible germline origin of the mutations. Among these, one patient displayed the same mutation in his leukaemia-free bone marrow sample. The mutated exon of the remission sample was then sequenced using GS Junior 454 to obtain the MAF at remission. The mutation, a single-nucleotide deletion within the zinc finger 3 coding sequence was present in 52- and 50% of the reads at diagnosis and at remission respectively, indicating a potential germline nature of the mutation. This case will be further discussed in the forth chapter of this thesis.

The clinical characteristics of the 12 mutated patients are described in Table 3.2. Among the 6 mutated patients that had been treated before the introduction of TKI (pre-TKI cohort) 4 relapsed and 1 died in continuous complete remission (CCR). The latter is in line with the previously reported impact of *IKZF1* deletions in pre-TKI patients and suggests that *IKZF1* mutations behave in the same manner as deletions in terms of their associations with poor outcome in Ph+ patients. Of the 6 mutated patients that were treated with imatinib (EsPhALL cohort) one failed (died in CCR), which is in line with the behaviour of *IKZF1* deleted patients in the imatinib era.

Patient ID	Sex	Age	WBC Cells 10^9/L	Early Response*	Protocol	Outcome	Mutation	%MAF
DCOG-6	M	5.07	17.02	NK	pre-TKI	Rel	p.G142Pfs*49	60
							p.R144Q	25
EORTC-9	F	5.03	8.07	yes	pre-TKI	AlCCR	p.N159S	36
MRC-UK-4	F	2.04	43.3	NK	pre-TKI	Rel-Dead	p.L160V	51,5
							p.R274*	36
BFM-G-22	M	5.07	12.54	yes	pre-TKI	Dead in CCR	p.D186Tfs*7	52
EORTC-1	M	5.04	7.04	yes	pre-TKI	Rel-Dead	p.E465Dfs*6	41
BFM-G-20	M	15.08	148.5	no	pre-TKI	Rel	p.C483Pfs*22	42
AIEOP-28	F	10.09	630.08	no	EsPhALL	Dead in CCR	p.C150R	41
MRC-UK-12	F	3.03	5.05	yes	EsPhALL	AlCCR	p.N159S	21
BFM-G-13	M	3.06	32.27	yes	EsPhALL	AlCCR	p.N159S	36
MRC-UK-13	M	12.09	64.07	no	EsPhALL	AlCCR	p.R162W	40
BFM-G-1	M	2.05	246	no	EsPhALL	AlCCR	p.H421Pfs*40	24
AIEOP-24	M	11.03	259	no	EsPhALL	AlCCR	p.F490Yfs*21	11

Table 3.2: clinical characteristics of mutated patients. The characteristics of mutated patients do not differ significantly from patients enrolled in the Van der Veer study in terms of sex (p=1), age (p=0,37) and early response (p=0,06). *Early clinical Response was defined as <1000 cells/μL in peripheral blood after 7 days of treatment with prednisone and a single intrathecal dose of methotrexate, or ≤5% leukemic blast cells in the bone marrow at day 21 (depending on national induction protocols). WBC, White Blood Cell Count; AlCCR, alive continuous complete remission; CCR, Clinical Complete Remission; MAF, mutant allele frequency calculated as number of mutated reads/number of total reads.

Recently, we reported the impact of *IKZF1* deletions on outcome of Ph+ BCP-ALL[14]. This study included 191 patients; 84 recruited in the pre-TKI cohort and 107 in the EsPhALL, post TKI cohort. Overall, 65 patients (40%) were defined as 'wild-type' on the basis of the absence of *IKZF1* deletions, and among them, 64 where included in our screening (one was excluded due to lack of material) (Figure 3.2A). Six of these carried *IKZF1* deleterious mutations, 3 from the pre-TKI cohort and 3 from the EsPhALL cohort.

IKZF1-mutated and -deleted patients were grouped together (N=132, '*IKZF1*-aberrant' patients) and their outcome compared to that of 'true' WT *IKZF1* (without deletion or mutations) Ph+ BCP-ALL patients (N=59). The new DFS curves of pre-TKI and EsPhALL cohorts confirmed the poor prognosis of patients with *IKZF1* aberrations (deletions plus mutations) (4-year DFS 28.1% [SE 6.4] vs. 64.3% [SE 9.7], P=0.0036 in pre-TKI; 4-year DFS 55.7% [SE 6.8] vs. 59.8% [SE 11.6] (P= 0.348) in EsPhALL) (Figure 3.2C).

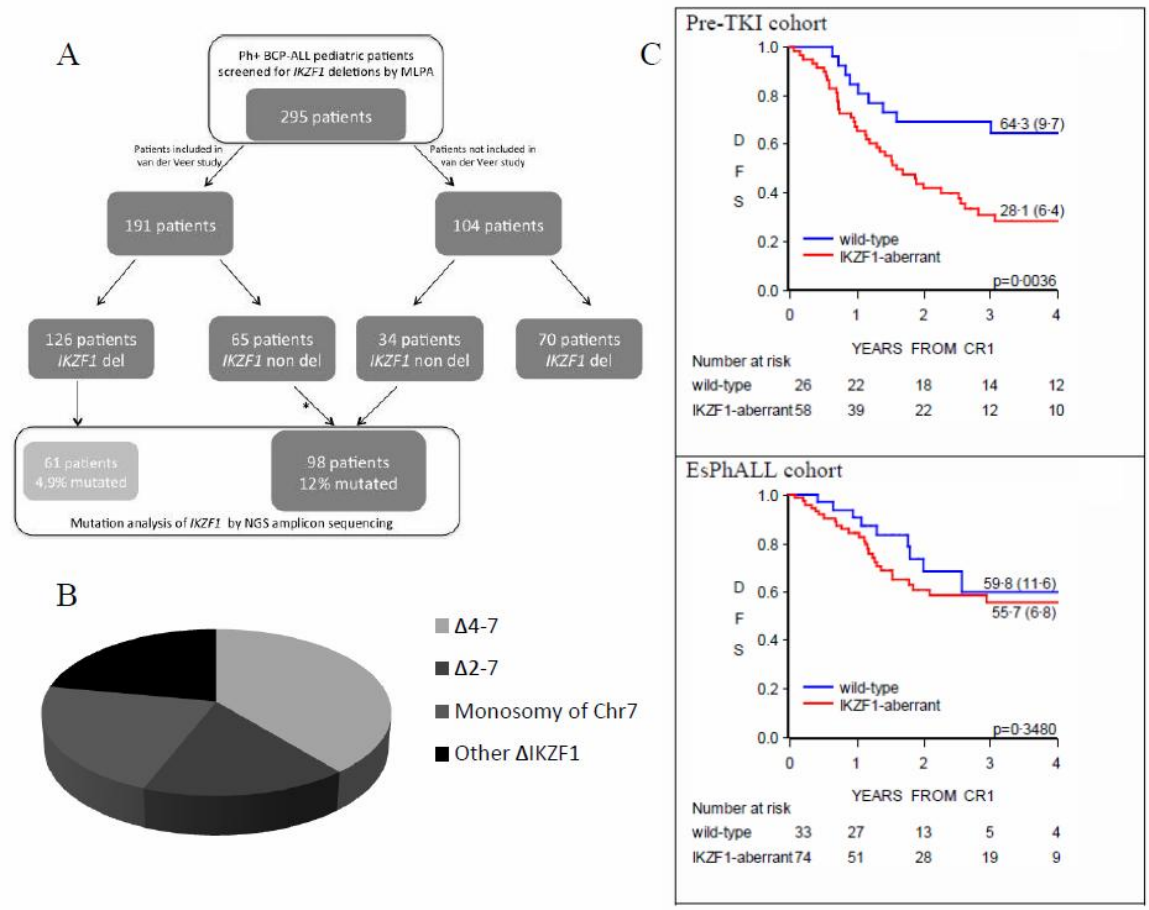

Figure 3.2: Description and outcome of *IKZF1*- aberrant and -WT cohorts. A) Scheme of the Ph positive BCP ALL patient cohort analyzed by MLPA and patients subsequently analyzed by amplicon NGS for *IKZF1* aberrations at the single nucleotide level. B) Percentages of different *IKZF1* deletions in *IKZF1*-deletet cohort. C) Outcome by *IKZF1* status in pre- and post-TKI cohorts. DFS was analyzed in patients with and without *IKZF1* aberrations (deletions and missense/frameshift mutations) in pre TKI cohort (*IKZF1*-aberrant n = 58; *IKZF1*-wild-type n = 26) (Top), in EsPhALL cohort (*IKZF1*-aberrant n = 74; *IKZF1*-wild-type n = 33) (Bottom)

As *IKZF1* mutations could also occur in conjunction with *IKZF1* deletions[19], we screened by GS Junior 454 61 pediatric Ph+ BCP-ALL samples at diagnosis previously identified as *IKZF1* deleted[14]. We sequenced Exons 4 and 8 as they are the exons most frequently mutated in the previous *IKZF1* wild type cohort. 39% of deleted patients carried the most common Δ4-7 deletion, 17% carried the Δ2-7 and 22% of them carried monosomy of chromosome 7 or large deletions that comprehend the entire IKZF1 locus (Figure 3.2B). We identified point mutations in 3 patients: p.R143>W (probably deleterious" for PolyPhen2 and "damaging" for SIFT), p.L411>F (probably deleterious for PolyPhen2 and neutral for SIFT) and p.I509>T (possibly damaging for PolyPhen2 and damaging for SIFT). The MAF of the variants (28% for p.R143>W, 11.5% for p.L411>F and 12.8% for p.I509>T) suggest the presence of an *IKZF1*-mutated blasts subpopulation. p.I509>T and p.R143>W are carried by 2 patients presenting a Δ4-7 deletion, while p.L411>F is present in conjunction with the Δ2-7 deletion. The p.R143>W is necessary located in the non-deleted allele, as located in the exon4, whereas the other 2 single-nucleotide mutations, located in exon8, it is not possible to know whether they occurred in the deleted or the non-deleted allele.

3.4 DISCUSSION

In conclusion, this work has demonstrated the presence of *IKZF1* mutations in >10% of pediatric Ph+ BCP-ALLs previously classified as *IKZF1* WT on the basis of deletion analysis alone. The higher incidence of *IKZF1* mutations identified in our study compare to previous papers[19,20] can be attributed to the difference in sensitivity of technologies (NGS in our study and Sanger sequencing in the others[19,20]). NGS is more sensitive and permits to identify mutations present in percentages lower than the detection limit of Sanger sequencing. This data strengthened our decision to take advantage of NGS for our screening to depict a more comprehensive landscape of *IKZF1* alternations in Ph+ pediatric ALL patients.

Exon5, which encodes for ZF2 and ZF3 domains, carried 9 out of 14 aberrations: 7 point mutations and 2 deletions. The presence of the high number of mutations in these domains and the recurrence of one of the mutations in 3% of patients prompted us to consider this region as a hotspot locus for mutation acquisition. All missense mutations are predicted to be deleterious by two bioinformatic tools and by *in vitro* mutagenesis studies[9], and all small in-del aberrations lead to the formation of premature stop codons. Overall, our observations have contributed to the refinement of DFS analysis of Ph+ BCP-ALL patients

with *IKZF1* aberrations. Separate Kaplan Meyer curves for *IKZF1* deleted, mutated, and WT patients are not feasible, due to the small number of mutated patients for which complete clinical data were available. Nevertheless, considering the pre- and post- TKI cohorts, some observations can be made. In the pre-TKI cohort, *IKZF1*-mutated patients showed a similar outcome as compared to *IKZF1* deleted patients (four out of six patients experienced an adverse event, such as relapse or death). The prognostic impact of the *IKZF1* mutations in imatinib-treated patients is more attenuated and may indicate the presence of other pathogenic mechanisms[21], as well as a possible effect of TKI therapy on the activation status of *IKZF1*. Recently, another group published an *IKZF1* mutational screening in pediatric ALL patients with different cytogenetic characteristics using Illumina MultiSeq sequencing[13]. They Identified *IKZF1* mutations in 5.7% of patients (9 out of 140 patients), none of them in BCR-ABL1 subgroup, probably due to the very low number of Ph+ patients included in their screening (6 out of 140 patients). Of note, 5 out of 9 *IKZF1*-aberrations (3 point mutations and 2 indels) occurred in the exon 5, corroborating our observation of an increased mutational rate in this locus. *IKZF1* mutated and WT patients do not significantly differ in terms of EFS and CIR, but when *IKZF1* deletions and mutations are combined, aberrant *IKZF1* patients presented a lower EFS compare to *IKZF1* WT patients. Considering the high incidence of nucleotide aberrations observed in our study (and in the Olsson L. et al., study, in a more heterogeneous cohort of pediatric leukemic patients), in both *IKZF1* deleted or non-deleted patients, we would like to stress the importance of including these mutations in the overview of *IKZF1* aberrations (Figure 3.3). This new category of *IKZF1* mutated patients, previously masked in the *IKZF1* WT group, behaves in a way similar to *IKZF1* deleted patients in both the pre and post TKI era, and needs to be considered for a precise estimation of the impact of aberrant *IKZF1* in leukemogenesis and disease progression.

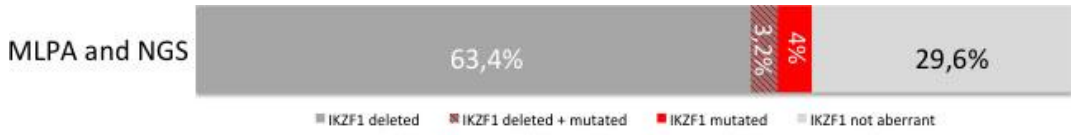

Figure 3.3: Overview of *IKZF1* status in Ph positive BCP-ALL pediatric patients. Percentages were calculated for each group based on the number of *IKZF1* mutated patients detected by NGS Amplicon sequencing in 98 non deleted and 61 deleted *IKZF1* patients. The *IKZF1* mutations detected in *IKZF1* deleted patients were: p.R143>W, p.L411>F and p.I509>T.

3.5 REFERENCES

1. Ribeiro RC, Abromowitch M, Raimondi SC, Murphy SB, Behm F, Williams DL. Clinical and biologic hallmarks of the Philadelphia chromosome in childhood acute lymphoblastic leukemia. Blood. 1987 Oct;70(4):948–53.

2. Biondi A, Schrappe M, De Lorenzo P, Castor A, Lucchini G, Gandemer V, et al. Imatinib after induction for treatment of children and adolescents with Philadelphia-chromosome-positive acute lymphoblastic leukaemia (EsPhALL): a randomised, open-label, intergroup study. Lancet Oncol. 2012 Sep;13(9):936–45.

3. Mullighan CG, Miller CB, Radtke I, Phillips LA, Dalton J, Ma J, et al. BCR-ABL1 lymphoblastic leukaemia is characterized by the deletion of Ikaros. Nature. 2008 May 1;453(7191):110–4.

4. Mullighan CG, Su X, Zhang J, Radtke I, Phillips LAA, Miller CB, et al. Deletion of IKZF1 and prognosis in acute lymphoblastic leukemia. N Engl J Med. 2009 Jan 29;360(5):470–80.

5. Palmi C, Valsecchi MG, Longinotti G, Silvestri D, Carrino V, Conter V, et al. What is the relevance of Ikaros gene deletions as a prognostic marker in pediatric Philadelphia-negative B-cell precursor acute lymphoblastic leukemia? Haematologica. 2013 Aug;98(8):1226–31.

6. Asai D, Imamura T, Suenobu S, Saito A, Hasegawa D, Deguchi T, et al. IKZF1 deletion is associated with a poor outcome in pediatric B-cell precursor acute lymphoblastic leukemia in Japan. Cancer Med. 2013 Jun;2(3):412–9.

7. Sun L, Liu A, Georgopoulos K. Zinc finger-mediated protein interactions modulate Ikaros activity, a molecular control of lymphocyte development. EMBO J. 1996 Oct 1;15(19):5358–69.

8. Molnár A, Wu P, Largespada DA, Vortkamp A, Scherer S, Copeland NG, et al. The Ikaros gene encodes a family of lymphocyte-restricted zinc finger DNA binding proteins, highly conserved in human and mouse. J Immunol. 1996 Jan 15;156(2):585–92.

9. Cobb BS, Morales-Alcelay S, Kleiger G, Brown KE, Fisher AG, Smale ST. Targeting of Ikaros to pericentromeric heterochromatin by direct DNA binding. Genes Dev. 2000 Sep 1;14(17):2146–60.

10. Schjerven H, McLaughlin J, Arenzana TL, Frietze S, Cheng D, Wadsworth SE, et al. Selective regulation of lymphopoiesis and leukemogenesis by individual zinc

fingers of Ikaros. Nat Immunol. 2013 Oct;14(10):1073–83.

11. Kastner P, Dupuis A, Gaub M-P, Herbrecht R, Lutz P, Chan S. Function of Ikaros as a tumor suppressor in B cell acute lymphoblastic leukemia. Am J Blood Res. 2013 Jan;3(1):1–13.

12. Roberts KG, Morin RD, Zhang J, Hirst M, Zhao Y, Su X, et al. Genetic alterations activating kinase and cytokine receptor signaling in high-risk acute lymphoblastic leukemia. Cancer Cell. 2012 Aug 14;22(2):153–66.

13. Olsson L, Albitar F, Castor A, Behrendtz M, Biloglav A, Paulsson K, et al. Cooperative genetic changes in pediatric B-cell precursor acute lymphoblastic leukemia with deletions or mutations of IKZF1. Genes Chromosomes Cancer. 2015 May;54(5):315–25.

14. van der Veer A, Zaliova M, Mottadelli F, De Lorenzo P, Te Kronnie G, Harrison CJ, et al. IKZF1 status as a prognostic feature in BCR-ABL1-positive childhood ALL. Blood. 2014 Mar 13;123(11):1691–8.

15. Kumar P, Henikoff S, Ng PC. Predicting the effects of coding non-synonymous variants on protein function using the SIFT algorithm. Nat Protoc. 2009 Jan;4(7):1073–81.

16. Adzhubei IA, Schmidt S, Peshkin L, Ramensky VE, Gerasimova A, Bork P, et al. A method and server for predicting damaging missense mutations. Nat Methods. 2010 Apr;7(4):248–9.

17. Kohlmann A, Klein H-U, Weissmann S, Bresolin S, Chaplin T, Cuppens H, et al. The Interlaboratory RObustness of Next-generation sequencing (IRON) study: a deep sequencing investigation of TET2, CBL and KRAS mutations by an international consortium involving 10 laboratories. Leukemia. 2011 Dec;25(12):1840–8.

18. Ng PC, Henikoff S. Predicting deleterious amino acid substitutions. Genome Res. 2001 May;11(5):863–74.

19. Roberts KG, Li Y, Payne-Turner D, Harvey RC, Yang Y-L, Pei D, et al. Targetable Kinase-Activating Lesions in Ph-like Acute Lymphoblastic Leukemia. N Engl J Med. 2014 Sep 11;371(11):1005–15.

20. Churchman ML, Low J, Qu C, Paietta EM, Kasper LH, Chang Y, et al. Efficacy of Retinoids in IKZF1-Mutated BCR-ABL1 Acute Lymphoblastic Leukemia. Cancer Cell. 2015 Aug 26;28(3):343–56.

21. Raetz EA, Carroll WL. Refining prognosis in BCR-ABL1-positive ALL. Blood. 2014 Mar 13;123(11):1626–7.

CHAPTER 4

IKZF1 GERMLINE MUTATION UNCOVERS FAMILIAL PREDISPOSITION TO LEUKAEMIA

Tobia Lana[1], Erik Kowarz[2], Silvia Bresolin[1], Maddalena Paganin[1], Luca Trentin[1], Rolf Marschalek[2], Martin Stanulla[3], Rupert Handgretinger[4], Geertruy te Kronnie[1]

[1]Department of Women's and Children's Health, University of Padova, Padova, Italy; [2]Institute of Pharmaceutical Biology, Goethe-University of Frankfurt, Biocenter, Max-von-Laue-Str. 9, D-60438 Frankfurt/Main, Germany; [3]Department of General Paediatrics, University Hospital Schleswig-Holstein, Kiel; [4]Department I - General Paediatrics, Haematology/Oncology, Children's Hospital, University Hospital Tuebingen, Hoppe-Seyler-Str. 1, 72076, Tuebingen, Germany.

ABSTRACT

Although leukaemia is a somato-genetically well characterized disease, the bases of familial predisposition are poorly understood. Among leukemic hallmark aberrations, deletions of the lymphocyte transcription factor *IKZF1* are described to occur in 15% of BCP-ALL paediatric patients. Here we report the first case of a family showing transmission of a heterozygous single nucleotide deletion of the *IKZF1* coding sequence. The deletion causes a reading frame shift resulting in a depletion of the dimerization-activation domain, leading to haploinsufficiency in cells where IKAROS is expressed. The mutation is found in three generations of the family of which 5 cases were positive and 6 cases were negative for the mutation. Two members of the family in subsequent generations presented with pediatric leukaemia. The aberrant transcript was identified in bone marrow of the proband at diagnosis and remission and in peripheral-blood cells of an unaffected relative, and the truncated protein presented a diffuse nuclear localization in a cellular model, indicating impaired DNA binding. This is the first family with recurrent pediatric leukaemia in two generation associated with transmission of a deleterious heterozygous mutation in *IKZF1*, even if penetration of leukaemia is low.

4.1 INTRODUCTION

Acute Lymphoblastic Leukaemia, a malignant disorder of the hematopoietic lymphoid progenitors in the bone marrow, is the most common pediatric leukaemia, as well as the leading cause of childhood cancer-related mortality[1]. The disease is characterized by distinct somato-genomic alterations, including aneuploidy and chromosomal re-arrangements, and is further known to carry other submicroscopic DNA aberrations, such as small deletions/insertions or point mutations affecting genes involved in cell cycle regulation, apoptosis or lymphoid differentiation[2]

A particular unfavourable subgroup of acute leukaemia carries a somatic t(9;22) translocation encoding the BCR-ABL1 tyrosine kinase chimeric protein[3]. Despite the advent of tyrosine kinase inhibitors (TKI) that improved outcome of patients up to 70%, one third of pediatric patients with a t(9;22) translocation still suffer of relapse or decease during treatment[4].

IKZF1 is a Zinc Finger transcription factor primary involved in the specification and differentiation of the lymphoid lineage by activating the lymphoid transcription program and repressing the stem cell and myeloid/erythroid differentiation program in hematopoietic stem cells[5,6].

The most common *IKZF1* alterations are intragenic deletions of exons Δ3-6 (30% *IKZF1* aberrations) or exons Δ1-6 (15%), followed by other deletions of other combined-exons or large chromosome 7 deletions[7]. Despite pediatric ALL is a well characterized disease, little is known about genetic predisposition to leukaemia development[8]. Familial studies on Swedish offspring databases revealed a higher probability to develop leukaemia in individuals with affected siblings. These data are significant for individuals affected by AML[9], while the correlations between an ALL-affected sibling and probability to develop ALL is significant only in twins cases[10]. The latter could be attributed to the prenatal origin of leukemic cells in one twin that *in utero* passed to the co-twin. Only recently, a recurrent mutation of *PAX5* has been found in three unrelated families[11,12] with familial predisposition to B-ALL, linking the familial predisposition to leukaemia to a well-known somatically mutated gene in B-ALL.

In 2013, a case of a newborn child carrying an *IKZF1 de novo* germline mutation was described[13]. The newborn presented pancytopenia, selective B and NK lymphopenia and a T cell differentiation skewed for the TCR-αβ positive cells. Sanger sequencing analysis revealed a p.Tyr210Cys missense point mutation in the zinc finger 4 domain. The mutation resulted in DNA-binding affinity impairment and a consequent diffuse nuclear localization

of IKAROS. The newborn died of multi-organ failure within 40 days. Both parents displayed 2 copies of wt-*IKZF1*.

In the previous chapter of this thesis, we reported a screening of aberrations at the *IKZF1* locus, such as point mutations or very small insertions/deletions of pediatric Philadelphia positive B cell precursor Acute Lymphoblastic Leukaemia (Ph+ BCP-ALL). Analysis performed on remission samples of *IKZF1* mutated patients revealed that one patient carried a mutation at a high mutation frequency in the leukemic-free bone marrow, suggesting a potential germline origin of the mutation. Here we investigated the segregation of this mutation in the family of the proband and report preliminary molecular characterization of *IKZF1* c.556_delG.

4.2 MATERIAL AND METHODS

Sleeping beauty system

IKZF1 wt or c.556_delG coding sequences, fused with FLAG, were cut using the SfiI restriction enzyme and subsequently cloned into the p.UC19 vector between 2 tandem inverted repeats sequences, under the control of the EF1a promoter. A PGK promoter controls the translation of a polycistronic mRNA cassette encoding for GFP and a puromycin resistant protein.

In order to establish a stable cell line, HeLa cells were co-transfected with *IKZF1*-sleeping beauty vectors and SB-transposase vectors BS100X[14]. Transfection was carried out using *FuGENE*®-transfections following manufacturer's instructions. Twenty-four hours after transfection, positive transfected cells were selected by 1µg/ml of puromycin for 3 days.

HEK-293T transfection

For transient transfection, p.RRL vectors containing *IKZF1* wt or c.556_delG coding sequences fused with FLAG and a GFP reporter gene were used. 4µg of p.RRL vector were added to 500 µl of 0.4M $CaCl_2$ solution. 500µl of 2x HEBS (12mM dextrose, 50mM HEPES, 280mM NaCl, 10mM KCl, 1.5mM $Na_2HPO_4 + 2H_2O$ in sterile water) were then added to the plasmid mix drop by drop. The transfecting solution was then added to cells drop by drop. The cell medium was changed 12h after transfection.

Immunofluorescence

Cells were incubated for 24h in multi well chamber slides. Cells were washed with $PBS^{-/-}$ and fixed with 4% paraformaldehyde (PFA) in PBS-/- for 10' at room temperature. Fixed samples were washed twice in $PBS^{-/-}$ and then permeabilized with 0.5% of TritonX-100 for 5'. Cells were incubated for 30' at room temperature with blocking solution (3% normal

goat serum, 0.1% TritonX-100 in PBS-/-). Primary antibodies were diluted 1:1000 in blocking solution and added to the samples overnight at 4 °C in a humidity chamber. Coverslips were washed 3x with PBS-/- and incubated with secondary antibodies conjugated with appropriate fluorophores diluted 1:10000 in blocking solution for 1h at room temperature in a humidity chamber in the dark. Coverslips were washed 3x PBS-/- and mounted in Vecatsheald (Vector laboratories) with DAPI 0.1µg/ml. samples were visualised using a Leica DMBL microscope. Images were analysed using Leica IM1000 software.

Reverse transcription

Reverse transcription was performed using Superscript First-Strand Synthesis system (Invitrogen). 1µg of RNA was mixed with 1µl of 10mM dNTPs mix and 1µl of 0.25mM random primers, topped up to 13µl with RNase-free H2O. The RNA mix is incubated at 65 °C for 5' and then 1' at 4 °C. A mix composed by 1µl of 0.1M of DTT, 1µl RNasi-OUT, 5µl of 4x first strand buffer and 1µl of 200U/µl Superscript III reverse transcriptase was added to the RNA mix. The final mix was incubated at 25 °C for 5', at 50 °C for 1h and at 75°C for 15'. The obtained cDNAs were diluted 10x.

Sanger Sequencing

PCR reactions were performed using FastStart High Fidelity Taq Polymerase (Roche Diagnostic, D), using 10ng of patient's genomic DNA or 10ng of cDNA. Primers used are reported here below. PCR products were purified using Agercount Ampure XP beads (Beckman coulter, Inc. CA USA). Sequencing was carried out using the BigDye Terminator Kit (version 3.1, Life technologies) and run on the ABI 310 Analyzer (Life technologies).

DNA_*IKZF1*_Exon5_fw	AAGGAGCTGGCAGGTTTAGTC
DNA_*IKZF1*_Exon5_rv	GGTTAGCCAGCAAGGACACA
c.DNA_*IKZF1*_Exon5_fw	CCCTTCAAATGCCACCTCT
c.DNA_*IKZF1*_Exon5_rv	AGGTCTTCTGCCATTTCACTG
rs4132601_fw	TCTGCTCACAGAAGGGTGTG
rs4132601_rv	AGGAAAGGGCAAAGCAGTTT

Protein extraction and quantification

One to 3 x106 cells are washed once in cold PBS-/- supplemented with protein inhibitor cocktail (Roche) and then resuspended in 1 volume of cold PBS-/- supplemented with protein inhibitor cocktail. One volume of 2x sample buffer (100mM Tris pH 6.8, 20%

glycerol and 2% of sodium dodecyl sulphate (SDS)) is added to cells, and the cell mix is subsequently boiled at 95 °C for 10'. Protein concentration is measured using the PierceTM BCA protein assay kit (Thermo scientific) according to manufacturer's instruction. After quantification, 10% v/v of β-mercaptoethanol and 0.002% of bromophenol blue are added to the protein assay. Proteins are stored at -20 °C.

Western blot

Proteins and Benchmark pre-stained protein ladder (Beckman) are loaded on a SDS-polyacrylamide gel. The gel is formed by an upper staking gel (4% w/v acrylamide, 125mM Tris-HCl pH 6.8, 0.1% SDS, 0.067% ammonium persulphate (APS) and 0.12% N,N,N'tetramethylethylenediamine (TEMED)) and a running gel (10% acrylamide, 390mM Tris-HCl pH 8.8, 0.1% SDS, 0.05% APS and 0.1% TEMED). Bio-Rad minigel system is used for the electrophoretic run together with running buffer (25mM Tris base, 192mM glycin and 0.1% SDS). The electrophoretic run is performed at 30mA per gel for 90'. Proteins are transferred to polyvinylidene fluoride (PVDF) using the trans-blot® SD semi-dry transfer cell (Bio-Rad) in transfer buffer (48mM Trizma base, 39mM glycin, 0.037% w/v SDS and 20% v/v ethanol) for 1h at 140mA/25mV per gel. The membrane is incubated 1h in blocking solution (5% w/v fat free milk powder (Marvel), 1.2g/l Tris pH 7.4 and 8.75g/l NaCl) and subsequently incubated ON at 4 °C with diluted primary antibody IKAROS H-100 (Santa Cruz biotech) in blocking solution with agitation. Membrane is then washed 3x10' in T-TBS (1.2g/l Tris pH 7.4, 8.75g/l NaCl and 0.1% tween20 20%) and subsequently incubated with horseradish peroxidase-coupled secondary antibodies (αRabbit and αMouse secondary antibodies are provided by Amersham) diluted 1:5000 in blocking solution for 1h at room temperature. The membrane is washed 3x10' with T-TBS and the detection is done using Luminata Crescendo Western HRP substrate (Millipore) following manufacturer's instruction with Kodak X-Omat photographic films.

4.3 RESULTS

Identification of an IKZF1 germline mutation

Recently, we applied amplicon next generation sequencing (NGS) to determine the status of *IKZF1* regarding nucleotide mutations and small indels at single nucleotide level[15].

NGS (next generation sequencing) allows to determine the presence of mutations and in addition provides quantitative information on the mutant allele frequency (MAF), calculated as a percentage of mutated reads upon the total number of reads obtained for a specific amplicon. Generally speaking, mutations with a MAF well below 50% point to a

somatogenetic mutation in the leukemic blast population, whereas mutations with MAFs of 50% and above maybe attributed to a germline mutation (with our without LOH).

As reported in Chapter 3, we identified 14 new deleterious mutations at the *IKZF1* locus. One of these mutations with MAF of 50% indicating a potential germline origin was further explore here.

The mutation consisted of a single nucleotide deletion c.556_delG located in the fifth exon of *IKZF1,* within the zinc finger 3 coding sequence. At the mRNA level the deletion would lead to a change in the reading frame and the formation of a premature stop codon (p.Asp186Thrfs*7) depleting ZF4 and the C-terminal dimerization domain resulting in a truncated protein. The mutation originally detected by NGS was confirmed by Sanger sequencing and was detected with the same MAF (50%) in a remission, blast-free, bone marrow sample both by NGS and Sanger sequencing (Figure 4.1 A&B), corroborating a potential germline origin of the mutation or, at least, a mutation in very early hematopoietic progenitors. The second allele carried neither mutations nor deletions, as confirmed by NGS and MLPA analysis respectively.

As *IKZF1* could be transcribed in at least 10 different isoforms, some of which do not incorporate exon5, we performed Sanger sequencing on cDNA derived from proband's remission specimen, with specific primers that mapped within exon5. The *IKZF1*-mutated allele was transcribed in leukemic-free bone marrow of the proband (Figure 4.1 B).

The patient was diagnosed at the age of 5 years with acute lymphoblastic leukaemia carrying the BCR-ABL1 translocation. At diagnosis, the WBC was $12.5x10^9$ cells/l, with a 50% of blasts in the bone marrow identified by cytomorphological analysis. The patient was classified as good early responder on the basis of a blood-cell count <1000 blast/µl after 7 days of glucocorticoid therapy, and achieved cytomorphological complete remission after induction therapy. Despite of this, the patient died in clinical complete remission. To further explore the germline origin of the proband's mutation, efforts were put to re-contact his family. Following consultation and informed consent the family agreed to collaborate in order to establish the nature of the *IKZF1* mutation. At first consent was obtained to screen DNA of the parents, and the mother was identified with *IKZF1* c.556_delG establishing the inherited nature of the *IKZF1* mutation (Figure 4.1 C).

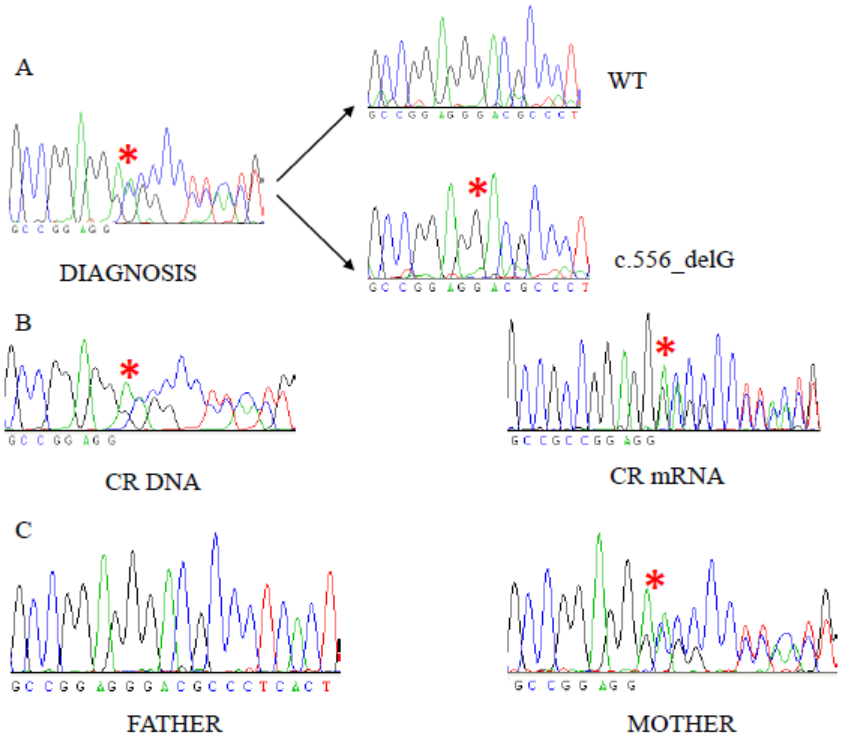

Figure 4.1: Sequencing of *IKZF1* exon5 of the proband. Sanger sequence at diagnosis (A) and at complete remission (B), and sequencing of proband's father and mother (C). The mutation is indicated by a red star. CR, complete remission.

Thanks to further cooperation of the family, we were able to track the transmission of the mutated allele through three generations (Figure 4.2). DNA from oral-swabs of 8 relatives were analyzed. The 2 sisters of the proband (IIIb and IIIc) both carry the mutation, as well as the daughter (IVa) of (IIIb). In the second generation, the maternal uncle of the proband (IId) does not carry the mutation. The second leukaemia case in this family was a second brother (IIc) of proband's mother who was reported to have died of leukaemia during childhood. The latter event dated back to more than 40 years and no material is available to screen for the mutation status of *IKZF1*. Four healthy mutation carriers do not present a clinical history of haematological disturbances, but further follow-up is ongoing to verify uncommon characteristics not subjected to routine clinical tests.

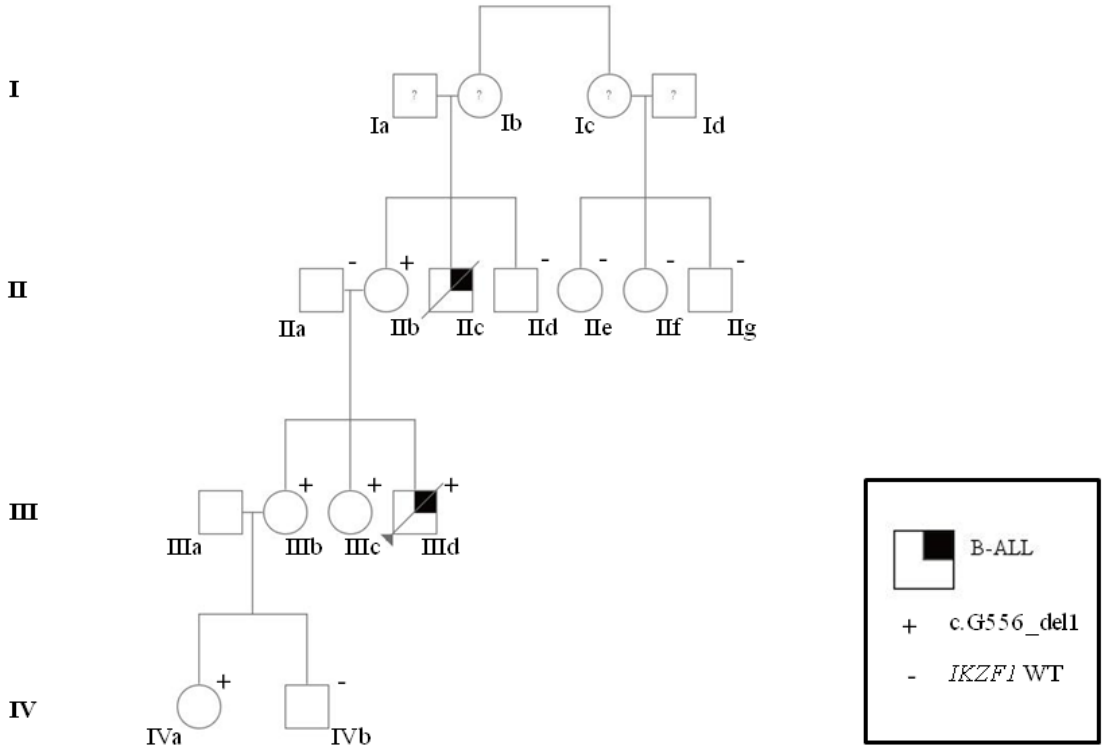

Figure 4.2: pedigree of the family. The proband is indicated by an arrow. Small black squares indicated B-ALL affected children. (+) marks carriers of the c.G556_del1 mutated allele.

Recent Genome Wide Association studies identified particular SNPs as risk variants for ALL[16,17]. Among these the *IKZF1* risk allele rs4132601 showed the strongest association with leukemic risk[16]. Testing of the proband for the presence of the *IKZF1* risk allele rs4132601 resulted negative.

Functional evaluation of the c.556_delG deletion

To test the impact of the frameshift mutation on IKAROS protein, HeLa cells were permanently transfected with wt- or c.556_delG- *IKZF1* coding sequence using the sleeping beauty transposase technique. *IKZF1* sequence was fused with a FLAG-sequence to ease identification of the ectopic protein. Sleeping beauty is a transposable element (DNA elements that have the unique ability to move around in the genome) derived from fish genome that has the feature to permanently integrate in vertebrate genomes. The translation of the mutated *IKZF1* transcript was verified by western blotting, using an α-FLAG (F7425, Sigma Aldrich) for IKAROS protein detection. As reported in Figure 4.3 A, the aberrant allele was translated in a truncated protein at the predicted molecular weight of ~28 KDa. The presence of different bands in the wt-IKAROS samples may be due to different post-translational modifications.

We next examined the sub-cellular localization of truncated protein by Leica DMBL fluorescent microscopy in HEK-293T cells transiently transfected with wt- or c.556_delG-

IKZF1 coding sequence (Figure 4.3 B). IKAROS protein was detected by an α-IKAROS antibody (red) designed to recognize the N-terminus, that is maintained in the truncated form (IKAROS H100, Santa Cruz biotechnology), while nuclei were stained with DAPI (blue). 293T cells do not expressed endogenous IKAROS and were already used in previous studies for IKAROS sub-cellular localization[13,18]. Wt-IKAROS was localized in the nuclei and showed the typical dotted staining, indicating its binding to heterochromatic pericentromeric regions (HC-PC) as described in the literature[19–22]. On the contrary, c.556_delG-IKAROS aberrant protein displayed a diffused pattern in the nuclear region. As we applied fluorescent microscopy we were not able to precisely determine if truncated IKAROS localized in the nuclei or at perinuclear regions. Nevertheless, these data demonstrate that the c.556_delG deletion compromised IKAROS DNA binding.

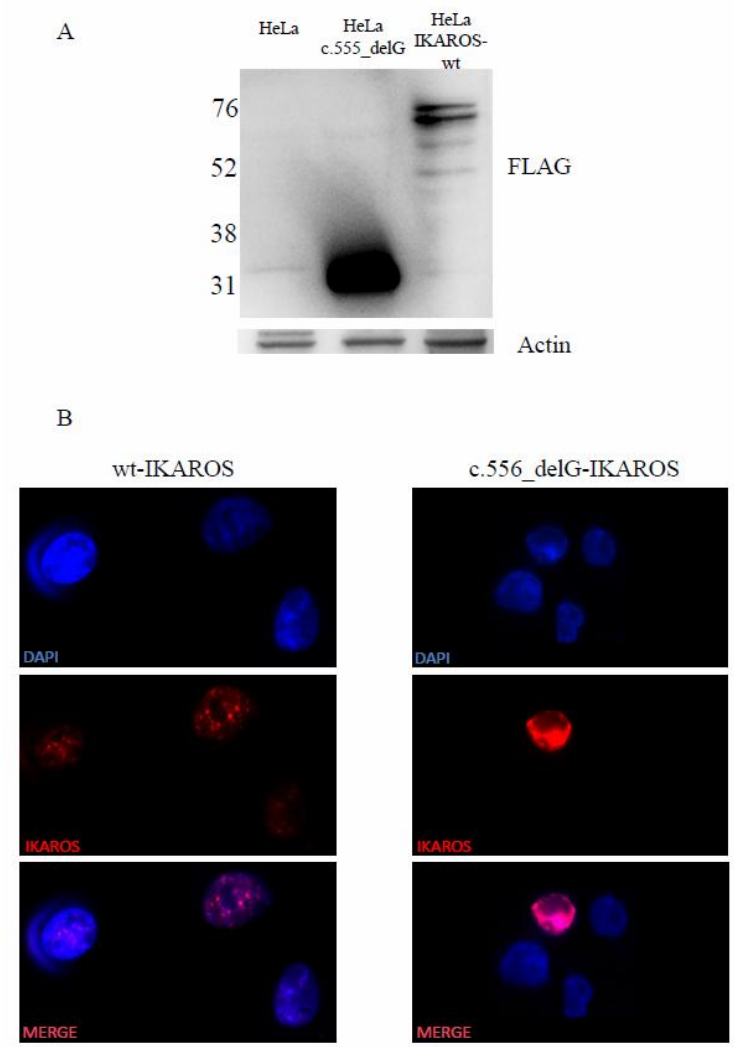

Figure 4.3: Functional analysis on c.556_delG-IKAROS. A) HeLa transfected cells were lysed and 10µg of proteins were loaded in a gel. Wt-HeLa cells were loaded as negative control. Ectopic IKAROS was detected using an α-FLAG antibody. B) Pictures show IKAROS localization in HEK-293T cells transiently transfected with wt- and c.556_delG IKAROS sequences. IKAROS protein was stained using an α-IKAROS antibody against the N-terminus.

One of the proband's sisters, IIIb, decided to cooperate in order to deepen the effect of the mutation in blood cells.

Peripheral-blood mononuclear cells (PBMC) were isolated by ficoll-hypac technique. RNA and proteins were extracted from 10M cells for further experiments. The expression of the mutated allele was evaluated by mRNA retro-transcription and Sanger sequencing of the fifth exon. As reported in Figure 4.4, the mutated allele was expressed in PBMC cells of the proband's sister. We then assessed if the mutated transcript is translated into a truncated protein by western blotting. Anti-IKAROS antibody against the N-terminus part of the protein was used.

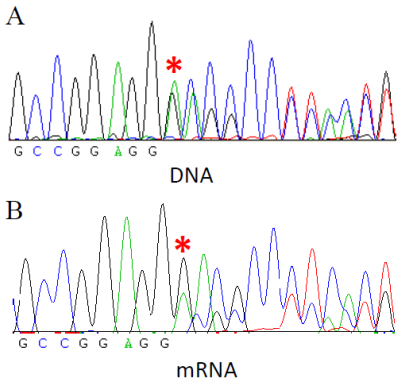

Figure 4.4: Sanger sequencing of proband's sister IIIb: Sanger sequencing of the fifth exon of *IKZF1* performed on the DNA (A) and mRNA (B) samples of IIIb. The mutation is indicated with a red star.

Proteins were extracted from whole PBMC of IIIb; as a positive control, we loaded proteins derived from the c.556_delG-HeLa cell line. PBMC-proteins from a normal donor were included in the analysis as negative control. The truncated protein was detected in IIIb PBMC (Figure 4.5). Of note, the abundance of truncated protein was much lower compare to the normal, longer isoforms, suggesting a high degradation rate of the aberrant protein[23] or the presence of post-transcriptional/translational mechanisms that modify its expression. Taking together, these data indicated that the mutant allele is expressed in normal peripheral blood cells.

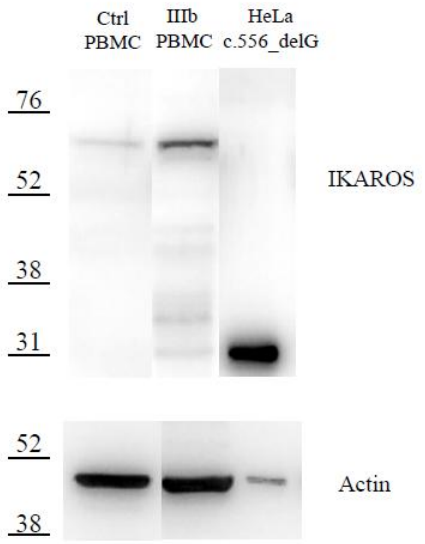

Figure 4.5: Western blot analysis of truncated-IKAROS in blood cells of IIIb. 30µg of proteins were extracted from PBMCs of IIIb(second lane) and loaded in a 12% acrylamide/bis-acrylamide gel. Control PBMC extracted proteins from a healthy donor was loaded as a negative control. 10µg of proteins extracted from a HeLa cell line transfected with c.556_delG-*IKZF1* sequence were loaded as positive control. IKAROS was detected using an α-IKAROS N-terminal antibody.

4.4 DISCUSSION

In conclusion, we identified a reading frame-shift mutation affecting *IKZF1*, one of the most studied genes in relation to pediatric and adult B-ALL, in a family with recurrent ALL in two generations. The mutation was identified during a screening of *IKZF1* mutations in a cohort of Ph+ B-ALL pediatric patients, and the familial recurrence of the mutation was confirmed starting from detection of the mutation in the mother of the proband. The mutation shows reduced penetrance with one known carrier (proband) that developed Ph+ BCP-ALL and IIc who succumbed from leukaemia during childhood (material to establish the *IKZF1* mutation status was not available in this case), while the other four mutation carriers do not display manifested haematological disorders.

Aberrant *IKZF1* is known to be involved in ALL but considered a secondary mutation that occurs after the appearance of strong pathogenic first hit aberrations such as the BCR/ABL1 fusion (Philadelphia chromosome)[24]. Interestingly, in the case of the proband of this study the *IKZF1* alteration being of germline nature acts as a primary leukemic event, whereas the BCR-ABL1 translocation appeared later. Considering the low penetrance of leukaemia in the family, it is reasonable that second-hits acting in synergy with the c.556_delG need to occur in haematopoietic cells in order to establish a leukemic clone.

The difference between the mild phenotype observed in our cases and the severe condition described in the *de novo IKZF1* germline case[13] may be attributed to the precise nature of the respective mutation. In the case of the newborn patient, the mutation was a missense point mutation that compromised the DNA-binding affinity but not the dimerization domain, leading to a dominant negative phenotype, in which case wt-IKAROS would be sequestered by the mutated protein. In our case, the mutation leads to a shift in the reading frame, erasing the forth zing finger and the C-terminal dimerization domain, generating a truncated protein. This aberrant protein lost DNA binding and dimerization capacity in which case the wt-IKAROS protein retains physiological functions.

An Epstein-Barr virus-immortalized cell line[25] was established from the mature B lymphocytes isolated from IIIb. Further analysis on this cell line in addition to a deeper clinical investigation on the healthy mutation carriers will help to understand the impact of an *IKZF1*-haploinsufficient mutation on the human haematopoietic system.

4.5 REFERENCES

1. Woo JS, Alberti MO, Tirado CA. Childhood B-acute lymphoblastic leukemia: a genetic update. Exp Hematol Oncol. 2014 Jan;3:16.

2. Mullighan CG, Downing JR. Global genomic characterization of acute lymphoblastic leukemia. Semin Hematol. 2009 Jan;46(1):3–15.

3. Ribeiro RC, Abromowitch M, Raimondi SC, Murphy SB, Behm F, Williams DL. Clinical and biologic hallmarks of the Philadelphia chromosome in childhood acute lymphoblastic leukemia. Blood. 1987 Oct;70(4):948–53.

4. Biondi A, Schrappe M, De Lorenzo P, Castor A, Lucchini G, Gandemer V, et al. Imatinib after induction for treatment of children and adolescents with Philadelphia-chromosome-positive acute lymphoblastic leukaemia (EsPhALL): a randomised, open-label, intergroup study. Lancet Oncol. 2012 Sep;13(9):936–45.

5. Ng SY-M, Yoshida T, Zhang J, Georgopoulos K. Genome-wide lineage-specific transcriptional networks underscore Ikaros-dependent lymphoid priming in hematopoietic stem cells. Immunity. 2009 Apr 17;30(4):493–507.

6. Ferreirós-Vidal I, Carroll T, Taylor B, Terry A, Liang Z, Bruno L, et al. Genome-wide identification of Ikaros targets elucidates its contribution to mouse B-cell lineage specification and pre-B-cell differentiation. Blood. 2013 Mar 7;121(10):1769–82.

7. Kastner P, Dupuis A, Gaub M-P, Herbrecht R, Lutz P, Chan S. Function of Ikaros as a tumor suppressor in B cell acute lymphoblastic leukemia. Am J Blood Res. 2013 Jan;3(1):1–13.

8. Pui C-H, Robison LL, Look AT. Acute lymphoblastic leukaemia. Lancet. 2008 Mar 22;371(9617):1030–43.

9. Hemminki K, Jiang Y. Familial myeloid leukemias from the Swedish Family-Cancer Database. Leuk Res. 2002 Jun;26(6):611–3.

10. Risks among siblings and twins for childhood acute lymphoid leukaemia: results from the Swedish Family-Cancer Database. Nature Publishing Group; 2002 Jan 21;16(2).

11. Shah S, Schrader KA, Waanders E, Timms AE, Vijai J, Miething C, et al. A recurrent germline PAX5 mutation confers susceptibility to pre-B cell acute

lymphoblastic leukemia. Nat Genet. 2013 Oct;45(10):1226–31.

12. Auer F, Rüschendorf F, Gombert M, Husemann P, Ginzel S, Izraeli S, et al. Inherited susceptibility to pre B-ALL caused by germline transmission of PAX5 c.547G>A. Leukemia. Macmillan Publishers Limited; 2014 May;28(5):1136–8.

13. Goldman FD, Gurel Z, Al-Zubeidi D, Fried AJ, Icardi M, Song C, et al. Congenital pancytopenia and absence of B lymphocytes in a neonate with a mutation in the Ikaros gene. Pediatr Blood Cancer. 2012 Apr;58(4):591–7.

14. Mátés L, Chuah MKL, Belay E, Jerchow B, Manoj N, Acosta-Sanchez A, et al. Molecular evolution of a novel hyperactive Sleeping Beauty transposase enables robust stable gene transfer in vertebrates. Nat Genet. Nature Publishing Group; 2009 Jun;41(6):753–61.

15. Lana T, de Lorenzo P, Bresolin S, Bronzini I, den Boer ML, Cavé H, et al. Refinement of IKZF1 status in pediatric Philadelphia-positive acute lymphoblastic leukemia. Leukemia. 2015 Oct;29(10):2107–10.

16. Papaemmanuil E, Hosking FJ, Vijayakrishnan J, Price A, Olver B, Sheridan E, et al. Loci on 7p12.2, 10q21.2 and 14q11.2 are associated with risk of childhood acute lymphoblastic leukemia. Nat Genet. Nature Publishing Group; 2009 Sep;41(9):1006–10.

17. Prasad RB, Hosking FJ, Vijayakrishnan J, Papaemmanuil E, Koehler R, Greaves M, et al. Verification of the susceptibility loci on 7p12.2, 10q21.2, and 14q11.2 in precursor B-cell acute lymphoblastic leukemia of childhood. Blood. 2010 Mar 4;115(9):1765–7.

18. Gurel Z, Ronni T, Ho S, Kuchar J, Payne KJ, Turk CW, et al. Recruitment of ikaros to pericentromeric heterochromatin is regulated by phosphorylation. J Biol Chem. 2008 Mar 28;283(13):8291–300.

19. Cobb BS, Morales-Alcelay S, Kleiger G, Brown KE, Fisher AG, Smale ST. Targeting of Ikaros to pericentromeric heterochromatin by direct DNA binding. Genes Dev. 2000 Sep 1;14(17):2146–60.

20. Brown KE, Guest SS, Smale ST, Hahm K, Merkenschlager M, Fisher AG. Association of transcriptionally silent genes with Ikaros complexes at centromeric heterochromatin. Cell. 1997 Dec 12;91(6):845–54.

21. Brown KE, Baxter J, Graf D, Merkenschlager M, Fisher AG. Dynamic repositioning of genes in the nucleus of lymphocytes preparing for cell division. Mol Cell. 1999 Feb;3(2):207–17.

22. Kim J, Sif S, Jones B, Jackson A, Koipally J, Heller E, et al. Ikaros DNA-binding proteins direct formation of chromatin remodeling complexes in lymphocytes. Immunity. 1999 Mar;10(3):345–55.

23. Goldberg AL. Protein degradation and protection against misfolded or damaged proteins. Nature [Internet]. Nature Publishing Group; 2003 Dec 18 [cited 2015 Mar 26];426(6968):895–9.

24. Bungaro S, Irving J, Tussiwand R, Mura R, Minto L, Molteni C, et al. Genomic analysis of different clonal evolution in a twin pair with t(12;21) positive acute lymphoblastic leukemia sharing the same prenatal clone. Leukemia. 2008 Jan;22(1):208–11.

25. Tosato G, Cohen JI. Generation of Epstein-Barr Virus (EBV)-immortalized B cell lines. Curr Protoc Immunol. 2007 Feb;Chapter 7:Unit 7.22.

CHAPTER 5

CHARACTERIZATION OF AN *IKZF1* KNOCK-OUT PRE-B CELL MODEL TO STUDY IKAROS-MEDIATED GENE EXPRESSION REGULATION

Tobia Lana[1], Ziwei Liang[2], Giuseppe Basso[1], Matthias Merkenschlager[2], Geertruy te Kronnie[1]

[1]Department of Women's and Children's Health, University of Padova, Padova, Italy; [2]Lymphocyte Development Group, and 2Epigenetics Section, MRC Clinical Sciences Centre, Faculty of Medicine, Imperial College London, London, United Kingdom

ABSTRACT

Ikaros is a zinc finger transcription factor protein that pays a pivotal role in haematopoiesis. It is expressed from haematopoietic stem cell progenitors, and its level increases dramatically during lymphoid commitment. In lymphoid progenitors, Ikaros switches off myeloid, erythroid and stem-cell primed-genes and activates lymphoid-specific genes, piloting B and T cells progenitors towards differentiation. Despite the importance of Ikaros in haematopoiesis, till recently a clear genome-wide map of Ikaros-target genes was not available, and still now the underlying mechanisms of Ikaros-mediated gene expression regulation are not fully understood. In this study, we combine an inducible Ikaros system with Ikaros-ko cell model, to discern the real effects of inducible Ikaros activation from pre-existing modifications caused by active endogenous Ikaros. Firstly, we confirmed the absence of endogenous Ikaros protein, and then we verified the ability of exogenous inducible Ikaros to translocate in the nucleus in response to 4-hydroxytamoxyfen treatment and to bind the promoter of a previously described Ikaros target gene. Inducible Ikaros is able to up-regulate the *Lig4* and *Zfp36* genes, but failed to repress the expression of *Myc*, *Ccnd2* and *Igll1* genes. In Ikaros-ko cells, inducible Ikaros did not significantly arrest the cell cycle, as demonstrated by cell cycling profiling experiments.

5.1 INTRODUCTION

B cell development progress through a series of developmental stages aimed at maturation of a functional, not self-responsive, B cell receptor. At the pre-proB stage starts the immunoglobulin heavy chain (IgH) recombination process. The rearranged IgH is assembled with the surrogate light chains (SLC) λ5 and VpreB proteins to form the preB cell receptor (preBCR). PreBCR expression induces a proliferative expansion in cycling-preB cells, and simultaneously induces a negative feedback signal that down-regulates SLC proteins expression and the cell cycle regulator *c-Myc*. PreBCR signal termination pilots cells out of the cell cycle and starts the rearrangement of the immunoglobulin light chain (IgL) locus. This stage is defined as resting-preB. The assembling of mature IgL with the IgH give rise to a mature BCR that identifies immature B cells[1,2]. A network of transcription factors that in a combinatorial manner specify cell fate orchestrates each step of the differentiation process. Ikaros is a transcription factor expressed from the HSC stage that plays a pivotal role in the commitment and specification of the lymphoid lineage[3]. Studies on transgenic mice highlighted a severe phenotype connected to *Ikzf1* depletion, with a complete ablation of B and NK progenitors, and an impaired development of T-cell progenitors[4,5]. These mice invariantly developed a aggressive form of T-leukaemia/lymphoma within 6 weeks after birth[4]. In human, IKZF1 is rarely mutated/deleted in T-cell acute lymphoblastic leukaemia (T-ALL), but was found frequently deleted in paediatric and adult B-cell acute lymphoblastic leukaemia (B-ALL), in particular in cases harbouring the BCR-ABL chromosomal translocation[6].

During Haematopoiesis, Ikaros is essential for priming the lymphoid-specific genes in HSC and multipotent progenitor (MPP) cells. In *Ikzf1* null mice, MPP failed to give rise to common lymphoid progenitor (CLP) cells, explaining the severe phenotype observed in mice. Moreover, MPP cells displayed an abnormal up-regulation of stemness- and myeloid-related genes. Therefore, Ikaros is involved in both lymphoid commitment and in extinguishing stem-cells and other lineage-specific genes signatures[7]. Ikaros deficiency in proB cells arrested them at this stage, due to defects in preBCR signalling[8]. At the cycling-preB stage, Ikaros acts in synergy with Aiolos to silence the SLC encoding-genes *Igll1* and *VpreB* and to activate *Rag1/2* to promote the *IgL* rearrangement [9,10]. In parallel, Ikaros and Aiolos downregulate *c-Myc* [11] and other cell-cycle promoters such as cyclines *Ccnd2, Ccnd3* and the cyclin-dependent kinase 6 (*Cdk6*), leading to arrest in cell cycle and accumulation of cells in G1 phase[10]. Although Ikaros targets were intensively investigated in the last years, the mechanisms by which Ikaros exploits its function are still poorly

understood. As a transcription-repressor, Ikaros is frequently associated with the NuRD complex, composed by the Mi-2β nucleosome remodeler sub-unit and by the HDAC deacetylase proteins[12]. Ikaros-NuRD complex was shown to localize at pericentromeric-heterochromatic regions of the genome together with their repressed-genes[13]

5.2 MATERAL AND METHODS

Cell Culture

The murine preB cell line B3 was isolated and cloned in Professor Fisher's lab from a lymphoma in an IL-7 transgenic mouse (Fisher et al 1995). This cell line was maintained in culture in Iscove's modified Dulbecco medium (IMDM) containing 10% (v/v) foetal calf serum (FCS) (Biosera) and antibiotics (100U/ml Penicillin and 100µg/ml Streptomycin, GIBCO, Invitrogen). Cells were kept in culture at a density between 0.1 and 1 x 10^6 cells/ml. The human embryonic kidney 293T cell line cells were cultured in Dulbecco modified Eagle medium (DMEM) supplemented with 10% (v/v) FCS, 2mM L-glutamine and antibiotics.

Virus production

293T cells were cultured in 10cm petri dishes at approximately 40% of confluence in 9 ml of DMEM medium. MSCV vector (4µg) and 4µg of pECO or 10A1 envelop helper plasmid DNA were added to 500 µl of 0.4M $CaCl_2$ solution. 500µl of 2x HEBS (12mM dextrose, 50mM HEPES, 280mM NaCl, 10mM KCl, 1.5mM Na_2HPO_4 + $2H_2O$ in sterile water) and were then added to the plasmid mix drop by drop. The transfecting solution was then added to cells drop by drop. The cell medium was changed 12h after transfection. After 24h, 3.5ml of fresh media was added to cells, and virus-containing media were collected at 36, 48 and 60 hours from transfection, and pooled together.

Infection

The retroviral media was filtered with a 0.22µm filter, and is supplemented with 10mM pH 7.6 HEPES and 4µg/ml polybrene (Sigma-Aldrich). 1.3 millions B3 cells were suspended in 3ml of retroviral media and plated in a 6-well plate. Cells were then centrifuged for 90' at 37 °C at 2500rpm to increase the infection rate. Retroviral media was then changed with fresh one and cells were put at 37 °C. 48h later, infected cells were sorted by FACS for positivity of specific fluorophores.

Cell sorting

Cells were sorted using a FACSAria IIu, based on positivity to mCherry. For sorting, cells were resuspended in basic sorting buffer (1x phosphate buffered saline (PBS) Ca/Mg^{++} free, 1mM EDTA, 25mM HEPES pH 7.0, 1% FCS) and collected in PBS Ca/Mg^{++} free supplemented with 20% of FCS. Sorted cells were then cultured for at least 24h in complete media supplemented with 5µg/ml of gentamycin.

Cell cycle analysis

$0.5x10^6$ cells were washed once in PBS-/-, and then resuspended in 300µl of propidium iodide buffer (PBS-/- supplemented with 10µg/ml RNAsi A (life technologies, NY, USA), 50µg/ml propidium iodide (Sigma-Aldrich) and 0.05% v/v NP40 (Calbiochem, Merck Millipore)). Cells were incubated 10' at room temperature and 20' on ice and subsequently analysed using a DB LSRII flow cytometer.

Immunofluorescence

B3 cells were plated for 1h in 12-well plates with poly-L-lysine coated coverslips (BioCoat). Coverslips were washed with $PBS^{-/-}$ and fixed with 4% paraformaldehyde (PFA) in $PBS^{-/-}$ for 10' at room temperature. Fixed samples were washed twice in $PBS^{-/-}$ and then permeabilized with 0.5% TritonX-100 for 5'. Cells were incubated for 30' at room temperature with blocking solution (3% normal goat serum, 0.1% TritonX-100 in $PBS^{-/-}$). Primary antibodies were diluted 1:1000 in blocking solution and added to the samples overnight at 4 °C in a humid chamber. Coverslips were washed 3x with $PBS^{-/-}$ and incubated with secondary antibodies conjugated with appropriate fluorophores diluted 1:10000 in blocking solution for 1h at room temperature in a humid chamber in the dark. Coverslips were washed 3x $PBS^{-/-}$ and mounted in Vecatshield (Vector laboratories) with DAPI 0.1µg/ml. samples were viewed using a TCS SP5 Leica laser scanning confocal microscope. Images were analysed using Leica confocal software.

Protein extraction and quantification

1 to 3 $x10^6$ cells were washed once in cold PBS-/- supplemented with protein inhibitor cocktail (Roche) and then re-suspended in 1 volume of cold $PBS^{-/-}$ supplemented with protease inhibitor cocktail. One volume of 2x sample buffer (100mM Tris pH 6.8, 20% glycerol and 2% of sodium dodecyl sulphate (SDS)) was added to cells, and the cell mix was subsequently boiled at 95 °C for 10'. Protein concentration was measured using the Pierce™ BCA protein assay kit (Thermo scientific) according to manufacturer's instruction. After quantification, 10% v/v of β-mercaptoethanol and 0.002% of bromophenol blue were added to the protein assay. Protein were stored at -20 °C.

Western blot

Proteins and Benchmark pre-stained protein ladder (Beckman) were loaded on a SDS-polyacrylamide gel. The gel is formed by an upper staking gel (4% w/v acrylamide, 125mM Tris-HCl pH 6.8, 0.1% SDS, 0.067% ammonium persulphate (APS) and 0.12% N,N,N'tetramethylethylenediamine (TEMED)) and a running gel (10% acrylamide, 390mM Tris-HCl pH 8.8, 0.1% SDS, 0.05% APS and 0.1% TEMED). Bio-Rad minigel system is used for the electrophoretic run together with running buffer (25mM Tris base, 192mM glycin and 0.1% SDS). The electrophoretic run was performed at 30mA per gel for 90'. Proteins were transferred to a polyvinylidene fluoride (PVDF) membrane using the trans-blot® SD semi-dry transfer cell (Bio-Rad) with transfer buffer (48mM Trizma base, 39mM glycin, 0.037% w/v SDS and 20% v/v ethanol) for 1h at 140mA/25mV per gel. The membrane was incubated 1h in blocking solution (5% w/v fat free milk powder (Marvel), 1.2g/l Tris pH 7.4 and 8.75g/l NaCl) and subsequently incubated ON at 4 °C with diluted primary antibodies in blocking solution with agitation. The membrane was then washed 3x10' in T-TBS (1.2g/l Tris pH 7.4, 8.75g/l NaCl and 0.1% tween20 20%) and subsequently incubated with horseradish peroxidase-coupled secondary antibodies (αRabbit and αMouse secondary antibodies are provided by Amersham) diluted 1:5000 in blocking solution for 1h at room temperature. The membrane was washed 3x10' with T-TBS and the detection was done using Luminata Crescendo Western HRP substrate (Millipore) following manufacturer's instruction with Kodak X-Omat photographic films.

RNA extraction

At least $1x10^6$ cells were washed once in cold $PBS^{-/-}$. RNA extraction was performed using QIAshredder and RNeasy Mini kit (Qiagen) following manufacturer's instruction. Residual DNA was cleared using the DNA-free kit (Ambion) according to manufacturer's instruction. RNA was quantified using Nanodrop

Reverse transcription

Reverse transcription was performed using Superscript First-Strand Synthesis system (Invitrogen). 1µg of RNA was mixed with 1µl of 10mM dNTPs mix and 1µl of 0.25mM random primers, topped up to 13µl with RNase-free H_2O. The RNA mix was incubated at 65 °C for 5' and then 1' at 4 °C. A mix composed of 1µl of 0.1M of DTT, 1µl RNasi-OUT, 5µl of 4x first strand buffer and 1µl of 200U/µl Superscript III reverse transcriptase was added to the RNA mix. The final mix was incubated at 25 °C for 5', at 50 °C for 1h and at 75°C for 15'. The obtained cDNA was diluted 10x.

Real-time quantitative PCR

The real-time reaction mix was composed by 2x SYBR Green qPCR mastermix (Qiagen), 0.3mM primers and 1µl of cDNA in a final volume of 12µl. The program used for RT-qPCR was: 95 °C for 15', then 40x(94 °C for 15', 60 °C for 30' and 72 °C for 30'). The melting curve was determined from 72 to 90 °C at 0.2 °C intervals. qPCR quantification was performed using Bio-Rad CFX96 real-time PCR machine, and was analysed using CFX96 Manager Software. The relative abundance of detected transcripts was calculated using the ΔΔC(t) method. Briefly, C(t) is the number of amplification steps needed to detect the fluorescence of PCR products above background. The relative abundance of the gene of interest C(t)1 compared to a reference C(t)2 can be calculated as $2^{-\Delta C(t)1}/2^{-\Delta C(t)2}$. For gene expression, housekeeping genes were used for normalization.

Chromatin Immune Precipitation (ChIP)

$30x10^6$ cells were washed once in cold PBS-/- and resuspended in 18ml of PBS-/- supplemented with 1mM Disuccinimidyl glutarate (DSG, Thermo Scientific) and incubated at a very low speed on a rotating incubator for 30' at room temperature. Cells were then washed once with PBS-/- and re-suspended in 18ml of PBS-/-, and fixed again with 1% formaldehyde adding 2ml of fixation buffer (0.5mM EGTA pH 8.0, 100mM NaCl, 1mM EDTA, 50mM HEPES pH8.0 and 10% formaldehyde in sterile water). The cells were incubated at a very low speed on a rotating incubator for 10' at room temperature. Fixation was stopped by adding glycine at a final concentration of 140mM and incubated for 5' more. Fixed cells were centrifuged at 4 °C at 3000rpm for 5', and washed twice with cold PBS-/-. Cell pellet was then re-suspended in 0.5ml of cell lysis buffer (25mM HEPES, 1.5mM $MgCl_2$, 0.1% v/v NP40 in sterile H_2O) supplemented with protease inhibitor cocktail (Roche), and lysed on ice for 15'. Samples were then pelleted by centrifuging at 4 °C for 20' at 900rcf, and re-suspended in nuclear lysis buffer (50mM Tris-HCl pH 8.1, 10mM EDTA and 0.5% v/v SDS) for 5' on ice. Fragmentation of chromatin was done by sonication at high speed for 30', 30'' on and 30'' off at 4 °C using a Bioruptor® (Diagenode). Un-sonicated chromatin and debris were eliminated by centrifugating the sample at 25000rcf for 15' at 4 °C, and supernatant was taken for ChIP. Chromatin was quantified by a 10x dilution in 0.1M NaOH and measured by Nanodrop. 100µg of chromatin was used for IP. 10µl of Dynabeads® protein G (Life technologies) was washed twice in 10 times volume of cold RIPA buffer (150mM NaCl, 10mM Tris-HCl pH 7.5, 1mM EDTA pH 8.0, 0.5mM EGTA pH 8.0, 1% v/v TritonX-100, 0.1% SDS, 0.1% sodium deoxycholate) and incubated with α-IK-C or control α-IgG for 3h at 4 °C in

agitation. Beads were then washed twice with cold RIPA buffer on a magnetic stand. 100µg of chromatin was incubated ON with beads-antibodies at 4 °C on a rotating platform. Unbound chromatin and non-specific binding were washed away by 3x 5' washes with RIPA buffer, 3x 5' washes with high salt RIPA buffer (RIPA buffer with a final concentration of NaCl of 500mM), 2x 5' washes with LiCl buffer (RIPA buffer with the addition of 250mM LiCl) and TE buffer (10mM Tris-HCl pH 7.5, 1mM EDTA). Washed beads were suspended in 300µl of elution buffer (50mM Tris, 1mM EDTA, 1% v/v SDS, 100µg/ml RNasi A and 50µg/ml protease K) and incubated 2h at 37 °C and ON at 65 °C with agitation. DNA was extracted using a phenol/chloroform protocol and precipitated with ethanol and sodium acetate. For qPCR analysis, 1µl of 50µl was used per reaction in a final volume of 12µl.

Ikaros induction

Exogenous ERt2-Ikaros was induced from the cytoplasm to the nucleus by adding 0.5µM 4hydroxytamoxifen (4OHT, Sigma-Aldrich). Time course experiments were performed by inducing Ikaros translocation at different time point and processed at the same end time point for subsequent analysis.

5.3 RESULTS

Construction of an Ikzf1-ko cell line model

The murine preB B3 cell line, isolated from an IL-7 transgenic mouse [14], was used as a model of cycling preB lymphocytes to study the role and kinetics of Ikaros in gene expression regulation. The *Ikzf1* locus was disrupted using the CRISPR-Cas9 gene editing system. Briefly, The CRISPR-Cas9 complex is composed of a small single guide RNA (sgRNA) and a non-specific CRISPR-associated endonuclease,–Cas9. The sgRNA is formed by a scaffold sequence and a user-defined 20 nucleotide target sequence, complementary to the genomic DNA to be edited. Cas9 is recruited to target DNA by sgRNA, and cuts the double strand DNA with its 2 endonuclease domains. The double-strand break will be repaired by the error-prone non-homologous end joining (NHEJ) system that inserts small indels at the break site.

The Ikaros knock-out (Ikaros-ko) experiments were performed by Lee Cooper, a PhD student in Prof Merkenschlager's lab. The single guide RNA (sgRNA) was designed complementary to the first 53 nucleotides of the second exon of *Ikzf1*, which contains the start codon. The sgRNA, the human codon optimized SnCas9 and a GFP expressing vector

were co-transfected into wt-B3 cells. Single GFP positive cells were sorted into 96-well plate to let them proliferate.

Individual clones were then tested by restriction fragment length polymorphism (RFLP) analysis. Briefly, a region of 530 nucleotides containing the target exon was amplified by PCR and the products were then digested with TaqaI, a restriction enzyme that cuts within the Cas9 target sequence. PCR products from WT clones containing the intact restriction site were cut by TaqaI, while in the mutated clones small indels disrupted the site, resulting in non-digested PCR products. Heterozygous clones displayed one uncut band and two cut fragments, and homozygous clones had 2 uncut bands. DNA sequencing confirmed the presence of indels. Following the above method, six clones were selected: C2, D6, E2, E3, E9, and G11.

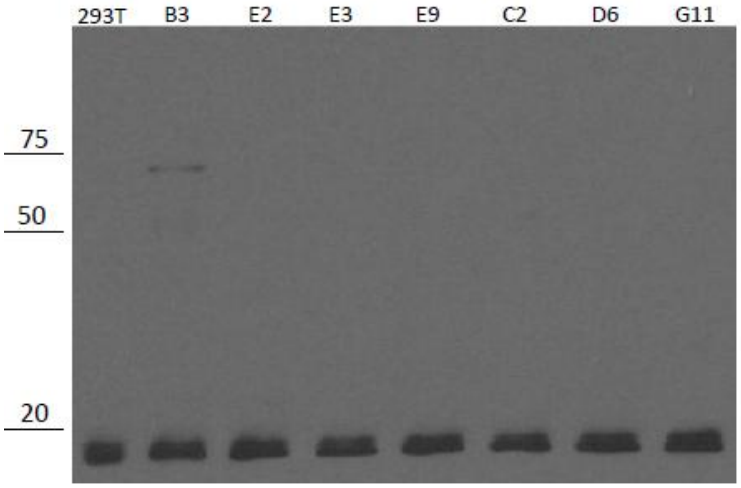

Figure 5.1: Detection of endogenous Ikaros in CRISPR-Cas9 clones. Proteins extracted from 293T cell line, wt-B3 cells and from the 6 *Ikzf1-ko* cell lines C2, D6, E2, E3, E9 and G11 were loaded in the western blot. 293T and wt-B3 proteins were loaded as negative and positive controls respectively. Endogenous Ikaros was detected using Ikaros antibody. α-tubulin was used as a loading control. The band present in wt-B3 sample identified Ikaros. No Ikaros was detected in CRISPR-Cas9 clones.

The presence of endogenous Ikaros in this cell line model was checked by immunoblotting using an antibody to the C-terminal part of the protein (Figure 5.1). Wt-B3 cells are loaded in the gel as positive control, while 293T cells proteins are included as negative control, as this human embryonic kidney cell line does not express endogenous IKAROS [15]. The Ikaros band was detected in the wt-B3 cells lane but not in the 6 CRISPR-Cas9 *Ikzf1*-ko clones, as shown by western blot. This data demonstrated the absence of endogenous Ikaros in the ko clones, and validated the Ikaros-ko model.

The Ikaros-ko clones were then transducted with an inducible Ikaros system, developed in prof Merkenschlager's lab. The system consists in a full-length Ikaros sequence fused with

a hemagglutinin (HA) epitope at the N-terminus and with the ligand-binding domain of the estrogen receptor (ERt2) at the C-terminus. The HA-Ikaros-ERt2 sequence is inserted upstream of an internal ribosome entry site (IRES)-mCherry sequence, so HA-Ikaros-ERt2 protein and the fluorescent mCherry protein are translated from the same transcript (Figure 5.2A). mCherry fluorescence intensity was used as an indicator of fusion protein expression and to sort transfected B3 cells.

The HA-Ikaros-ERt2 fusion protein is constitutively expressed but is sequestrated in the cytoplasm by heat-shock proteins (HSP) that bind the ERt2 domain. To induce the translocation of the Ikaros fusion protein to the nucleus, 4-hydroxytamoxifen (4OHT), an ERt2 ligand, is added to the culture media. 4OHT abolishes the HSP-Ikaros fusion protein interaction, leading to the translocation of the fusion protein to the nucleus thanks to its nuclear localization sequence (Figure 5.2B).

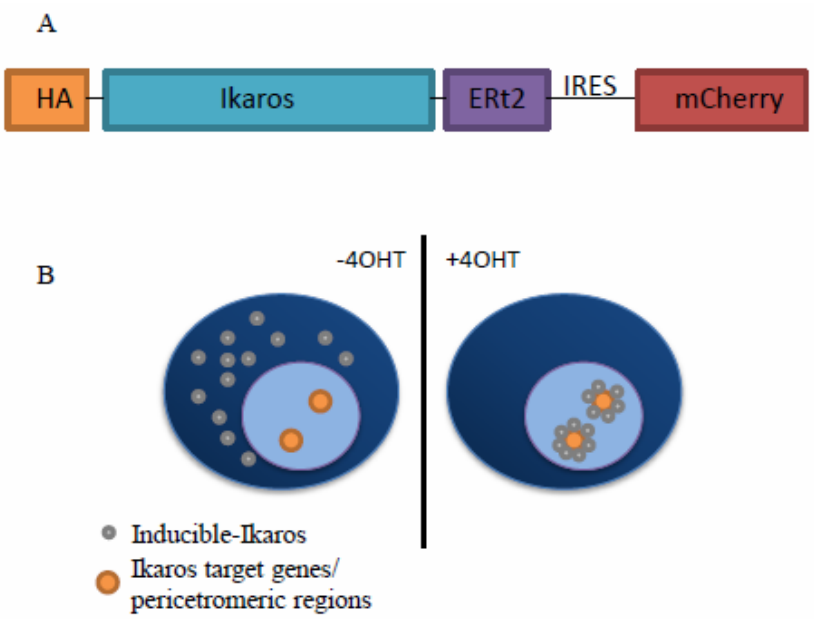

Figure 5.2: Schematic representation of the inducible Ikaros system. A) Schematic representation of the inducible Ikaros construct cloned in MSCV vector. HA, hemagglutinin; Ikaros, the longest Ikaros isoform; ERt2, ligand binding domain of the oestrogen receptor; IRES, internal ribosome entry site; mCherry, a red-fluorescent protein. B) Schematic representation of the experimental system. Inducible Ikaros is constitutively expressed by cells and is retained in the cytoplasm. Addition of 4-hydroxytamoxifen-induces Ikaros nuclear translocation. In the nucleus inducible Ikaros binds to target genes. Adapted from Ferreirós-Vidal I., et al., 2013.

Inducible Ikaros localization and translocation

The sub-cellular localization of the Ikaros fusion protein was evaluated in non 4OHT-treated cells by immunofluorescence (IF) microscopy. Inducible Ikaros was detected by α-HA antibody (green), while the nuclei were marked with DAPI (blue). Cells are imaged by confocal microscopy (Figure 5.3). The Ikaros signal localized most abundantly in the

cytoplasm, but a fraction of inducible Ikaros co-localized with DAPI staining in the nuclei of all B3 clones as well. The same issue was previously observed in the wt-B3 inducible Ikaros model expressing endogenous Ikaros.

Ikaros ability to translocate to the nucleus was then tested by IF (Figure 5.4). Cells were treated with 0.5μM of 4OHT for 1h and then fixed, stained and imaged at confocal microscopy as previously described. After 1h of 4OHT induction, the majority of inducible Ikaros translocated to the nucleus and showed the characteristic toroidal spots at pericentromeric regions. Taken together, these data indicate that inducible Ikaros can efficiently translocate into the nucleus after 4OHT induction and formed clusters at pericentromeric regions.

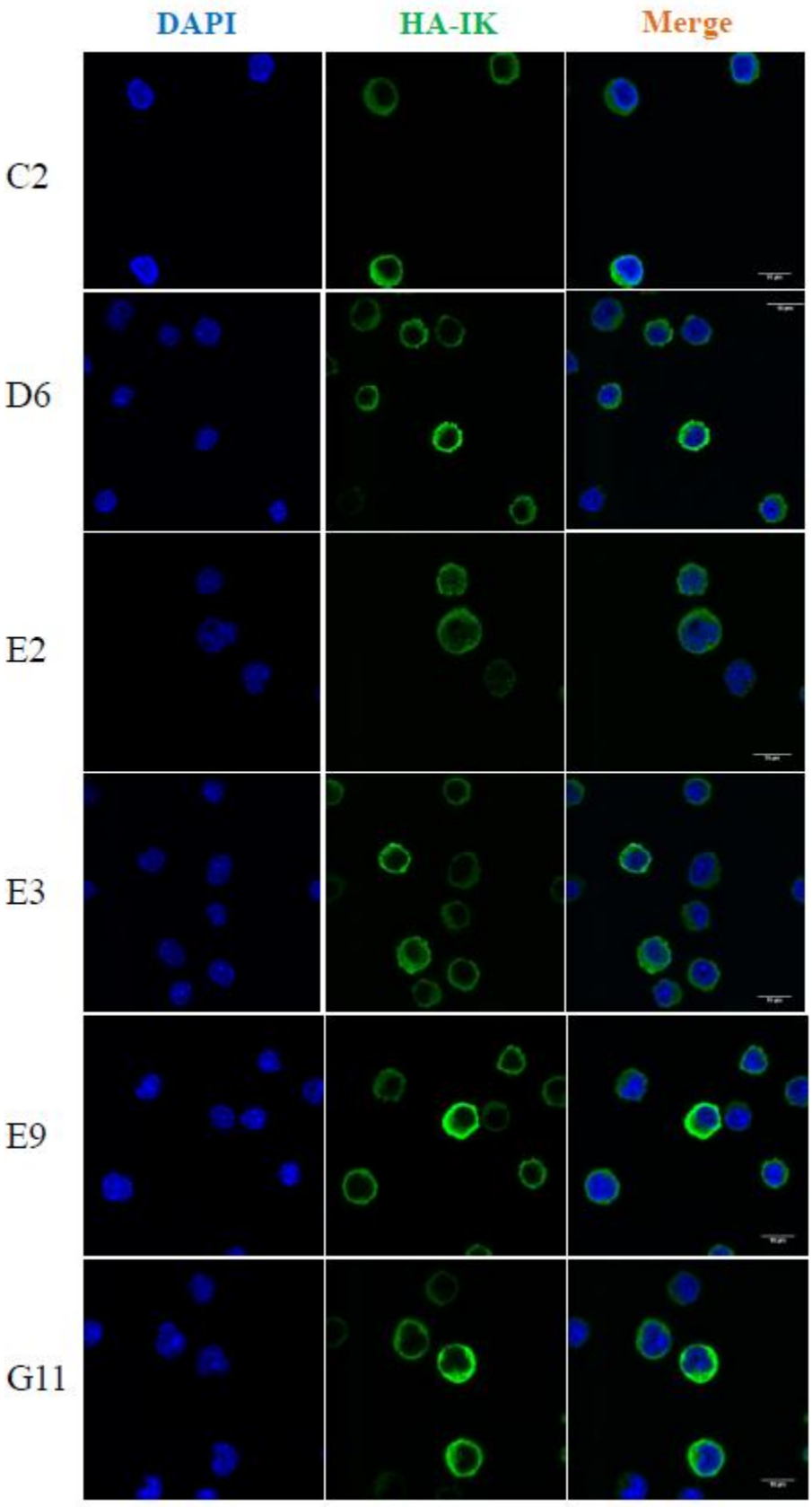

Figure 5.3: Inducible Ikaros localization before 4OHT treatment. Inducible Ikaros was detected by α-HA antibody (green). Nuclei were stained with DAPI (blue). Images were acquired using a TCS SP5 Leica laser scanning confocal microscope.

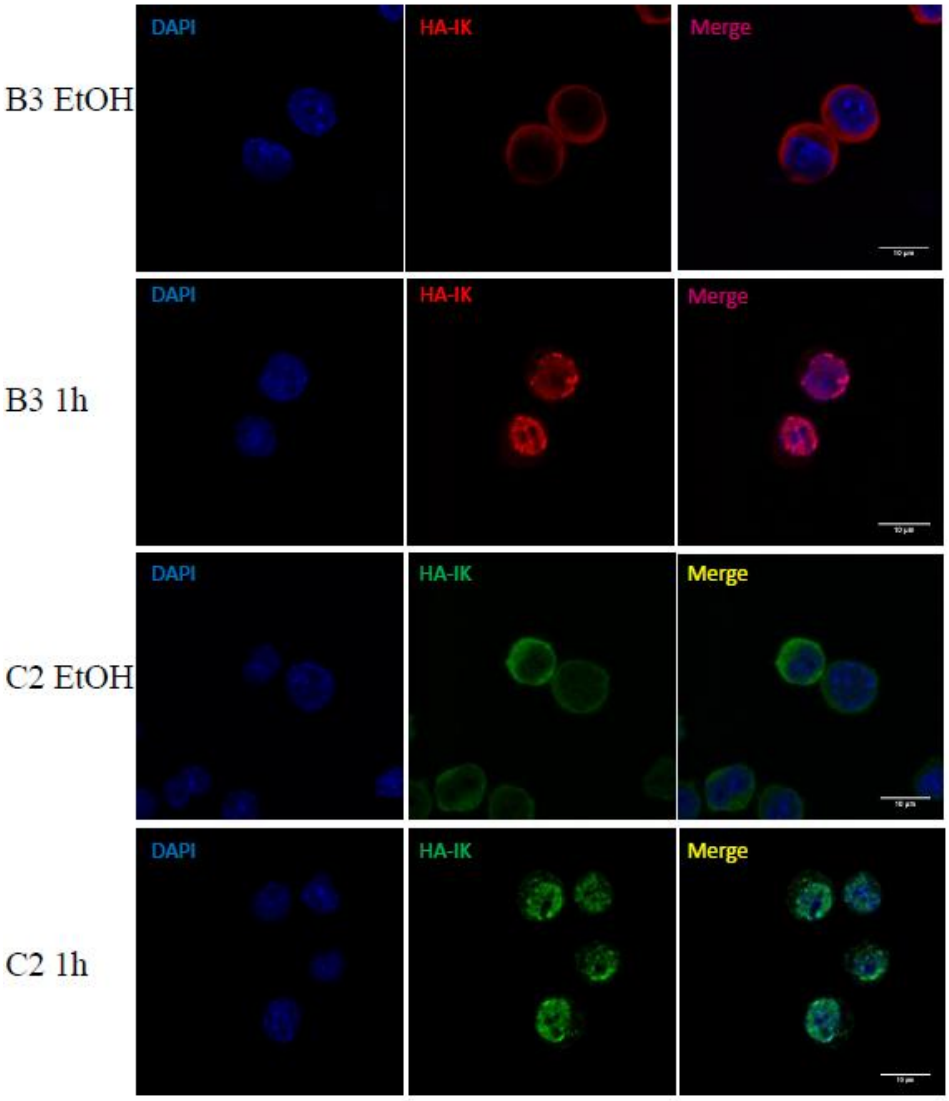

Figure 5.4: Ikaros translocation induced by 4OHT treatment. Ikaros-wt B3-inducible Ikaros cells and Ikaros-ko E2 clones were imaged by TCS SP5 Leica laser scanning confocal microscope before (EtOH) and after 1 hour (1h) of 4OHT treatment. After 1h most of inducible Ikaros translocated in the nuclei, and formed clusters at pericentromeric heterochromatic regions.

For the further characterization of our cellular model, the experiments were conducted in the C2 and E9 clones, because these clones displayed the lowest level of Ikaros nuclear localization in un-induced cells.

Inducible Ikaros binding at a target gene

To further characterize inducible Ikaros function in Ikaros-ko cells, we evaluated its binding to the promoter region of *Igll1*, which encodes the λ5 component of the preB cell receptor (preBCR). Ikaros down-regulates *Igll1* expression, guiding preB cells from a proliferative state to a resting state and initiating the rearrangement of the BCR light chains locus [9].

We addressed the capacity of inducible Ikaros to bind to the *Igll1* promoter by ChIP experiments after 1h of 4OHT induction. To control for carrier effects, cells were treated with ethanol (EtOH) for 1h as control. Ikaros ChIP was performed using α-Ikaros antibody to the C-terminus. Ikaros enrichment was evaluated by RQ-PCR and normalized to input signal. As a negative control, IgG was included in the experiment. To obtain a precise map of Ikaros binding sites at the *Igll1* promoter, we used primers that amplified the surrounding region on either side of the expected Ikaros binding sites.

Without 4OHT induction (EtOH), modest Ikaros binding was observed at -200bp and 100bp from the transcription star site (TSS) consistent with the presence of some inducible Ikaros proteins in the nuclei detected by IF. After one hour of induction (4OHT), the Ikaros binding at -200bp showed a 5-fold increased in the C2 clone and 11-fold in the E9 clone. A second smaller peak appeared at -1300bp in both clones (Figure 5.5). This data suggests that inducible Ikaros was able to bind at the *Igll1* promoter after 4-hydroxytamoxifen induction.

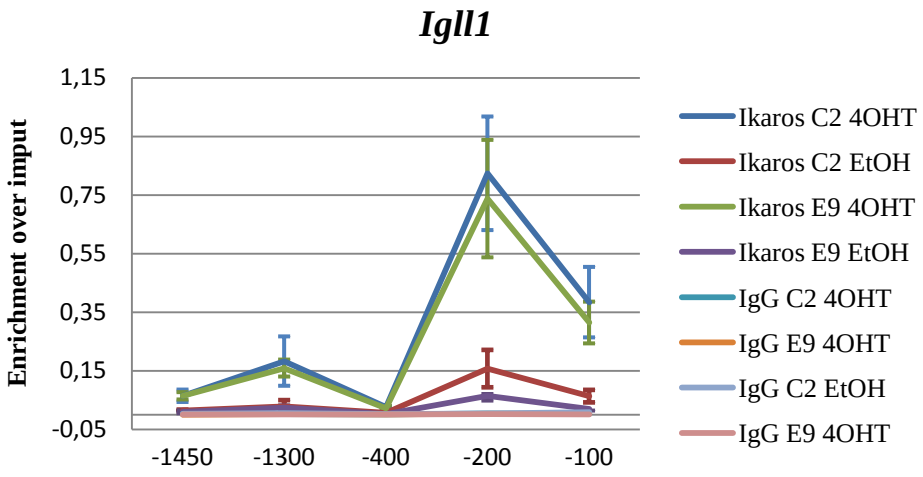

Figure 5.5:Inducible Ikaros binding to *Igll1* promoter. The Ikaros binding to *Igll1* promoter was detected by ChIP-RQ-PCR using Ikaros antibody in untreated (EtOH) or 4OHT treated sample for 1h (4OHT). IgG negative controls are reposted. Data shown is an average of 3 biological replicates. Standard errors are reported.

Regulation of gene expression

We then tested the ability of inducible Ikaros to regulate transcription. For this purpose, we selected genes that were previously described to be bound and regulated by Ikaros in B3 cells [10]. We analyzed 2 Ikaros up-regulated genes, *Lig4* and *Zfp36*, and 3 down-regulated genes: *Ccnd2*, *Igll1* and *Myc*. For gene expression analysis, C2 and E9 cells were sorted for high levels of mCherry, corresponding to high levels of inducible Ikaros protein. Cells were sorted to obtain comparable inducible Ikaros level between the two clones and the B3

inducible Ikaros control. As Ikaros was demonstrated to regulate transcription very shortly after its translocation into the nucleus (Liang Z., personal communication), we monitored the expression of candidate genes after 5', 15', 30' and 1h, and finally at 6h after induction with 4OHT. To follow these rapid changes in gene expression, intronic-exonic primers were used, in order to detect the level of primary unspliced (immature) transcripts. Transcript levels were evaluated by RQ-PCR. Expression was normalized to the *Ubc* and *Ywhaz* housekeeping genes and values were normalized to the EtOH, un-induced sample. We performed gene expression experiments also on wt-B3 inducible Ikaros cells and wt-B3 cells transduced with inducible HA-ERt2-mCherry control vector, as positive and negative control of the experiment. Firstly, we analyzed the gene expression of the Ikaros up-regulated genes (Figure 5.6).

In wt-B3 inducible Ikaros cells, *Lig4* was up-regulated after 1h and *Zfp36* after 15' of 4OHT induction, and their level of expression became progressively higher over the 6 hours.

C2 and E9 Ikaros-ko clones showed a significant up-regulation of *Lig4* after 6h, and after 1h for the *Zfp36*. The *Lig4* and *Zfp36* up-regulation was faster and stronger in magnitude in wt-B3 cells compare to the Ikaros-ko clones. These differences could be ascribed to the presence of endogenous Ikaros in the nuclei of wt-B3 cells, that could facilitate inducible Ikaros binding to target genes, as well as of small difference in the inducible Ikaros level between wt-B3 and Ikaros-ko cells.

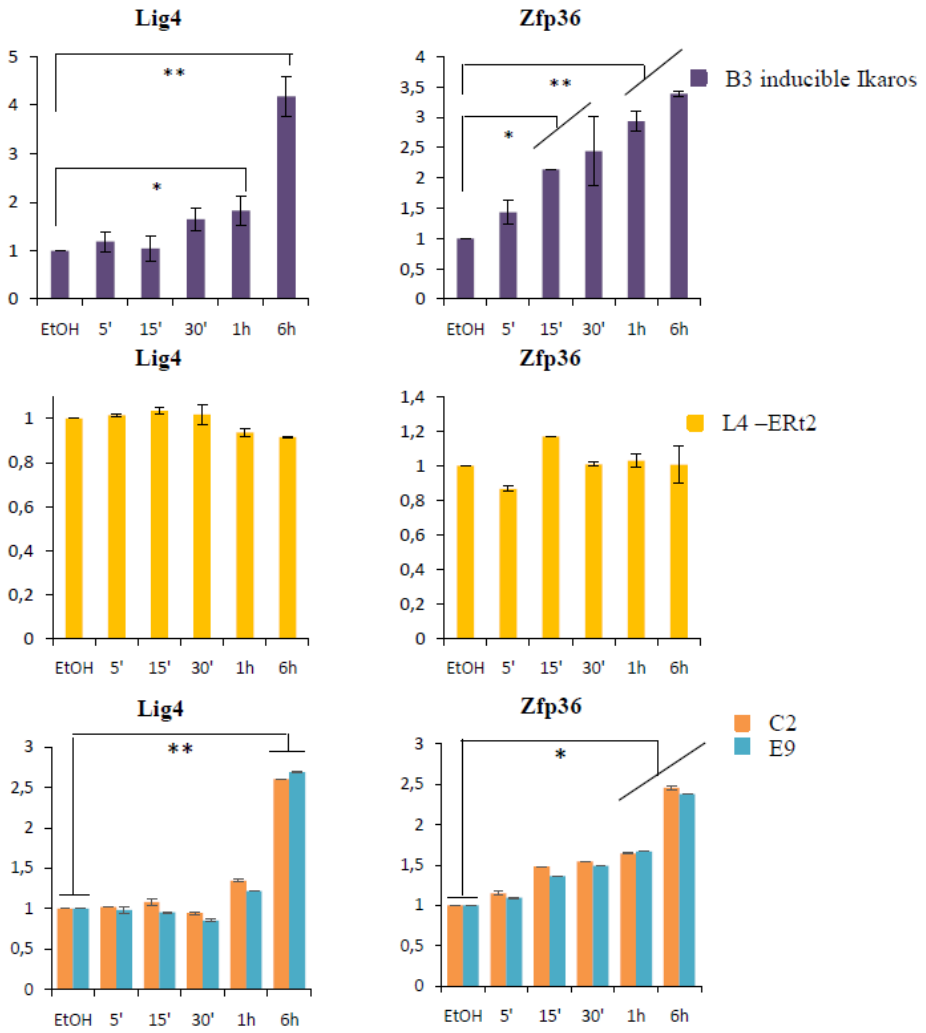

Figure 5.6: Transcriptional regulation of selected Ikaros up-regulated target genes. Histograms show the relative expression of candidate genes normalized to the untreated control (EtOH). RNA samples were collected after 5', 15',30', 1h and 6h after addition of 4OHT. The gene expression changes were monitored in wt-B3 inducible Ikaros, empty vector control and in Ikaros-ko C2 and E9 cell lines. Student's T test p value: *p<0.05, **p<0.01. Data shown is an average of 3 biological replicates. Standard errors are reported.

The behaviour of the down-regulated genes was then analyzed in C2, E9 and wt-B3 inducible Ikaros cell lines (Figure 5.7). None of these 3 genes were significatively down-regulated in C2 and E9 cell lines. C2 displayed a small down-regulation of *Ccnd2* after 1h, and of *Igll1* after 30', but the changes were not significant. *Myc* was not regulated after 6 hours of Ikaros induction. In B3 cells *Myc* and *Ccnd2* levels decreased after 15' of induction, and the down-regulation became statistically significant at 1h. *Igll1* significantly reduced its expression at 30', and the transcript level decreased dramatically during time till the 6h. Taken together, these data highlighted an impaired down-regulation mechanism of Ikaros target genes in Ikaros-ko cells.

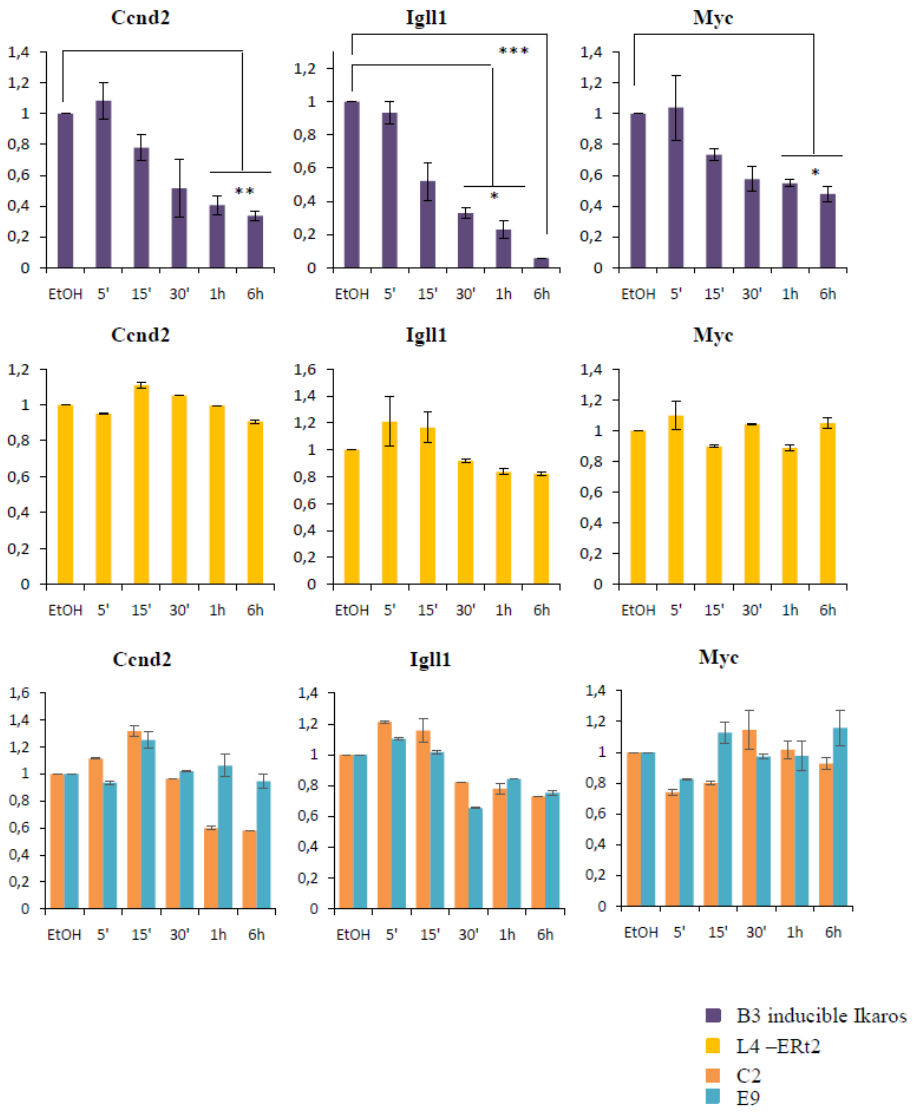

Figure 5.7: Transcriptional regulation of selected Ikaros down-regulated target genes. Histograms show the relative expression of candidate genes normalized to the untreated control (EtOH). RNA samples were collected after 5', 15',30', 1h and 6h after addition of 4OHT. The gene expression changes were monitored in wt-B3 inducible Ikaros, empty vector control and in Ikaros-ko C2 and E9 cell lines. Student's T test p value: *p<0.05, **p<0.01, ***p<0.001. Data shown is an average of 3 biological replicates. Standard errors are reported.

Myc is an important Ikaros target genes. Its Ikaros-dependent down-regulation is crucial for the transition from immature cycling preB cells to maturing resting preB cells[11]. To corroborate the gene expression analysis, the cell cycle profiles of C2 and E9, as well as B3 inducible Ikaros cells were analysed using PI DNA staining. As a 4OHT control, B3 cells transduced with HA-ERt2-mCherry control vector are included in the analysis. The DNA content profile was examined after 16 hours of 4OHT induction at FACS (Figure 5.8).

Wt-B3 inducible Ikaros untreated cells displayed a profile of 40% G1 phase, 40% S phase and 20% of G2 phase. After 16h of 4OHT treatment, G1 phase increased to 63%, while the

S and G2 phases decreased to 22% and 15%, indicating an arrest of the cell cycle at G1 phase (Figure 4). Both C2 and E9 clones failed to show any difference in cell cycle between 4OHT-treated and untreated cells. Of note, C2 cells present a lower percentage of cells in S and G2 phases in untreated sample compare to E9 and B3 inducible Ikaros. In conclusion, Inducible Ikaros is able to induce cell cycle arrest in B3 cells, but fails to do so in Ikaros-ko cells.

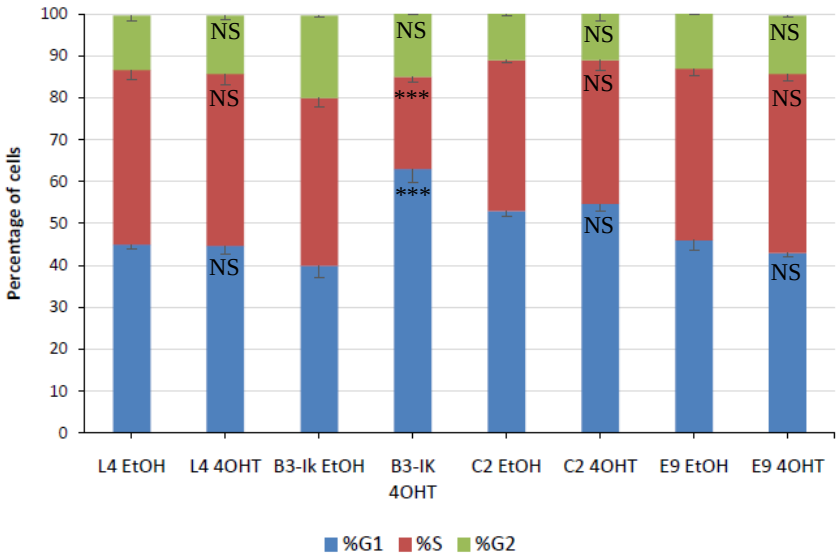

Figure 5.8: Cell cycle analysis of inducible Ikaros cells. The histogram shows the percentage of cells in different cell cycle stages after 16 hours of induction (4OHT) or in control (EtOH) treated cells. The significance reported in the 4OHT bars referred to control (EtOH) treated cells. Student's T test p value: ***p<0.001. Data shown is an average of 3 biological replicates. Standard errors are reported.

5.4 DISCUSSION

The aim of this work was the characterization of an Ikaros-ko cellular model designed to elucidate the underlying mechanisms of Ikaros gene expression regulation in the absence of endogenous Ikaros. Previously, an inducible Ikaros system was set up and characterized to deeply elucidate the genome-wide Ikaros target genes[10], and the kinetic and mechanisms of the gene expression changes in a temporal fashion (Liang et al., unpublished data). To do that, the B3 murine cycling preB cell line was used as a model. Our model combines the power of the inducible Ikaros system for studying Ikaros function with an endogenous Ikaros-ko model. Our system should decrease the background noise in the analysis, and allowed us to investigate the order of events that occur after Ikaros translocation in an "Ikaros-free" nucleus. The *Ikzf1* knock–out was confirmed by western blot analysis, and the function of the inducible Ikaros system was then tested. Inducible Ikaros was able to

translocate into the nucleus and formed toroidal structures at pericentromeric-heterochromatic regions, as previously reported in the literature[9,10,16,17]. IF analysis revealed a small amount of inducible Ikaros in the nucleus before the induction, while the majority of Ikaros was located in the cytoplasm. For further characterization of our model, we selected the C2 and E9 clones because they displayed the lowest amount of nuclear-Ikaros. Ikaros could efficiently bind to *Igll1* promoter, as demonstrated by ChIP experiments. The E9 clone showed a greater difference after induction than C2, with an increased in the signal of 11-fold, mostly due to the lower peak in untreated control compare to the other clone. A second peak, not present in untreated controls, appeared after induction at -1300bp from the TSS, in a secondary Ikaros binding site[9]. The presence of a small peak at -220bp in the untreated controls could be explained by binding of some inducible Ikaros proteins already present in the nuclei. Interestingly, a peak was found in B3 inducible Ikaros cells (expressing the endogenous Ikaros) using an α-HA antibody specific for the inducible Ikaros, corroborate the hypothesis of a contamination of nuclear inducible Ikaros both models. In wt-B3 system, the interaction between endogenous and inducible Ikaros is supposed to be the cause of inducible Ikaros nuclear localization before induction. It is also possible that, as inducible Ikaros is over-expressed in cells, HSPs are not enough to sequester all inducible Ikaros proteins in the cytoplasm, allowing a small portion of them to translocate in the nuclei. The latter would be the explanation of why we observed inducible Ikaros nuclear localization in our Ikaros-ko cell lines.

We next tested the gene-expression modulation by inducible Ikaros in our model. The candidate genes we selected were all direct target of Ikaros, with a strong Ikaros binding and a strong change of their expression upon Ikaros induction[10]. For gene expression experiments, we chose to sort our cells for high expression of inducible Ikaros. Upregulation of *Lig4* and *Zfp36* was observed in our model, but the increased amount of their transcripts after 6h was significantly lower compare to the previous model which expressed the endogenous Ikaros. Surprisingly, the Ikaros-repressed genes *Igll1, Ccnd2* and *Myc* do not showed any significant down-regulation after Ikaros induction. *Igll1* and *Ccnd2* displayed a mild decreased in their expression after 1h of induction in C2 clone (even if not significant), while in E9 no significant change was observed. *Myc* does not display any difference in gene expression within the 6 hours 4OHT of treatment.

Indirect evidence corroborating our observation came from the cell cycle analysis. Experiments performed in Merkenschlager's lab showed that Ikaros induction guide cells from a cycling state to a resting state after 16h of induction. This shift in cell state mimics

the physiological transition between cycling preB and resting preB cells, and is orchestrated by Ikaros, at least partially by direct down-regulation of *Myc* and subsequently of *Myc*'s target genes[10,11]. B3 with endogenous Ikaros displayed an arrest in G1 phase after 24h of induction, while both C2 and E9 are not affected by 4OHT treatment. This data, even if indirect, suggests us that the gene expression experiments are reliable.

The impairment of Ikaros repressor activity will need further investigations. It is worth to note that between the down-regulated tested genes was present *Igll1*, whose promoter was bound by inducible Ikaros, as previously demonstrated in this work by ChIP-RQ-PCR experiments. The same analysis needs to be done for the other genes to verify the Ikaros status at their promoters. The Ikaros capacity to regulate gene expression is mediated by other complexes that interact with it, as histones modifiers and nucleosome remodelers. One of the major Ikaros partner involved in gene silencing is the Nucleosome Remodeler Deacetylase complex (NuRD)[12,17], containing the nucleosome remodeler Mi-2β and the deacetylases HDAC1 and -2. Liang et al. demonstrated that the rapid changes in gene expression are, at least partially, related to changes in nucleosome occupancy at promoter and TSS sites (Liang Z. et al., unpublished data). Considering this information, Mi-2β, the nucleosome remodeler protein present in the Ikaros-NuRD complex, could be a candidate factor for further investigations.

In conclusion, we demonstrated that the Ikaros-ko B3 cell line transduced with the inducible Ikaros cassette is a functional and efficient system to study Ikaros-mediated regulation of gene expression. The comparison between our model and the previous one that maintains endogenous Ikaros protein will allow us to deepen our understanding of Ikaros mediated regulation of gene expression.

5.5 REFERENCES

1. Hardy, R. R. Resolution and characterization of pro-B and pre-pro-B cell stages in normal mouse bone marrow. *J. Exp. Med.* **173,** 1213–1225 (1991).

2. Herzog, S., Reth, M. & Jumaa, H. Regulation of B-cell proliferation and differentiation by pre-B-cell receptor signalling. *Nat. Rev. Immunol.* **9,** 195–205 (2009).

3. Georgopoulos, K. Haematopoietic cell-fate decisions, chromatin regulation and ikaros. *Nat. Rev. Immunol.* **2,** 162–74 (2002).

4. Wang, J. H. *et al.* Selective defects in the development of the fetal and adult lymphoid system in mice with an Ikaros null mutation. *Immunity* **5,** 537–49 (1996).

5. Nichogiannopoulou, A., Trevisan, M., Neben, S., Friedrich, C. & Georgopoulos, K. Defects in hemopoietic stem cell activity in Ikaros mutant mice. *J. Exp. Med.* **190,** 1201–14 (1999).

6. Mullighan, C. G. *et al.* BCR-ABL1 lymphoblastic leukaemia is characterized by the deletion of Ikaros. *Nature* **453,** 110–4 (2008).

7. Ng, S. Y.-M., Yoshida, T., Zhang, J. & Georgopoulos, K. Genome-wide lineage-specific transcriptional networks underscore Ikaros-dependent lymphoid priming in hematopoietic stem cells. *Immunity* **30,** 493–507 (2009).

8. Schwickert, T. A. *et al.* Stage-specific control of early B cell development by the transcription factor Ikaros. *Nat. Immunol.* **15,** 283–93 (2014).

9. Thompson, E. C. *et al.* Ikaros DNA-binding proteins as integral components of B cell developmental-stage-specific regulatory circuits. *Immunity* **26,** 335–44 (2007).

10. Ferreirós-Vidal, I. *et al.* Genome-wide identification of Ikaros targets elucidates its contribution to mouse B-cell lineage specification and pre-B-cell differentiation. *Blood* **121,** 1769–82 (2013).

11. Ma, S. *et al.* Ikaros and Aiolos inhibit pre-B-cell proliferation by directly suppressing c-Myc expression. *Mol. Cell. Biol.* **30,** 4149–58 (2010).

12. Koipally, J., Renold, A., Kim, J. & Georgopoulos, K. Repression by Ikaros and Aiolos is mediated through histone deacetylase complexes. *EMBO J.* **18,** 3090–100 (1999).

13. Brown, K. E. *et al.* Association of transcriptionally silent genes with Ikaros complexes at centromeric heterochromatin. *Cell* **91,** 845–54 (1997).

14. Fisher, A. G., Burdet, C., Bunce, C., Merkenschlager, M. & Ceredig, R. Lymphoproliferative disorders in IL-7 transgenic mice: expansion of immature B cells which retain macrophage potential. *Int. Immunol.* **7,** 415–23 (1995).

15. Cobb, B. S. *et al.* Targeting of Ikaros to pericentromeric heterochromatin by direct DNA binding. *Genes Dev.* **14,** 2146–60 (2000).

16. Brown, K. E. *et al.* Association of transcriptionally silent genes with Ikaros complexes at centromeric heterochromatin. *Cell* **91,** 845–54 (1997).

17. Kim, J. *et al.* Ikaros DNA-binding proteins direct formation of chromatin remodeling complexes in lymphocytes. *Immunity* **10,** 345–55 (1999).

CHAPTER 6

A FRET-BASED SYSTEM TO STUDY METABOLIC CHANGES IN B-LYMPHOCYTE DEVELOPMENT

Tobia Lana[1], Ziwei Liang[2], Alessandro Sardini[3], Giuseppe Basso[1], Matthias Merkenschlager[2], Geertruy te Kronnie[1]

[1]Department of Women's and Children's Health, University of Padova, Padova, Italy; [2]Lymphocyte Development Group, and 2Epigenetics Section, MRC Clinical Sciences Centre, Faculty of Medicine, Imperial College London, London, United Kingdom; [3]MRC Clinical Sciences Centre, Imperial College London, Hammersmith Hospital Campus, London W12 0NN, UK

ABSTRACT

During the progression along the B-cell lineage, B cell progenitors underwent a series of proliferation and quiescence stages, in which the immunoglobulin loci were sequentially rearranged and expressed. Thus, different stages in the developmental process present distinct energetic and biomass precursors demand. The transcription factor Ikaros promotes the cycling to resting transition during B-cell development by down-regulating proliferation genes, such as *Ccnd2/3* and *Myc*, and up-regulating genes relating to B cell differentiation, such as *Rag1* and *Rag2*. Moreover, Ikaros has been shown to down-regulate genes related to glycolysis and oxidative phosphorylation, indicating an active role in cell metabolism changes. Here we report the construction and characterization of 3 cycling preB cell lines expressing the inducible Ikaros cassette and 3 different FRET-based sensors to detect the cellular metabolic changes mediated by Ikaros expression. The 3 FRET sensors are specific for the detection of cytoplasmic ATP (Ateam) and glucose (FLII^{12}Pglu_700Δ6) levels and for the AMPK activation status (AMPKAR-NES). We set up a fluorescence microscopy- and a FACS- based assays to monitor the FRET intensities before and after Ikaros induction. Preliminary results from fluorescence microscopy indicate a minor glucose uptake and AMPK activation in Ikaros-induced cells, while for the ATP level, no clear results have been obtained so far with our experimental design.

6.1 INTRODUCTION

During lymphopoiesis, B cell precursors pass through different stages of proliferation and quiescence, necessary for antigen receptor loci rearrangement and cell maturation[1]. The succession of these developmental stages is orchestrated by different transcription factors acting in synergy or as antagonists[2,3]. At the preB stage, B cell precursors experience a burst in proliferation stimulated by preBCR signals guided by cell cycle regulator Cyclin D3 and the oncogene Myc[4]. Subsequently, components of the preBCR are down-regulated by piloting the cells out of cell cycle in order to rearrange the Ig light chain loci[1]. The transition from cycling preB to resting preB is driven by the activation of the transcription factors Ikaros and Aiolos, which directly repress Myc and thereafter Cyclin D3 expression[5].

Cells regulate their metabolism depending on the energetic demand as well as on the availability of biomass precursors[6]. In lymphocytes the transition from a resting to a proliferative state is accompanied by a switch from a metabolism based on oxidative phosphorilation to one based mainly on glycolysis[7,8], also called aerobic glycolysis since oxygen even if present is not required. Although the amount of the ATP produced by glycolysis is 18 times lower than by oxidative phosphorylation, the glycolytic process is much faster, providing a higher rate of ATP production compared to the tricarboxylic acid cycle (TAC). Moreover, glycolysis intermediate products are used by cells as precursors in different biosynthetic pathways, essential for biomass production of proliferating cell[9]. Both in T and B cell activation, the up-regulation of aerobic glycolysis and TAC down-regulation are piloted by Myc activation[8,10], whereas during the cycling to resting preB transition, glycolytic genes are shown to be down-regulated after Ikaros activation. The role of Ikaros in the metabolic switch is dual: an indirect one caused by Ikaros-mediated down-regulation of Myc and its downstream target genes, and a direct one, as ChIP experiments demonstrated Ikaros binding at promoters of glycolysis genes (Ferreirós-Vidal I., et al, unpublished data). Here, we reported the construction and characterization of a FRET-based model to study the metabolic state of preB cells during the cycling to resting transition. Förster resonance energy transfer (FRET) is a quantum mechanical effect observed when 2 fluorophores are located in the near-field. Light energy absorbed by a donor fluorophore is transferred to a nearby acceptor fluorophore with an absorption spectrum that overlaps the emission spectrum of the donor. In our study, we used 3 FRET sensors able to detect ATP concentration (Ateam[11]), glucose concentration (FLII[12]Pglu_700Δ6[12]) and AMPK activation status (AMPKAR-NES[13]). ATP concentration

is a direct measurement of the energetic state of cells; glucose uptake level is an indicator of the type of metabolism used by cells, as glycolysis needs more glucose uptake compared to oxidative phosphorylation to produce a comparable amount of ATP. Finally, AMPK is activated by a high AMP/ATP ratio[14] and is therefore considered as a physiological sensor of cellular energetic state.

6.2 MATERAL AND METHODS

Plasmids

The inducible-Ikaros sequence, as well as the Ateam, FLII^{12}Pglu_700Δ6 and AMPKAR-NES FRET sensors were contained assembled in murine stem cell virus (MSCV) retroviral plasmids. The transcription was driven by the 5' MSCV long terminal repeat.

Cell Culture

The murine preB cell line B3 was isolated and cloned in Professor Fisher's lab from a lymphoma occurring in an IL-7 transgenic mouse (Fisher et al 1995). This cell line was maintain in culture in Iscove's modified Dulbecco medium (IMDM) containing 10% (v/v) foetal calf serum (FCS) (Biosera) and antibiotics (100U/ml Penicillin and 100µg/ml Streptomycin, GIBCO, Invitrogen) . Cells were kept in culture at a density between 0.1 and 1 x 10^6 cells/ml.

The human embryonic kidney 293T cell line was cultured in Dulbecco modified Eagle medium (DMEM) supplemented with 10% (v/v) FCS, 2mM L-glutamine and antibiotics.

Virus production

293T cells were cultured in 10cm petri dish at approximately 40% of confluence in 9 ml of DMEM medium. 4µg of MSCV vector and 4µg of pECO or 10A1 envelop helper plasmid DNA were added to 500 µl of 0.4M $CaCl_2$ solution. 500µl of 2x HEBS (12mM dextrose, 50mM HEPES, 280mM NaCl, 10mM KCl, 1.5mM Na_2HPO_4 + $2H_2O$ in sterile water) were then added to the plasmid mix drop by drop. The transfecting solution was added to the cells drop by drop-wise. The cell medium was changed 12h after transfection. After 24h, 3.5ml of fresh media was added to cells, and virus-containing media were collected at 36, 48 and 60 hours from transfection, and pooled together.

Infection

The retroviral media was filtered with a 0.22µm filter, and supplemented with 10mM pH 7.6 HEPES and 4µg/ml polybrene (Sigma-Aldrich). 1.3 millions of B3 cells were suspended in 3ml of retroviral media and plated in a 6-well plate. Cells were then

centrifuged for 90' at 37 °C at 2500rpm to increase the infection rate. Retroviral media was then changed with fresh one and cells were put at 37 °C. 48h later, infected cells were sorted by FACS for the positivity at mCherry and eCFP fluorophores.

Cell sorting

Cells were sorted using FACSAria IIu, based on positivity to specific panels of fluorescent proteins (mCherry). For sorting, cells were resuspended in basic sort buffer (1x phosphate buffered saline (PBS) Ca/Mg^{++} free, 1mM EDTA, 25mM HEPES pH 7.0, 1% FCS) and collected in PBS Ca/Mg^{++} free supplemented with 20% of FCS. Sorted cells were then cultured for at least 24h in complete media supplemented with 5µg/ml of gentamycin.

Cell cycle analysis

Cells ($0.5x10^6$) were washed once in $PBS^{-/-}$, and then re-suspended in 300µl of propidium iodide buffer (PBS-/- supplemented with 10µg/ml RNAsi A (life technologies, NY, USA), 50µg/ml propidium iodide (Sigma-Aldrich) and 0.05% v/v NP40 (Calbiochem, Merck Millipore)). Cells were incubated 10' at room temperature and 20' on ice and subsequently analysed using a DB LSRII flow cytometer.

Ikaros induction

Exogenous ERt2-Ikaros was induced to transfer from cytoplasm to the nucleus by adding 0.5µM of 4hydroxytamoxifen (4OHT, Sigma-Aldrich). Time course experiments were performed by inducing Ikaros translocation at different times and processed at the same endpoint for subsequent analysis.

FRET analysis by fluorescent microscopy

Glass-bottom culture dishes were coated with Poly-L-Lysine (Sigma-Aldrich) for 1h at 37 °C and then washed twice with PBS-/-. 1x 10^6 cells were re-suspended in 2ml of complete IMDM media and seeded in coated plates for 2h. Ikaros induction was performed as previously described, 16h before the analysis. Cells were washed once and then topped up with 2ml of DMDM media (Sigma-Aldrich) without phenol-red, supplemented with 25mM D-glucose, 25mM HEPES, 1mM sodium pyruvate, 2mM L-glutamine and 10% v/v FCS. Living cells were imaged using an OLYMPUS IX70 (Leica) microscope with a Coolsnap HQ camera through a 40X dry objective lens in an environmental chamber at 37 °C. eCFP-eYFP/mVenus and mCherry were excited using 434/17 and 565/25 nm excitation filters and were acquired with 470/24, 559/38 and 632/60 nm emission filters respectively. Every 5' 8 image recordings were made for each sample. After the second image, different compounds were added to the dishes and changes in FRET signal were monitored every 5'

for a total of 30'. For the Ateam sensor, 10μM of Rotenone and 20μM of antimycin (Sigma Aldrich) are used (to inhibit the oxidative phosphorylation); 20μM of Phloretin (Sigma Aldrich) is used for FLII12R sensor (to inhibit the glucose transporter), and 50μM of 991 is added at AMPKAR-NES sensor cells (to activate the AMPK kinase). Analysis were performed using Fiji software. The FRET value was calculated as the yellow-to-cyan ratio.

FRET analysis by FACS

Ikaros induction was performed as previously described, 16h before the analysis. 2 million cells were washed once with warm PBS-/-, and then re-suspended in 2ml of DMDM media (Sigma-Aldrich) without phenol-red, supplemented with 25mM D-glucose, 25mM HEPES, 1mM sodium pyruvate, 2mM L-glutamine and 10% v/v FCS. FRET measurements were performed wt FACSAria IIu. To measure eCFP and FRET, cells were excited with the 405 nm laser and fluorescence was collected in the eCFP channel with a 480/40 filter, while the FRET-signal was measured with a 525/50 filter. For each sample 10,000 eCFP/eYFP positive events were analyzed.

6.3 RESULTS

In order to study metabolic changes in developing-B cells, we took advantage of the murine preB cell line B3[15] established in Prof Merkenschlager's lab, as a model of cycling-preB cells. This cell line was transduced with an inducible Ikaros cassette that allows us to precisely control the nuclear translocation of Ikaros[16]. For an extensive explanation of the inducible Ikaros system, see the results paragraph of chapter 5.

To study the dynamic alterations in the cellular energetic status prompted by Ikaros, 3 different FRET sensors were adopted: The Ateam[11] (Adenosine 5′-Triphosphate indicator based on Epsilon subunit for Analytical Measurements) sensor was used to measure ATP levels and the FLII[12]Pglu_700Δ6[12] sensor was used to measure glucose concentration. An AMPKAR sensor was fused to a nuclear export signal to generate AMPKAR-NES[13], which selectively measures AMPK cytoplasmic activity (Chennel G. et al., unpublished data) (Figure 6.1). Ateam is composed by the ε subunit of the *Bacillus* sp. PS3 FoF1-ATP synthase[11]. The corresponding dissociation constant (k_d) is 7.4μM, so it can detect differences of ATP levels in the micro-molar range. The glucose-binding domain of the FLII[12]Pglu_700Δ6 sensor derived from the glucose/galactose chemotactic receptor from *E. coli*, with a k_d of 660μM, within the range of physiological glucose concentration changes. The AMPKAR-NES sensor is formed by a synthetic peptide optimized for the favourable

substrate motif of AMPK, and by the phosphothreonine-binding domain FHA1. Phosphorylation of the substrate reporter by AMPK caused its subsequent binding with FHA1, resulting in juxtaposition between the donor and the acceptor. In living cells, responses obtained by the AMPKAR-NES sensor were consistent with results obtained by western blotting with antibodies against AMPK phosphorylation-targets, indicating the suitability of the FRET-sensor for detecting AMPK activity[13].

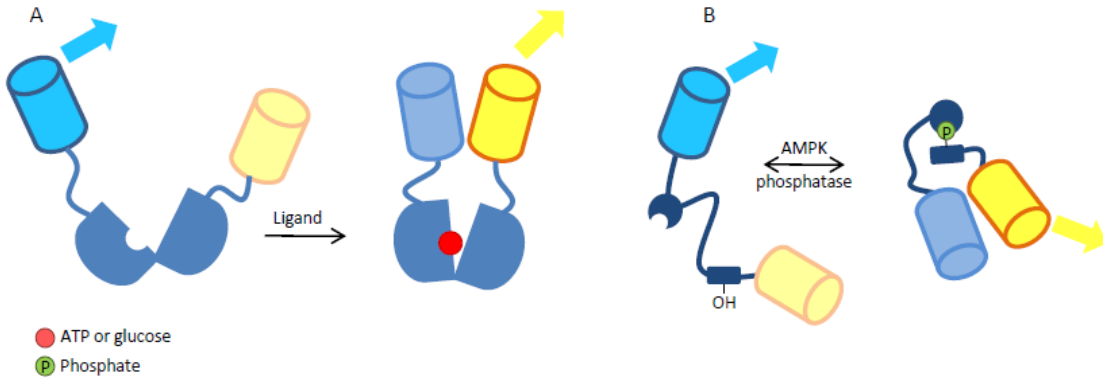

Figure 6.1: Schematic representation of the FRET-sensors used in this study. A) ATP and glucose sensors are formed by a single ligand recognition protein that changes conformation after ligand binding, while B) the AMPK-sensor is formed by an AMPK-phosphorylation recognition site that is bound by a phosphothreonine-binding module of the same sensor. Binding causes a conformational change that brings the fluorophores in close proximity and allows FRET. All sensors are formed by the FRET donor-acceptor pair eCFP-eYFP/mVenus (eYFP for FLII12Pglu_700Δ6, and mVenus for Ateam and AMPKAR-NES).

All the sensors were genetically linked with enhanced CFP (eCFP, a variant of the cyan fluorescent protein) at the N-terminus and with enhanced YFP (eYFP, in FLII[12]Pglu_700Δ6) or mVenus (in Ateam and AMPKAR-NES), 2 variants of the yellow fluorescent protein) at the C-terminus. These fluorochromes retain the excitation and emission spectra of the original CFP and YFP proteins, but were genetically engineered to increase the brightness and quantum yield in the case of eCFP[17], or to be less sensitive to pH changes and chloride ions in the case of eYFP/mVenus[17,18].

The 3 sensors were separately transduced into B3-inducible Ikaros cells. Each cell line was subsequently sorted for eCFP and mCherry to ensure high and homogeneous expression of FRET sensors and inducible Ikaros (for a more comprehensive explanation of inducible Ikaros and mCherry correlation, please see the results paragraph of chapter 5).

The cellular levels of Ikaros and FRET-sensors were verified by western blot (Figure 6.2). For Ikaros detection, a primary antibody against the C-terminal part of the protein was used, while the FRET sensors were detected by using a primary antibody (Clontech JL-8) that recognized GFP and GFP-derived variants such as eCFP and eYFP. Ikaros levels were

comparable between the 3 cell lines as expected, since they were sorted for the same levels of mCherry. The 3 FRET sensors had the predicted molecular weights and were present in comparable amounts.

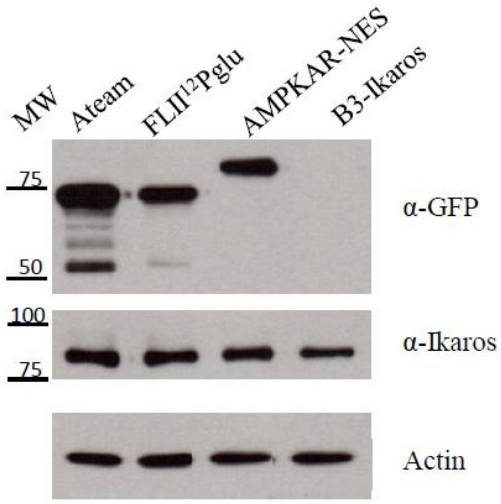

Figure 6.2: Evaluation of Ikaros and FRET-sensors by western blotting. Protein was extracted from the 3 FRET-sensor cell lines and from wt-B3 inducible Ikaros as a control. Inducible Ikaros was detected by an α-Ikaros antibody, the FRET sensors were detected using an α-GFP antibody that recognized GFP and GFP-derived variants such as eCFP and eYFP.

To test the efficiency of gene regulation by inducible Ikaros in established cell lines, we performed gene expression analysis by RQ-PCR after 30' and 1h of 4OHT induction, on 3 Ikaros down-regulated (*Ccnd2, Igll1* and *Myc*) and one up-regulated gene (*Lig4*). The expression was normalized to *Ubc* and *Ywhaz* housekeeping genes, and subsequently calculated relative to the EtOH control. *Igll1* and *Myc* were significantly down-regulated at 30', and *Ccnd2* after 1h; *Lig4* enhanced expression is detected after 1h 4OHT treatment. Thus, inducible Ikaros could efficiently regulate the expression of its target genes in our experimental model.

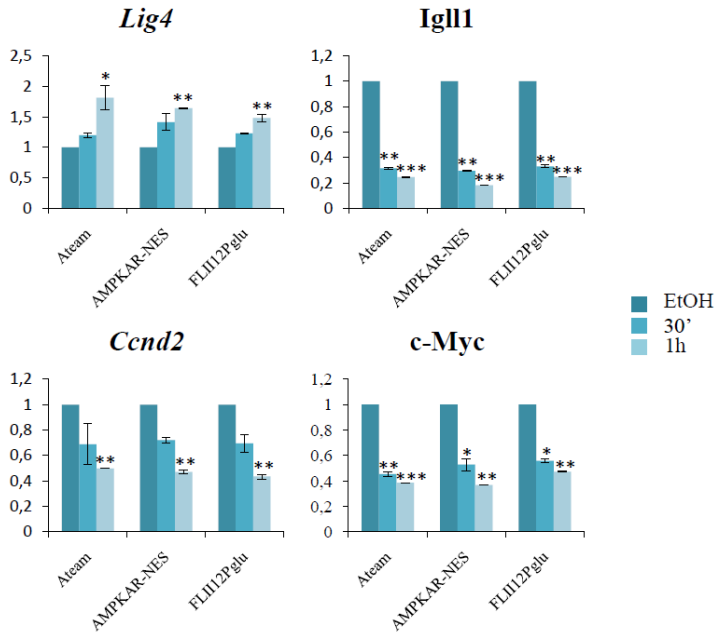

Figure 6.3: Regulation of gene expression triggered by Ikaros induction. Relative expression of genes in Ateam, AMPKAR-NES and FLII^{12}Pglu cells before (EtOH) or after 30' or 1h of 4OHT induction are displayed. Data shown are an average of 3 biological replicates. Standard errors are reported. Student T test p value: *p<0.05, **p<0.01, ***p<0.001.

It is important to keep in mind that the observed gene-expression changes referred to the level of immature transcripts. Alterations in cell metabolism are slower, and require that modifications at gene expression level are translated to protein levels.

During B cell development, the metabolic switches take places concomitantly with proliferation-state changes. Ikaros and the Ikaros family member Aiolos had previously been reported to block cell cycle progression in preB cells, mainly caused by direct down-regulation of transcription factor *Myc*, leading to an accumulation in the G1 phase[16,19]. To confirm the cell cycle block induced by Ikaros, the cell cycle profile of Ateam, AMPKAR-NES and FLII^{12}Pglu_700Δ6 cells was investigated at different time points by propidium iodide (PI) DNA staining (Figure 6.4).

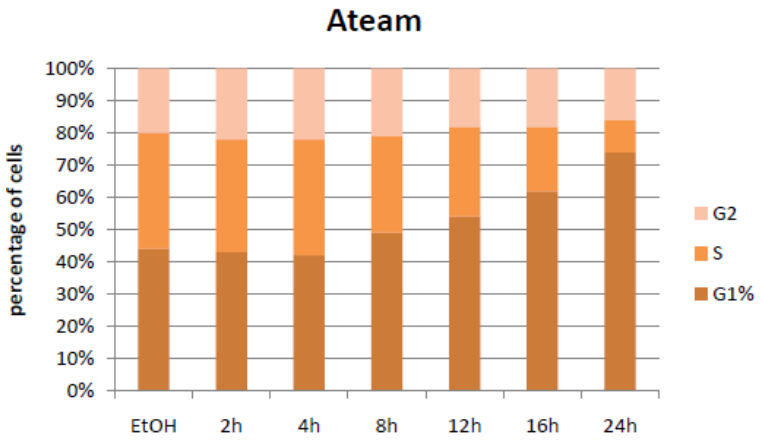

Figure 6.4: The cell cycle profile of Ateam cells after Ikaros induction. PI staining was performed at different time points after Ikaros induction. The graph reports the percentages of cells in G1, S and G2 phases of the cell cycle.

Cells were induced with 4OHT at different time points, and were analysed by FACS at 2h, 4h, 8h, 12h, 16h and 24hours after 4OHT treatment. The DNA content profile of Ateam cells, as an example, is displayed in Figure 6.4. The cell cycle arrest at G1 started at 8h and increased in magnitude during induction. G1 was more powerful in our models compared to the previously published data on the B3 inducible Ikaros cells[16]. This was probably due to the very high level of inducible Ikaros present in our cells. FACS analysis on Ateam cells at 24h revealed a population of cells with altered forward and side scatter parameters. Cell stress after long periods of Ikaros induction had been observed earlier and is probably due to an impairment of the differentiation process in preB cells due to the lack of a proper niche that normally provides for essential surviving signals. Considering that, further experiments were conducted on cells treated with 4OHT for 16h.

Ikaros translocation caused changes in the energetic state of B3 cells

To measure metabolic changes upon Ikaros induction, the 3 FRET-sensor cell lines were seeded in glass-bottom culture dishes coated with Poly-L-Lysine, and were cultured for 16h in the presence of 4OHT or carrier (EtOH). Cell medium was changed to DMDM (Sigma-Aldrich) without phenol-red, to limit the auto-fluorescence of the media, and supplemented with 25mM D-glucose, 25mM HEPES, 1mM sodium pyruvate, 2mM L-glutamine and 10% v/v FCS to maintain the same concentration of these metabolites as compared to the usual cell culture medium. Cells were then positioned in an environmental chamber at 37°C and were imaged using an OLYMPUS IX70 (Olympus) epi-fluorescence microscope. For each experiment, 4OHT-treated samples and controls were imaged synchronously. To measure the resonance energy transfer between the eCFP donor fluorochrome and the eYFP/mVenus acceptor, we excited the eCFP with a 434/14 nm

excitation filter and we acquired the eYFP/mVenus emission (sensitizedYFP, sYFP) with a YFP 559/38nm emission filter. eCFP and mCherry emission signals were acquired as well for further analysis with a 470/24nm and 632/60nm emission filters respectively. In our experimental conditions, the sYFP signal can be influenced by 2 factors: 1) direct YFP excitation caused by eCFP excitation filter, and 2) a bleed-through of eCFP emission in the sYFP detection filter. By using the 434/14nm excitation filter to excite eCFP, the direct excitation of YFP is negligible. Instead, the eCFP signal partially bled through into the YFP emission filter. The bleed-through component is consistent between the treated and control samples, so we initially wanted to see if changes in FRET signal could be detected over the bleed-thought noise. For every experiment, 2 images were taken every 5 minutes. As control of the functionality of the biosensors, after the second image, either inhibitors or activators were added to the cell medium and the response monitored by acquiring additional 6 images every 5 minutes. Specifically, in order to perturb ATP production, we added rotenone and antimycin that inhibit oxidative phosphorylation. To block glucose uptake, we used phlorerin, that inhibits the GLUC- transmembrane glucose-transporters[20]. To assess AMPK activation we used compound 991, a direct activator of AMPK[21].

FRET was calculated as the ratio between sYFP/eCFP emissions at the different time points. We first evaluated the possible photo-bleaching of eCFP. To do that, we acquired eCFP signal 3 times every 5'. eCFP signal did not significantly change over time in our experimental conditions, indicating the absence of photo-bleaching.

Figure 6.5 reports the results obtained from one replicate of the FLII[12]Pglu_700Δ6 cell line as an example of the performed analysis. eCFP, sYFP and mCherry levels were extrapolated, for each time point, from 368 and 306 treated and control cells, respectively. The FRET value of 4OHT and EtOH treated samples was calculated as the average of the excitedYFP and eCFP signals of the first 2 images. FRET ratio was significantly lower in Ikaros-induced cells compare to control sample, suggesting a lower glucose uptake in these cells (Figure 6.5A). This result was confirmed when eCFP and sYFP channels were analyzed individually. As shown in Figure 6.5B, the eCFP signal was higher and the sYFP was lower in 4OHT treated cells compared to control samples. Finally, we analyzed the cellular response to the glucose transport inhibitor phloretin (Figure 6.5C). Five minutes after phloretin addition, the eCFP signal increased, and the increment remained constant over the 30' of the experiment. The sYFP decreased its intensity over time, but in a lower amount compared the increment of eCFP signal. This phenomenon could be explained by a bleed-through effect of eCFP in the eYFP channel, as the eCFP emission spectrum

partially overlaps with that of eYFP. These results were confirmed in another biological replicate. Taken together, these data demonstrate that after Ikaros induction, the glucose uptake in cells diminished. In our experimental conditions, we were able to detect changes in FRET values caused by Ikaros induction and by the addition of phloretin. Analysis of single channels behaviour corroborated our results, showing that a change in the FRET ratio value was due to a change in both eCFP and sYFP channels, at opposite directions.

Similar experiments were conducted on the Ateam and AMPKAR-NES expressing cells. AMPK activity as detected by the AMPKAR-NES sensor was significantly decreased after Ikaros induction, as demonstrated by a lower FRET ratio in 4OHT treated cells compared to the EtOH control (Figure 5.6D). Analysis of individual channels before addition of compound 991 showed a higher eCFP signal in Ikaros induced- compare to controlled cells, while the sYFP channel was lower respect to the control sample, confirming the FRET-ratio data. However, the results obtained for this sensor did not reach statistical significance in the second biological replicate we performed. For Ateam cells, in our experimental conditions we were not able to detect any clear difference between 4OHT and EtOH controls neither between pre and post inhibitor addition. One possible explanation could be that the differences we were trying to detect were too small for the sensitivity of our sensors, or the bleed-through of the eCFP covered the small changes in the FRET signal between Ikaros-induced and un-induced cells. In this regard, increasing the number of analyzed cells might allow to detect small significant differences between 4OHT treated- and control samples.

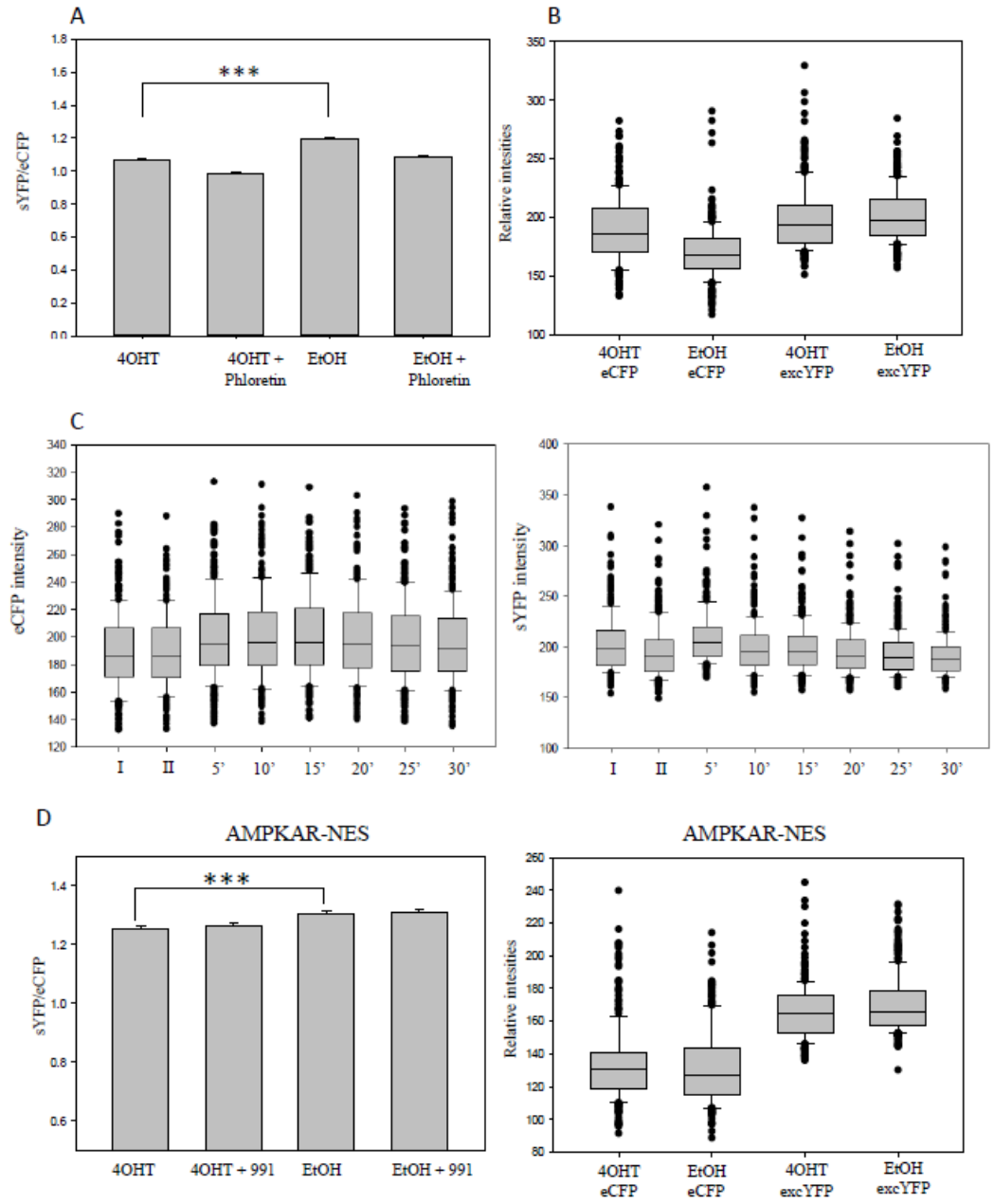

Figure 6.5: FRET measurements by epi-fluorescence microscopy. FLII^{12}Pglu_700Δ6 cells were treated with 4OHT or EtOH for 16h and subsequently imaged by fluorescence microscopy. Cells were then treated with 20μM Phloretin and imaged every 5' for a total of 30'. A) FRET was calculated as sensitizedYFP/eCFP signals. The FRET value before phloretin addition was calculated as the average of the 2 acquired images, while the signal after phloretin addition refers to the last acquisition, after 30' of phloretin treatment. 368 treated cells and 306 control cells were acquired; B) Relative intensities of eCFP and excitedYFP of 4OHT and EtOH treated cells before phloretin addition; C) Variation over time of eCFP and excitedYFP signals before and after addition of phloretin of 4OHT treated cells; D) FRET intensities in AMPKAR-NES cells treated with 4OHT or EtOH for 16h. After 2 acquired images, 50μM of compound 991 was added to AMPKAR-NES cells. 410 treated 4OHT- and 495 EtOH control cells were analyzed for AMPKAR-NES. Mann-Whitney Rank Sum test p value: ***p<0.001.

To overcome these problems, we set up a methodology to read the FRET signal by flow cytometry. To establish a FACS assay, we produced 2 cell lines expressing only CFP or YFP fluorochromes. To do that, we permanently transduced wt-B3 cells with a MSCV

vector containing the CFP coding sequence under the control of MSCV long terminal repeat. CFP positive cells were then sorted by FACS. The eYFP single positive cells were primary lymph node cells from a CD4Cre transgenic mouse with lox-STOP-lox-YFP targeted into the endogenous Rosa26 locus. 24h before the FACS reading, T cells were activated using α-CD3 and α-CD28 antibodies to more closely resemble B3 cells in size and background fluorescence. We gated on living cells according to forward and sideward scatter parameters and then adjusted the photomultiplier tube voltages and compensation to avoid bleed-through between the channels. CFP was excited at 405nm and the signals were acquired at 480nm for CFP and at 525nm for YFP.

Ateam and FLII^{12}Pglu_700Δ6 cells were then analyzed (Figure 6.6). We took 2 measurements of each sample, before and after 30' of rotenone and antimycin or phloretin treatment. After compound treatments, FACS detected an increase in eCFP signal and a decrease in the excitedYFP signal, indicating that our assay was able to detect changes in the FRET ratio.

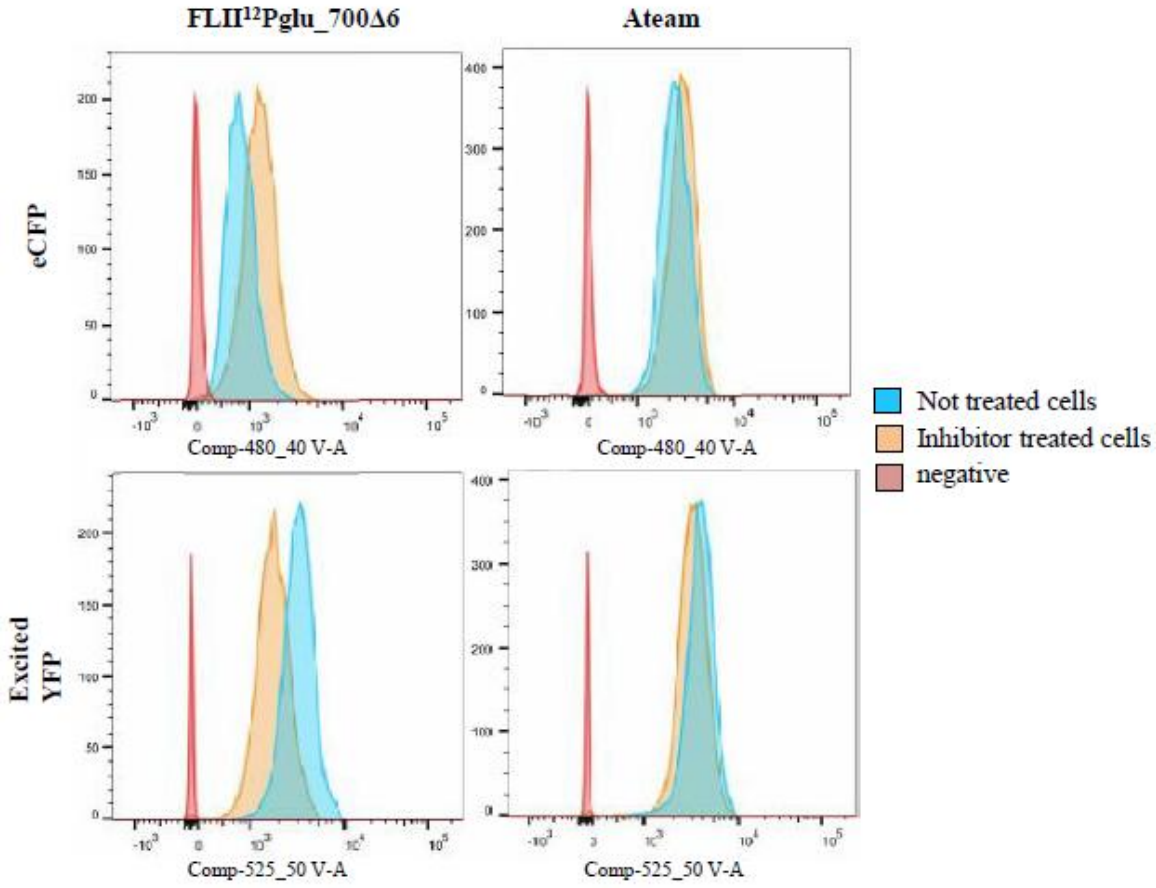

Figure 6.6: FRET measurements by flow cytometry. Ateam and FLII12Pglu_700Δ6 cells were analyzed by FACS before and after 30' of inhibitor treatment (Rotenone and antimicyn for Ateam, phloretin for FLII12Pglu_700Δ6). eCFP was excited at 405nm, and eCFP and excitedYFP were acquired with 480_40 and 525_50 emission filters respectively.

6.4 DISCUSSION

In this chapter, we constructed and characterized 3 preB cell lines in order to study changes in the cellular metabolism triggered by Ikaros activation. Three FRET sensors were transduced in wt-B3 cells already transduced with the inducible Ikaros cassette. The 3 FRET sensors were specific for ATP, glucose, and the AMPK activity, 3 important indicators of cellular energetic state. Using FRET-based analysis, we attempted to measure changes induced by Ikaros induction in real time and in living cells.

To test our models, we induced Ikaros translocation and analysed the effects 16hours later, when cells had stopped cycling. Preliminary results obtained by fluorescence microscopy showed a decreased glucose level in cells hence a decreased uptake by Ikaros induced cells and a decrease in AMPK activity. Taken together, the information obtained from the 2 sensors suggested a metabolic switch from aerobic glycolysis (2 ATP produced from every glucose molecule) to oxidative phosphorylation (36 ATPs produced from a single glucose molecule). Switching to oxidative phosphorylation as the main metabolic pathway, cells would require less glucose to produce a higher amount of ATP that results in a lower activation of AMPK decreasing the ratio of AMP/ATP. The data analysed so far were consistent with a lower uptake of glucose in Ikaros induced cells, while for the other 2 sensors data did not in all cases reach statistical significance and further analysis is required. The possible causes of discrepancies between biological replicates can be the very small change in ATP level before and after Ikaros induction, hard to detect for our FRET sensor, as well as the bleed-through between the eCFP and eYFP channels. To refine our analysis, CFP and YFP single positive cells were generated and will be imaged by microscopy. FRET analysis will be performed with the aid of software designed to correct the FRET-channel signal to the undesired bleed-through signal[22].

In parallel to microscopy analysis, we started to set up a FACS-based methodology to detect and quantify the FRET signal. Flow cytometry will allow us to acquire in a reasonable amount of time the eCFP, excitedYFP and mCherry levels of a large number of cells, adding robustness to our analysis. Moreover, FACS is a powerful tool to reduce the bleed-through signal between channels, by means of compensation and gating. Very preliminary experiments performed at FACS on Ateam and FLII^{12}Pglu_700Δ6 cells before and after addition of inhibitors demonstrated that FACS can detect a difference in FRET signal, indicating that this technique can be applied for further experiments. Next we will test Ateam, FLII^{12}Pglu_700Δ6 and AMPKAR-NES cells after Ikaros induction.

6.5 REFERENCES

1. Hardy RR. Resolution and characterization of pro-B and pre-pro-B cell stages in normal mouse bone marrow. J Exp Med. 1991 May 1;173(5):1213–25.

2. Busslinger M. Transcriptional control of early B cell development. Annu Rev Immunol. 2004 Jan;22:55–79.

3. Singh H, Medina KL, Pongubala JMR. Contingent gene regulatory networks and B cell fate specification. Proc Natl Acad Sci U S A. 2005 Apr 5;102(14):4949–53.

4. Herzog S, Reth M, Jumaa H. Regulation of B-cell proliferation and differentiation by pre-B-cell receptor signalling. Nat Rev Immunol. 2009 Mar;9(3):195–205.

5. Ma S, Pathak S, Mandal M, Trinh L, Clark MR, Lu R. Ikaros and Aiolos inhibit pre-B-cell proliferation by directly suppressing c-Myc expression. Mol Cell Biol. 2010 Sep 1;30(17):4149–58.

6. Stark H, Fichtner M, König R, Lorkowski S, Schuster S. Causes of upregulation of glycolysis in lymphocytes upon stimulation. A comparison with other cell types. Biochimie. 2015 Nov;118:185–94.

7. Maciver NJ, Jacobs SR, Wieman HL, Wofford JA, Coloff JL, Rathmell JC. Glucose metabolism in lymphocytes is a regulated process with significant effects on immune cell function and survival. J Leukoc Biol. 2008 Oct;84(4):949–57.

8. Wang R, Dillon CP, Shi LZ, Milasta S, Carter R, Finkelstein D, et al. The transcription factor Myc controls metabolic reprogramming upon T lymphocyte activation. Immunity. 2011 Dec 23;35(6):871–82.

9. Lunt SY, Vander Heiden MG. Aerobic Glycolysis: Meeting the Metabolic Requirements of Cell Proliferation. Annu Rev Cell Dev Biol. 2011 Nov 10;27(1):441–64.

10. Caro-Maldonado A, Wang R, Nichols AG, Kuraoka M, Milasta S, Sun LD, et al. Metabolic reprogramming is required for antibody production that is suppressed in anergic but exaggerated in chronically BAFF-exposed B cells. J Immunol. 2014 Apr 15;192(8):3626–36.

11. Imamura H, Nhat KPH, Togawa H, Saito K, Iino R, Kato-Yamada Y, et al. Visualization of ATP levels inside single living cells with fluorescence resonance energy transfer-based genetically encoded indicators. Proc Natl Acad Sci U S A.

2009 Sep 15;106(37):15651–6.

12. Takanaga H, Chaudhuri B, Frommer WB. GLUT1 and GLUT9 as major contributors to glucose influx in HepG2 cells identified by a high sensitivity intramolecular FRET glucose sensor. Biochim Biophys Acta. 2008 Apr;1778(4):1091–9.

13. Tsou P, Zheng B, Hsu C-H, Sasaki AT, Cantley LC. A fluorescent reporter of AMPK activity and cellular energy stress. Cell Metab. 2011 Apr 6;13(4):476–86.

14. Gowans GJ, Hawley SA, Ross FA, Hardie DG. AMP is a true physiological regulator of AMP-activated protein kinase by both allosteric activation and enhancing net phosphorylation. Cell Metab. 2013 Oct 1;18(4):556–66.

15. Fisher AG, Burdet C, Bunce C, Merkenschlager M, Ceredig R. Lymphoproliferative disorders in IL-7 transgenic mice: expansion of immature B cells which retain macrophage potential. Int Immunol. 1995 Mar;7(3):415–23.

16. Ferreirós-Vidal I, Carroll T, Taylor B, Terry A, Liang Z, Bruno L, et al. Genome-wide identification of Ikaros targets elucidates its contribution to mouse B-cell lineage specification and pre-B-cell differentiation. Blood. 2013 Mar 7;121(10):1769–82.

17. Rizzo MA, Springer GH, Granada B, Piston DW. An improved cyan fluorescent protein variant useful for FRET. Nat Biotechnol. Nature Publishing Group; 2004 Feb 29;22(4):445–9.

18. Nagai T, Ibata K, Park ES, Kubota M, Mikoshiba K, Miyawaki A. A variant of yellow fluorescent protein with fast and efficient maturation for cell-biological applications. Nat Biotechnol. 2002 Jan;20(1):87–90.

19. Ma S, Pathak S, Mandal M, Trinh L, Clark MR, Lu R. Ikaros and Aiolos inhibit pre-B-cell proliferation by directly suppressing c-Myc expression. Mol Cell Biol. 2010 Sep;30(17):4149–58.

20. Afzal I, Cunningham P, Naftalin RJ. Interactions of ATP, oestradiol, genistein and the anti-oestrogens, faslodex (ICI 182780) and tamoxifen, with the human erythrocyte glucose transporter, GLUT1. Biochem J. Portland Press Limited; 2002 Aug 1;365(Pt 3):707–19.

21. Xiao B, Sanders MJ, Carmena D, Bright NJ, Haire LF, Underwood E, et al. Structural basis of AMPK regulation by small molecule activators. Nat Commun. Nature Publishing Group; 2013 Jan 19;4:3017.

22. Hachet-Haas M, Converset N, Marchal O, Matthes H, Gioria S, Galzi J-L, et al. FRET and colocalization analyzer--a method to validate measurements of sensitized emission FRET acquired by confocal microscopy and available as an ImageJ Plug-in. Microsc Res Tech. 2006 Dec;69(12):941–56.

CHAPTER 7

DISCUSSION

Since its discovery in 1992[1], the transcription factor IKAROS and other protein family members became one of the most studied transcription factors in B-cell development and malignancies. Ikaros is expressed since the earliest stages of haematopoiesis, where contributes to CLP specification enhancing lymphoid-priming genes expressions and extinguishing genes related to stemness, myeloid and erythroid specification[2]. In lymphopoiesis, Ikaros expression pilots B cells through subsequent developmental stages, activating genes involved in immunoglobulin loci maturation and down-regulating genes involved preBCR signalling and proliferation[3–5]. *Ikzf1* transgenic mice models displayed severe haematological disorders, including delayed and impaired thymocytes differentiation, a complete block of B- and NK cells commintment[6–8], and developed T-cell leukaemia/lymphoma at high penetrance[9].

In human, *IKZF1* deletions were found in 15% of B cell precursors paediatric and adult acute lymphoblastic leukaemia, and in 70% of Philadelphia+ BCP-ALL[10]. The clinical relevance of *ΔIKZF1* in paediatric BCP-ALL, as well as its possible introduction as a risk stratification factor is however still debated. The *ΔIKZF1* prognostic impact was recently evaluated in 2 paediatric Ph+ BCP-ALL cohorts before and after the introduction of TKI in clinical protocols[11]. *ΔIKZF1* correlated with worse EFS and CIR in pre-TKI patients, and with a worse OS in post-TKI patients stratified as 'good-prognosis'. Considering the high incidence of *IKZF1* deletions and their negative impact on prognosis, we took advantage of next generation amplicon deep-sequencing to evaluate the presence of point mutations and very small indels in Ph+ BCP-ALL patients. Since Ph+ ALL represent 2% of the total ALL paediatric cases, we set up an European multicenter study collecting 98 *IKZF1*-not deleted and 61 *IKZF1*-deleted specimens. We found that 4% of *IKZF1* non deleted- and 3.2% of *IKZF1* deleted-patients carried mutations in the *IKZF1* coding sequence, mainly located in exons 5 and 8. Ikaros mutations and macrodeletions behaved in the same manner concerning the impact on prognosis, as the majority of *IKZF1* mutated patients that experienced an adverse event (relapse or dead) when treated before the introduction of TKI in clinical protocols. The milder effect of *IKZF1* aberrations on prognosis in TKI-treated patients may indicate a possible effect of imatinib on the activation status of *IKZF1*.

Thanks to our approach, we identified a new class of patients carrying previously under-estimated mutations[12,13], with an impact on IKAROS activity that has to be take into consideration in future studies in order to have a precise evaluation of *IKZF1*-aberrations impact in prognosis. This could be particularly important for other leukemic subgroups, such as Ph-like or B-other patients, where Δ*IKZF1* are still predictors of lower EFS and higher CIR[14–20].

A further advantage of NGS technique is its capacity to provide a quantification of the mutation load in terms of a MAF of the detected mutations. In the wake of this new approach we identified the first case of a familial *IKZF1* germline mutation. Genetic familial predisposition to leukaemia was thought to be an extremely rare event, and only recently 3 familial leukaemia cases related to a point mutation in a well-known leukemic gene were described [21,22]. The single nucleotide frameshift deletion was identified in both proband's diagnosis and remission samples with a MAF of 50%, was consistent with a constitutive heterozygous mutation. Sequencing analysis on proband's parents uncovered the same aberration in the mother's DNA. The mutation was then observed in 3 other members of the family among 3 generations, all without any manifested haematological disturbances; a brother of the mother had died of leukaemia during childhood, but no material was available to evaluate the genetic state of *IKZF1*. The mutated allele was found to be actively transcribed in proband's mRNA at remission and in his sister's mononuclear cells, and the predicted truncated proteins was identified in proband sister's peripheral cells. The mutated protein, expressed in a HeLa cell model, revealed a diffuse nuclear localization, indicating a null-effect of the mutation on IKAROS function. The low penetrance of leukaemia in mutation carriers points to the importance of secondary adverse events for the instauration of a leukemic cell clone. Indeed, the leukemic clone at diagnosis carried the t(9;22) translocation, a strong leukemogenic factor.

Even if the importance of Ikaros in lymphopoiesis is well established, mainly through genetic ablation studies in transgenic mice[6,7,9,23], the mechanisms and the temporal order of events that culminates in Ikaros-mediated gene expression regulation are only partially understood. Ikaros can interact with both inhibitors and activators of transcription, depending on the cell type and the developmental stage of a cell[5,24–27]. We took advantage of an inducible Ikaros system developed in Prof. Merkenschlager's lab[3] to construct and characterized 2 cellular models to further insight in the role of Ikaros in B-cell

development using a murine preB cell line. The inducible Ikaros system allowed us to control in a temporal fashion the translocation of Ikaros protein in the nuclei, where it exploits its functions.

In the first model, endogenous Ikaros was knocked-out using the CRISPR-Cas9 gene editing tool. As a result, we were able to study the effects of Ikaros in gene expression regulation in "Ikaros free" nuclei. Inducible Ikaros was able to efficiently translocate in the nuclei after induction with 4-hydroxytamoxyfen, and bound the promoter region of a well known Ikaros target gene, *Igll1*. The gene expression regulation of selected Ikaros target genes was then evaluated. In the endogenous Ikaros-ko context, inducible Ikaros was able to up-regulate target genes, but was not shown to down-regulate some of its most important targets, among which *Igll1* and *Myc*. After Ikaros induction, Ikaros-ko cells did not experience any block in the cell cycle, whereas in endogenous-Ikaros wt cells a prominent block in G1 phase after inducible Ikaros translocation was displayed.

The Ikaros-piloted cell cycle arrest in our preB cell model partially recapitulates the transition from cycling preB to resting preB cells, a crucial step during B-lymphocytes development.
In the second model, Inducible Ikaros was used to study the metabolic changes caused by its translocation in endogenous-Ikaros wt cells after the cell cycle arrest. Three FRET sensors were expressed in B3 inducible Ikaros cells, to monitor the cellular level of ATP and glucose, and the activation of AMPK protein. The FRET-reading was tested by fluorescent microscopy after 16 hours of Ikaros induction. Preliminary results on Ikaros induced cells show a diminished level of glucose uptake, and a lower level of AMPK activation, consistent with a metabolic switch from aerobic glycolysis to oxidative phosphorylation. These results need to be corroborated by further experiments and biological replicates. Finally, a method to read the FRET signal by flow cytometry was evaluate, and preliminary tests on ATP and glucose sensors showed that FACS can efficiently detect changes in donor and acceptor channels after treatment with inhibitors of glucose transporters and oxidative phosphorylation.

In conclusion, we studied the role of *IKZF1* in haematopoiesis and in paediatric leukaemia, in order to provide new insight and tools to better elucidate IKAROS' position in leukemogenesis and regulation of normal blood cell development.

REFERENCES

1. Georgopoulos K, Moore DD, Derfler B. Ikaros, an early lymphoid-specific transcription factor and a putative mediator for T cell commitment. Science. 1992 Oct 30;258(5083):808–12.

2. Ng SY-M, Yoshida T, Zhang J, Georgopoulos K. Genome-wide lineage-specific transcriptional networks underscore Ikaros-dependent lymphoid priming in hematopoietic stem cells. Immunity. 2009 Apr 17;30(4):493–507.

3. Ferreirós-Vidal I, Carroll T, Taylor B, Terry A, Liang Z, Bruno L, et al. Genome-wide identification of Ikaros targets elucidates its contribution to mouse B-cell lineage specification and pre-B-cell differentiation. Blood. 2013 Mar 7;121(10):1769–82.

4. Brown KE, Guest SS, Smale ST, Hahm K, Merkenschlager M, Fisher AG. Association of transcriptionally silent genes with Ikaros complexes at centromeric heterochromatin. Cell. 1997 Dec 12;91(6):845–54.

5. Kim J, Sif S, Jones B, Jackson A, Koipally J, Heller E, et al. Ikaros DNA-binding proteins direct formation of chromatin remodeling complexes in lymphocytes. Immunity. 1999 Mar;10(3):345–55.

6. Georgopoulos K, Bigby M, Wang JH, Molnar A, Wu P, Winandy S, et al. The Ikaros gene is required for the development of all lymphoid lineages. Cell. 1994 Oct 7;79(1):143–56.

7. Wang JH, Nichogiannopoulou A, Wu L, Sun L, Sharpe AH, Bigby M, et al. Selective defects in the development of the fetal and adult lymphoid system in mice with an Ikaros null mutation. Immunity. 1996 Dec;5(6):537–49.

8. Reynaud D, A Demarco I, L Reddy K, Schjerven H, Bertolino E, Chen Z, et al. Regulation of B cell fate commitment and immunoglobulin heavy-chain gene rearrangements by Ikaros. Nat Immunol. 2008 Jun 22;9(8):927–36.

9. Winandy S, Wu P, Georgopoulos K. A dominant mutation in the Ikaros gene leads to rapid development of leukemia and lymphoma. Cell. 1995 Oct 20;83(2):289–99.

10. Mullighan CG, Miller CB, Radtke I, Phillips LA, Dalton J, Ma J, et al. BCR-ABL1 lymphoblastic leukaemia is characterized by the deletion of Ikaros. Nature. 2008 May 1;453(7191):110–4.

11. van der Veer A, Zaliova M, Mottadelli F, De Lorenzo P, Te Kronnie G, Harrison CJ, et al. IKZF1 status as a prognostic feature in BCR-ABL1-positive childhood ALL. Blood. 2014 Mar 13;123(11):1691–8.

12. Mullighan CG, Su X, Zhang J, Radtke I, Phillips LAA, Miller CB, et al. Deletion of IKZF1 and prognosis in acute lymphoblastic leukemia. N Engl J Med. 2009 Jan 29;360(5):470–80.

13. Roberts KG, Morin RD, Zhang J, Hirst M, Zhao Y, Su X, et al. Genetic alterations activating kinase and cytokine receptor signaling in high-risk acute lymphoblastic leukemia. Cancer Cell. 2012 Aug 14;22(2):153–66.

14. Clappier E, Grardel N, Bakkus M, Rapion J, De Moerloose B, Kastner P, et al. IKZF1 deletion is an independent prognostic marker in childhood B-cell precursor acute lymphoblastic leukemia, and distinguishes patients benefiting from pulses during maintenance therapy: results of the EORTC Children's Leukemia Group study 58951. Leukemia. 2015 Nov;29(11):2154–61.

15. Palmi C, Valsecchi MG, Longinotti G, Silvestri D, Carrino V, Conter V, et al. What is the relevance of Ikaros gene deletions as a prognostic marker in pediatric Philadelphia-negative B-cell precursor acute lymphoblastic leukemia? Haematologica. 2013 Aug;98(8):1226–31.

16. Yamashita Y, Shimada A, Yamada T, Yamaji K, Hori T, Tsurusawa M, et al. IKZF 1 and CRLF 2 gene alterations correlate with poor prognosis in Japanese BCR - ABL 1 -negative high-risk B-cell precursor acute lymphoblastic leukemia. Pediatr Blood Cancer. 2013 Oct 27;60(10):1587–92.

17. Asai D, Imamura T, Suenobu S, Saito A, Hasegawa D, Deguchi T, et al. IKZF1 deletion is associated with a poor outcome in pediatric B-cell precursor acute lymphoblastic leukemia in Japan. Cancer Med. 2013 Jun;2(3):412–9.

18. Olsson L, Castor A, Behrendtz M, Biloglav A, Forestier E, Paulsson K, et al. Deletions of IKZF1 and SPRED1 are associated with poor prognosis in a population-based series of pediatric B-cell precursor acute lymphoblastic leukemia diagnosed between 1992 and 2011. Leukemia. 2013 Jul 4;28(2):302–10.

19. Dörge P, Meissner B, Zimmermann M, Möricke A, Schrauder A, Bouquin J-P, et al. IKZF1 deletion is an independent predictor of outcome in pediatric acute lymphoblastic leukemia treated according to the ALL-BFM 2000 protocol. Haematologica. 2013 Mar;98(3):428–32.

20. Song C, Gowda C, Pan X, Ding Y, Tong Y, Tan B-H, et al. Targeting casein kinase II restores Ikaros tumor suppressor activity and demonstrates therapeutic efficacy in

high-risk leukemia. Blood. 2015 Jul 28;

21. Auer F, Rüschendorf F, Gombert M, Husemann P, Ginzel S, Izraeli S, et al. Inherited susceptibility to pre B-ALL caused by germline transmission of PAX5 c.547G>A. Leukemia. Macmillan Publishers Limited; 2014 May;28(5):1136–8.

22. Shah S, Schrader KA, Waanders E, Timms AE, Vijai J, Miething C, et al. A recurrent germline PAX5 mutation confers susceptibility to pre-B cell acute lymphoblastic leukemia. Nat Genet. 2013 Oct;45(10):1226–31.

23. Nichogiannopoulou A, Trevisan M, Neben S, Friedrich C, Georgopoulos K. Defects in hemopoietic stem cell activity in Ikaros mutant mice. J Exp Med. 1999 Nov 1;190(9):1201–14.

24. Koipally J, Renold A, Kim J, Georgopoulos K. Repression by Ikaros and Aiolos is mediated through histone deacetylase complexes. EMBO J. 1999 Jun 1;18(11):3090–100.

25. Naito T, Gómez-Del Arco P, Williams CJ, Georgopoulos K. Antagonistic interactions between Ikaros and the chromatin remodeler Mi-2beta determine silencer activity and Cd4 gene expression. Immunity. 2007 Nov;27(5):723–34.

26. Payne KJ, Dovat S. Ikaros and tumor suppression in acute lymphoblastic leukemia. Crit Rev Oncog. 2011 Jan;16(1-2):3–12.

27. Bottardi S, Mavoungou L, Milot E. IKAROS: a multifunctional regulator of the polymerase II transcription cycle. Trends Genet. 2015 Jul 3;

APPENDIX

LIST OF PUBLICATIONS:

- APPENDIX 1: Lana T, de Lorenzo P, Bresolin S, Bronzini I, den Boer ML, Cavé H, et al. **Refinement of IKZF1 status in pediatric Philadelphia-positive acute lymphoblastic leukemia.** Leukemia. 2015 Oct;29(10):2107–10.

- APPENDIX 2: Palmi C, Lana T, Silvestri D, Savino A, Kronnie G Te, Conter V, et al. **Impact of IKZF1 deletions on IKZF1 expression and outcome in Philadelphia chromosome negative childhood BCP-ALL.** Reply to "incidence and biological significance of IKZF1/Ikaros gene deletions in pediatric Philadelphia chromosome negative and Philadelphia. Haematologica. 2013 Dec;98(12):e164–5.

- APPENDIX 3: Kumar S, Milani G, Takatsuki H, Lana T, Persson M, Frasson C, et al. **Sensing protein antigen and microvesicle analytes using high-capacity biopolymer nano-carriers.** Analyst. 2015 Nov 30

APPENDIX 1

3 Patel JP, Gönen M, Figueroa ME, Fernandez H, Sun Z, Racevskis J *et al.* Prognostic relevance of integrated genetic profiling in acute myeloid leukemia. *N Engl J Med* 2012; **366**: 1079–1089.
4 Gönen M, Sun Z, Figueroa ME, Patel JP, Abdel-Wahab O, Racevskis J *et al.* CD25 expression status improves prognostic risk classification in AML independent of established biomarkers: ECOG phase 3 trial, E1900. *Blood* 2012; **120**: 2297–2306.
5 Fernandez HF, Sun Z, Yao X, Litzow MR, Luger SM, Paietta EM *et al.* Anthracycline dose intensification in acute myeloid leukemia. *N Engl J Med* 2009; **361**: 1249–1259.
6 Walter RB, Othus M, Borthakur G, Ravandi F, Cortes JE, Pierce SA *et al.* Prediction of early death after induction therapy for newly diagnosed acute myeloid leukemia with pretreatment risk scores: a novel paradigm for treatment assignment. *J Clin Oncol* 2011; **29**: 4417–4423.
7 Cheson BD, Bennett JM, Kopecky KJ, Büchner T, Willman CL, Estey EH *et al.* Revised recommendations of the international working group for diagnosis, standardization of response criteria, treatment outcomes, and reporting `standards for therapeutic trials in acute myeloid leukemia. *J Clin Oncol* 2003; **21**: 4642–4649.
8 Marcucci G, Yan P, Maharry K, Frankhouser D, Nicolet D, Metzeler KH *et al.* Epigenetics meets genetics in acute myeloid leukemia: clinical impact of a novel seven-gene score. *J Clin Oncol* 2014; **32**: 548–556.
9 Marcucci G, Maharry KS, Metzeler KH, Volinia S, Wu YZ, Mrózek K *et al.* Clinical role of microRNAs in cytogenetically normal acute myeloid leukemia: miR-155 upregulation independently identifies high-risk patients. *J Clin Oncol* 2013; **31**: 2086–2093.
10 Walter MJ, Shen D, Ding L, Shao J, Koboldt DC, Chen K *et al.* Clonal architecture of secondary acute myeloid leukemia. *N Engl J Med* 2012; **366**: 1090–1098.
11 Elliott MA, Litzow MR, Letendre LL, Wolf RC, Hanson CA, Tefferi A *et al.* Early peripheral blood blast clearance during induction chemotherapy for acute myeloid leukemia predicts superior relapse-free survival. *Blood* 2007; **110**: 4172–4174.
12 Lacombe F, Arnoulet C, Maynadié M, Lippert E, Luquet I, Pigneux A *et al.* Early clearance of peripheral blasts measured by flow cytometry during the first week of AML induction therapy as a new independent prognostic factor: a GOELAMS study. *Leukemia* 2009; **23**: 350–357.
13 Terwijn M, van Putten WL, Kelder A, van der Velden VH, Brooimans RA, Pabst T *et al.* High prognostic impact of flow cytometric minimal residual disease detection in acute myeloid leukemia: data from the HOVON/SAKK AML 42A study. *J Clin Oncol* 2013; **31**: 3889–3897.
14 Freeman SD, Virgo P, Couzens S, Grimwade D, Russell N, Hills RK *et al.* Prognostic relevance of treatment response measured by flow cytometric residual disease detection in older patients with acute myeloid leukemia. *J Clin Oncol* 2013; **31**: 4123–4131.

Supplementary Information accompanies this paper on the Leukemia website (http://www.nature.com/leu)

Refinement of *IKZF1* status in pediatric Philadelphia-positive acute lymphoblastic leukemia

Leukemia (2015) **29,** 2107–2110; doi:10.1038/leu.2015.78

Philadelphia-positive B-cell precursor acute lymphoblastic leukemia (Ph+ BCP-ALL) identifies an unfavorable subgroup of pediatric ALL characterized by the presence of the BCR-ABL1 chimeric protein. However, clinically Ph+ BCP-ALL remains a heterogeneous disease with an unfavorable response to therapy in a critical percentage of patients. Even though introduction of tyrosine kinase inhibitors (TKIs) has improved outcome in pediatric Ph – BCP-ALL patients, 30% still relapse or die.[1]

Recurrent genomic deletions within the IKAROS (*IKZF1*) gene locus have been identified in Ph+ BCP-ALL[2] and BCP-ALL in general, and recent the work of van der Veer *et al.*[3] has shown that clinical heterogeneity in response to therapy at least in part may be attributed to the mutation status of *IKZF1* in Ph+ BCP-ALL patients.[4,5]

IKAROS is a transcription factor composed of two regions: the C terminal, including two zinc-finger (ZF) domains, that is responsible for the homo–hetero dimerization of the protein,[6] and a N-terminal domain with four ZFs, responsible for the DNA-binding activity: ZF2 and ZF3 ensure a stable DNA-binding, whereas ZF1 and ZF4 regulate the interaction to specific genomic sites.[7,8] Deletions of *IKZF1* can be subdivided into three categories: dominant-negative deletions, characterized by loss of the DNA-binding domain, deletions causing haploinsufficiency that lack the C-terminal dimerization domain and null deletions, that correspond to large chromosome 7 deletions or loss of the ATG codon.[9]

Even though the role of *IKZF1* deletions as a prognostic factor has been extensively investigated, remaining sometimes controversial,[5] little is known about other genetic alterations at the IKAROS locus.[4,10] The aim of this study was to assess the incidence of single-nucleotide mutations and in/del in the coding sequence of *IKZF1*.

Leukemic samples of 98 pediatric Ph+ BCP-ALL patients at diagnosis were collected from six European centers that participated in the 'Ponte di Legno' (pre-TKI) cohort[11] study and the European study for Ph+ ALL (EsPhALL).[1] The latter study used a combination of high-risk chemotherapy and imatinib treatment. The 98 patients we analyzed had previously been considered *IKZF1* wild type (WT) as they were free from *IKZF1* deletions as revealed using the MLPA analysis (see Supplementary Figure S3).

Sequencing analysis of *IKZF1*-coding exons, from exon2 to exon8 (Supplementary Table ST2), was performed using amplicon next generation sequencer GS Junior 454 (Roche Applied Science, Penzberg, Germany), using two-step universal-tailed amplicon sequencing. Today, next-generation sequencing-based sequencing strategies are a well-accepted robust substitute for Sanger sequencing[12] that can be applied in a clinical setting. Moreover, next-generation sequencing reliably detects mutations well below the detection rate of Sanger sequencing, provides a mutant allele frequency rate (MAF) and allows a robust and sensitive detection of insertions or deletions. Sequences of 882 amplicons were obtained with predicted average coverage per amplicon of 250 reads (range 102–853) and a minimum coverage of 50 reads in forward and reverse strands. Amplicon sequences were analyzed using the Amplicon Variant Analyzer (Roche Applied Science) software, obtaining a total of 313 variants. To identify predicted deleterious mutations a pipeline (Supplementary Figure S1) was applied that exclude intronic variants, homopolymeric stretches, known single-nucleotide polymorphisms and silent mutations. In addition, a threshold of 10% of variant detection in both strands was set. Finally, we obtained 14 variants with predicted deleterious effects in the *IKZF1*-coding sequence corresponding to 12 distinct mutations in 12 out of 98 patients (12.2%) including three patients from three different centers that were carrying the same mutation (Figure 1 and Supplementary Table ST1). The 12 mutations can be subdivided into two categories: those localized in the DNA-binding domain with a predictive dominant-negative effect (five missense mutations) and haploinsufficiency aberrations, that impaired the dimerization activity of IKAROS (seven frameshift mutations).

Accepted article preview online 17 March 2015; advance online publication, 14 July 2015

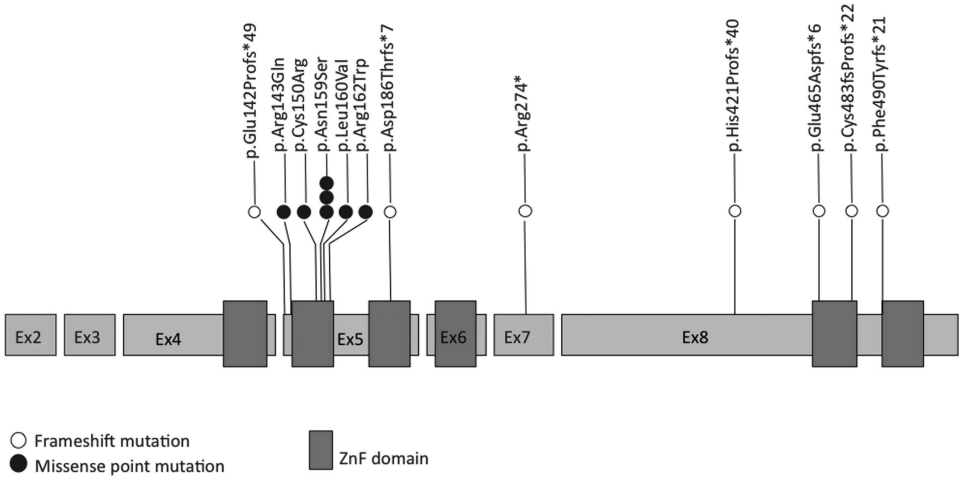

Figure 1. Location and type of *IKZF1* mutations: gray squares define the coding exons of *IKZF1*; red squares represent the zinc-finger domains. Each circle represents a detected mutation.

	MLPA	MLPA and NGS
IKZF1 deleted	66.4%	66.4%
IKZF1 mutated	-	4%
IKZF1 not deleted	33.6%	29.6%

Figure 2. Overview of *IKZF1* in Ph+ BCP-ALL pediatric patients. Percentages were calculated for each group on the basis of the number of *IKZF1*-mutated patients detected by amplicon NGS in 98 patients. NGS, next-generation sequencing.

The five missense mutations were located in exon5, of which four were localized within the ZF2-coding sequence, essential for DNA–protein interaction. All missense mutations were predicted to be 'probably deleterious' by PolyPhen2[13] (score 0.999) and 'damaging' by SIFT[14] (score 0.001) bioinformatic tools.

Regarding the mutated amino acids in the ZF2 domain, Asn159 and Arg162 (Figure 1) are known to be crucial for the maintenance of the α-helix domain structure, and their substitutions are described to have impaired the DNA-binding activity of the protein.[8] The Cys150 (mutated into Arg) is one of the four Cys/His residues that coordinate the zinc atom of the domain, and the mutation is predicted to severely impair the function of the domain as well. Of note, the p.Asn159Ser (c.A476 > G) substitution is carried by three patients (3% of *IKZF1* non-deleted patients). Altogether six patients carried point mutations in the ZF2-coding sequence with a predicted deleterious impact.

The seven frameshift mutations (two deletions, four insertions and one InDel) were identified at different positions within the *IKZF1* locus, two in exon5, one in exon7 and four in exon8. These mutations cause shifts in the reading frame that predict the formation of premature stop codons and consequent depletion the C-terminal dimerization domain of the protein.

The MAF of *IKZF1* mutations was in most cases consistent with a heterozygous mutation in the entire blast population (Supplementary Table ST1); only in three cases (MRC-UK-12, BFM-G-1 and AIEOP-24) MAF suggested a *IKZF1*-mutated subpopulation. Two patients carried double mutations: in one case, the two mutations in exon5 were reciprocally exclusive (p.Glu142Profs*49 and p.Arg143Gln), whereas in the second case mutations were located in different exons (p.Leu160Val in Exon5 and p.Arg274* in Exon7). In both cases one of the two mutations was present at a higher MAF (60% for p.Glu142Profs* versus 25% for p.Arg143Gln, and 51,5% for p.Leu160Val versus 36% for p.Arg274*), indicating the presence of leukemic subpopulations characterized by different *IKZF1* mutations. For six of 12 mutated patients, a remission sample was available, and Sanger sequencing demonstrated absence of the mutations in the tumor-free bone marrow.

The clinical characteristics of the 12 mutated patients are described in Supplementary Table ST1. Among the six mutated patients who had been treated before the introduction of TKI (pre-TKI cohort), four relapsed and one died in continuous complete remission (CCR). The latter is in line with the previously reported impact of *IKZF1* deletions in pre-TKI patients and suggests that *IKZF1* mutations behave in the same manner as deletions in terms of their associations with poor outcome in Ph+ patients. In the EsPhALL cohort, only one of the six mutated patients who were treated with imatinib failed (died in CCR), pointing to a diminished impact of aberrant *IKZF1* on patient outcome.

Recently, we reported the impact of *IKZF1* deletions on outcome of Ph+ BCP-ALL.[3] The study included 191 patients (see Supplementary Figure S3); 84 recruited in the pre-TKI cohort and 107 in the EsPhALL, post-TKI cohort. Overall, 65 patients (40%) were defined as 'wild-type' on the basis of the absence of *IKZF1* deletions and, of these, 64 had been included in our mutation screening (one was excluded because of lack of material). Six of these 64 patients carried *IKZF1* deleterious mutations, three from the pre-TKI cohort and three from the EsPhALL cohort. *IKZF1*-mutated and -deleted patients were grouped together ($N = 132$, '*IKZF1*-aberrant' patients) and their outcome compared with that of 'true' WT *IKZF1* (without deletion or mutations) Ph+ BCP-ALL patients ($N = 59$). The new disease-free survival curves of pre-TKI and EsPhALL cohorts confirmed the poor prognosis of patients with *IKZF1* aberrations (deletions plus mutations; 4-year disease-free survival 28.1% (standard error (SE) 6.4) versus 64.3% (SE 9.7), $P = 0.0036$ in pre-TKI; 4-year disease-free survival 55.7% (SE 6.8) versus 59.8% (SE 11.6; $P = 0.348$) in EsPhALL, 4-year disease-free survival 56.8% (SE 9.4) versus 75.0% (SE 21.7) in EsPhALL Good risk group; Supplementary Figure S2).

In conclusion, this work has demonstrated the presence of *IKZF1* mutations in $>10\%$ of pediatric Ph+ BCP-ALLs previously classified as *IKZF1* WT on the basis of deletion analysis alone. Exon5, which encodes ZF2 and ZF3 domains, carried 9 out of 14 aberrations: 7 point mutations and 2 deletions. The presence of the high number of mutations in the domain and the recurrence of one of them in three patients prompt us to consider this region as a hotspot locus for mutation acquisition. All missense mutations are predicted to be deleterious by two bioinformatic tools employed in this study and by *in vitro* mutagenesis studies,[8] and all the small in-del aberrations lead to the formation of premature stop codons. Overall, our observations have contributed to the refinement of disease-free survival analysis of Ph+ BCP-ALL patients with *IKZF1* aberrations. In the pre-TKI cohort, *IKZF1*-mutated patients showed a similar outcome as compared with *IKZF1*-deleted patients. The prognostic impact of the *IKZF1* mutations in imatinib-treated patients is more attenuated and may indicate the presence of other pathogenic mechanisms,[15] as well as a possible effect of therapy on the activation status of *IKZF1*. Considering the high incidence of nucleotide aberrations observed in our study, we would like to stress the importance of including these mutations in the overview of *IKZF1* aberrations (Figure 2 and Supplementary Figure SF4). This new category of *IKZF1*-mutated patients, previously masked in the *IKZF1* WT group, behaves in the same manner as *IKZF1*-deleted patients in both pre- and post-TKI era, and needs to be considered for a precise estimation of the impact of aberrant *IKZF1* in leukemogenesis and disease progression.

CONFLICT OF INTEREST

The authors declare no conflict of interest.

ACKNOWLEDGEMENTS

We thank Dr Aurélie Caye and all the pediatricians from the Société Française des Cancer de l'Enfant (SFCE). This work was supported by Czech Ministry of Health NT 13170-4 (to MZ), Czech Science Foundation GACR (grant P304/12/2214 to EF), the Italian Associations for Cancer Research (AIRC, to CG), the Italian Ministry of University and Research (MIUR, to AB) and the Fondazione Cariplo (to CG and GtK). The research leading to these results has received funding from the European Union's Seventh Framework Program (PF7/2007-2013) under the project ENCCA, grant agreement HEALTH-F2-2011-261474 (MGV, GtK, MS, GC, AB and MLdB) and ERA-net TRANSCAN project TRANSCALL (GB, MS, GC and GtK).

DISCLAIMER

These funding sources had no role in the collection, analysis or interpretation of the results, or in writing the manuscript and the decision for submission of this work.

T Lana[1], P de Lorenzo[2,3], S Bresolin[1], I Bronzini[1], ML den Boer[4,5], H Cavé[6], E Froňková[7], M Stanulla[8,9], M Zaliova[7,8,9], CJ Harrison[10], H de Groot[5], MG Valsecchi[3], A Biondi[2], G Basso[1], G Cazzaniga[2] and G te Kronnie[1]

[1]*Department of Women's and Children's Health, University of Padova, Padova, Italy;*
[2]*Clinica Pediatrica, Centro Ricerca Tettamanti, University of Milano-Bicocca, Monza, Italy;*
[3]*European Study for Philadelphia–Acute Lymphoblastic Leukemia Trial Data Center, Department of Health Sciences, University of Milano-Bicocca, Monza, Italy;*
[4]*Department of Pediatric Oncology, Erasmus University Medical Center-Sophia Children's Hospital, Rotterdam, The Netherlands;*
[5]*Dutch Childhood Oncology Group, The Hague, The Netherlands;*
[6]*Department of Genetics, Assistance Publique Hôpitaux de Paris, Hôspital Robert Debré, University Paris Diderot, Paris, France;*
[7]*Childhood Leukemia Investigation Prague, Second Faculty of Medicine, Charles University and University Hospital Motol, Prague, Czech Republic;*
[8]*Department of Pediatric Hematology and Oncology, Hannover Medical School, Germany;*
[9]*Department of General Pediatrics, University Hospital Schleswig-Holstein, Kiel, Germany and*
[10]*Leukemia Research Cytogenetics Group, Northern Institute for Cancer Research, Newcastle University, Newcastle upon Tyne, UK*
E-mail: truustekronnie@unipd.it

REFERENCES

1 Biondi A, Schrappe M, De Lorenzo P, Castor A, Lucchini G, Gandemer V *et al.* Imatinib after induction for treatment of children and adolescents with Philadelphia-chromosome-positive acute lymphoblastic leukaemia (EsPhALL): a randomised, open-label, intergroup study. *Lancet Oncol* 2012; **13**: 936–945.
2 Mullighan CG, Miller CB, Radtke I, Phillips LA, Dalton J, Ma J *et al.* BCR-ABL1 lymphoblastic leukaemia is characterized by the deletion of Ikaros. *Nature* 2008; **453**: 110–114.
3 Van der Veer A, Zaliova M, Mottadelli F, De Lorenzo P, Te Kronnie G, Harrison CJ *et al.* IKZF1 status as a prognostic feature in BCR-ABL1-positive childhood ALL. *Blood* 2014; **123**: 1691–1698.
4 Mullighan CG, Su X, Zhang J, Radtke I, Phillips LAA, Miller CB *et al.* Deletion of IKZF1 and prognosis in acute lymphoblastic leukemia. *N Engl J Med* 2009; **360**: 470–480.
5 Palmi C, Valsecchi MG, Longinotti G, Silvestri D, Carrino V, Conter V *et al.* What is the relevance of Ikaros gene deletions as a prognostic marker in pediatric Philadelphia-negative B-cell precursor acute lymphoblastic leukemia? *Haematologica* 2013; **98**: 1226–1231.
6 Sun L, Liu A, Georgopoulos K. Zinc finger-mediated protein interactions modulate Ikaros activity, a molecular control of lymphocyte development. *EMBO J* 1996; **15**: 5358–5369.
7 Schjerven H, McLaughlin J, Arenzana TL, Frietze S, Cheng D, Wadsworth SE *et al.* Selective regulation of lymphopoiesis and leukemogenesis by individual zinc fingers of Ikaros. *Nat Immunol* 2013; **14**: 1073–1083.
8 Cobb BS, Morales-Alcelay S, Kleiger G, Brown KE, Fisher AG, Smale ST. Targeting of Ikaros to pericentromeric heterochromatin by direct DNA binding. *Genes Dev* 2000; **14**: 2146–2160.
9 Kastner P, Dupuis A, Gaub M-P, Herbrecht R, Lutz P, Chan S. Function of Ikaros as a tumor suppressor in B cell acute lymphoblastic leukemia. *Am J Blood Res* 2013; **3**: 1–13.
10 Roberts KG, Morin RD, Zhang J, Hirst M, Zhao Y, Su X *et al.* Genetic alterations activating kinase and cytokine receptor signaling in high-risk acute lymphoblastic leukemia. *Cancer Cell* 2012; **22**: 153–166.
11 Aricò M, Schrappe M, Hunger SP, Carroll WL, Conter V, Galimberti S *et al.* Clinical outcome of children with newly diagnosed Philadelphia chromosome-positive

acute lymphoblastic leukemia treated between 1995 and 2005. *J Clin Oncol* 2010; **28**: 4755–4761.
12 Kohlmann A, Klein H-U, Weissmann S, Bresolin S, Chaplin T, Cuppens H *et al.* The Interlaboratory RObustness of Next-generation sequencing (IRON) study: a deep sequencing investigation of TET2, CBL and KRAS mutations by an international consortium involving 10 laboratories. *Leukemia* 2011; **25**: 1840–1848.
13 Adzhubei IA, Schmidt S, Peshkin L, Ramensky VE, Gerasimova A, Bork P *et al.* A method and server for predicting damaging missense mutations. *Nat Methods* 2010; **7**: 248–249.
14 Ng PC, Henikoff S. Predicting deleterious amino acid substitutions. *Genome Res* 2001; **11**: 863–874.
15 Raetz EA, Carroll WL. Refining prognosis in BCR-ABL1-positive ALL. *Blood* 2014; **123**: 1626–1627.

Supplementary Information accompanies this paper on the Leukemia website (http://www.nature.com/leu)

PD-L1/PD-1 presence in the tumor microenvironment and activity of PD-1 blockade in multiple myeloma

Leukemia (2015) **29,** 2110–2113; doi:10.1038/leu.2015.79

Despite remarkable therapeutic improvement in multiple myeloma (MM), prognosis is very poor once patients become refractory to or ineligible for proteasome inhibitors and immunomodulatory drugs. Accordingly, new drugs are clearly needed for this patient population, and extensive efforts are leading to a new breed of antimyeloma drugs.[1] In this regard, the PD-1/PD-L1 axis has recently emerged as a master immune checkpoint that controls antitumor immune responses against many neoplasms. Namely, PD-L1-expressing tumor cells in the tumor microenvironment engage PD-1 on tumor-infiltrating T lymphocytes to repress antigen-driven activation.[2] PD-L1 expression is also considered an adaptive resistance mechanism as PD-L1 is induced on tumor cells when under immune attack in response to immune-stimulating cytokines such as interferons.[2] Importantly, antibodies to PD-1 and PD-L1 have already shown clinical activity in melanoma,[3] renal-cell carcinoma,[4] non-small-cell lung cancer,[2] refractory Hodgkin lymphoma and bladder cancer. Predictive correlates of response mainly based on the expression of PD-L1 and the abundance of T lymphocytes are being intensively investigated.[3,4]

In MM, clinical trials targeting the PD-L1/PD-1 axis are already being conducted,[5] even though only two (discordant) studies have investigated expression of PD-L1 on $CD138^+$ PCs: one showed that PD-L1 is commonly present (although at low levels),[6] whereas the other report found PD-L1 to be positive in only ~25% of patients.[7] Accordingly, it could be the case that not all MM patients are equally likely to benefit from therapeutic targeting of the PD-1/PD-L1 axis, at least when used in monotherapy strategies. Discordant results have also emerged regarding levels of PD-1 expression on T and Natural killer (NK) cells from MM patients.[8–10] *In vitro* experiments showed increased MM cell death after enhancement of T-cells[9] and NK-cells[8] with anti-PD-1 monoclonal antibodies (mAb), whereas only two *in vivo* studies have been performed; both evaluated anti-PD-L1 mAb in the 5T33 mouse model either after autologous (syngeneic) stem-cell transplantation plus administration of a cell-based vaccine or after lymphodepleting irradiation, showing survival improvement.[9,11]

Here, we sought to define the expression of PD-L1 and PD-1 in clonal PCs as well as T and NK cells on bone marrow (BM) aspirates from monoclonal gammopathy of undetermined significance (MGUS) and MM patients at diagnosis, after treatment (minimal residual disease (MRD)) and upon relapse by using standardized multidimensional flow cytometry (MFC). We then evaluated efficacy of anti-PD-1 mAb therapy in a syngeneic mouse model after intravenous injection of 5TGM1 secretory MM cells.

We prospectively studied 107 patients, including 20 MGUS and 87 MM (47 at diagnosis, 25 after treatment to monitor MRD and 15 at relapse); normal BM samples were obtained from healthy volunteers or individuals undergoing orthopedic surgery ($n = 9$). All samples were collected after receiving informed consent, in accordance with local ethics committees and the Helsinki Declaration.

MFC was performed on EDTA anticoagulated BM samples, immunophenotyped using a direct 8-color immunofluorescence stain-and-lyse technique, with the following combination of monoclonal antibodies (PacB/OC515/FITC/PE/PerCP-Cy5.5/PE-Cy7/APC/APCH7): CD45/CD138/CD38/CD56/PD-1/CD19/PD-L1/CD3 and HLA-DR/CD27/CD45RA/CCR7/PD-1/CD25/CD8/CD4. In the first combination, we measured PD-L1 (Biolegend, San Diego, CA, USA; clone 29E.2A3) expression on normal and clonal PCs after careful discrimination according to aberrant phenotypic profiles,[12] as well as the percentage of PD-1^+ NK-cells ($SSC^{lo}CD45^+CD56^+CD19^-CD3^-$) using the Infinicyt software (Cytognos, Salamanca, Spain). In the second combination, we determined the percentage of PD-1^+ CD4 and CD8 T-cells, as well as the distribution of PD-1^+ versus PD-1^- according to peripheral maturation stage and activation status. Data acquisition was performed for $\geqslant 10^6$ leukocytes/tube in a FACSCantoII flow cytometer (BD Biosciences, San Jose, CA, USA) by using FACSDiva software (BD Biosciences; version 6.1). Instrument performance was monitored daily with cytometer setup beads (BD Biosciences) and rainbow 8-peak beads (Spherotech, Inc.; Lake Forest, IL, USA) after laser stabilization, following the EuroFlow guidelines; sample acquisition was systematically performed after longitudinal instrument stability was confirmed. Flow data were analyzed with Infinicyt software (Cytognos).

We established mouse 5TGM1 myeloma cells from the transplantable mouse 5T33 myeloma of spontaneous origin.[13] 5TGM-1 cells (0.75×10^6 per mouse) were intravenously inoculated via the tail vein into 6- to 8-week-old female naive C57BL/KaLwRijHsd mice.[14] Immediately after tumor cell inoculation, mice were randomly assigned for treatment with control rat immunoglobulin G antibody (Sigma-Aldrich, St Louis, MO, USA) or anti-PD-1 mAb (RPMP1-14 BioXcel). Doses were 100 μg of mAb every other day for three doses on days 3, 6, and 9 after tumor cell inoculation. Mice were checked twice weekly for survival or signs of terminal disease. Weight loss appeared only when mice reached a terminal status and could not be attributable to potential side effects. We assessed 5TGM1-specific monoclonal paraprotein (IgG2bκ) in sera prepared from whole blood obtained by submandibular vein puncture of tumor-bearing mice under light methoxyflurane-induced anesthesia. We assayed mouse IgG2bκ levels by using a specific in-house sandwich enzyme-

Accepted article preview online 17 March 2015; advance online publication, 17 April 2015

APPENDIX 2

Impact of IKZF1 deletions on IKZF1 expression and outcome in Philadelphia chromosome negative childhood BCP-ALL. *Reply to* "Incidence and biological significance of IKZF1/Ikaros gene deletions in pediatric Philadelphia chromosome negative and Philadelphia chromosome positive B-cell precursor acute lymphoblastic leukemia"

We thank Dr. Qazi and Dr. Uckun for their letter that focused on the biological relevance of *IKZF1* deletions in pediatric acute lymphoblastic leukemia (ALL), and in particular on the lack of correlation between *IKZF1* deletions and the expected deregulation of *IKZF1* expression. This information clearly supports the findings of our study[1] and our suggestion that the unfavorable prognostic role reported for Ikaros deletion may be due to general genetic instability rather than to Ikaros deletion *per se*, and justifies the hypothesis put forward by Qazi and Uckun that no specific biological effect is associated to Ikaros deletion. This issue is extremely relevant in this field, since a precise definition of the pathogenic mechanisms associated to *IKZF1* deletions is crucial for the ongoing efforts to define new targeted therapies for ALL.

Whilst the authors did infer *IKZF1* gene expression data without knowing the exact correspondence of *IKZF1* deleted and wild-type (wt) cases, to experimentally test the hypothesis, we have analyzed the gene expression data of *IKZF1* wild-type *versus* deleted cases in our own gene expression data set of pediatric ALL patients. From the MILE study[2] and further proprietary unpublished data, array-based gene expression was analyzed for 60 *IKZF1* wild-type and 10 deleted cases belonging to the cohort of 410 patients reported in our recent paper on *IKZF1*-related outcome.[1] Through analysis of the expression levels of two probe sets located in exon 4, no changes in *IKZF1* expression were observed that could be expected from heterozygous deletions of *IKZF1* (Figure 1). It has to be considered, however, that analysis of gene expression data of single probe sets is not the most appropriate method to detect gene expression variances of single genes or isoforms. In particular, probe sets 1565816_at and 1565818_s_at both show overall a very low expression, which largely reduces the probability to detect expression variance, if there is any. Therefore, we performed the analysis of *IKZF1* gene expression by real-time quantitative-PCR (Figure 2). Although there was a tendency for a lower *IKZF1* expression in *IKZF1* deleted cases compared to wt, this difference did not reach statistical significance, because of several outliers in both groups. This supports the hypothesis by Qazi and Uckun that *IKZF1* expression deregulation is very likely not a driving biological player in BCP-ALL cases with intragenic or entire deletions of *IKZF1*, thus raising the question on what is the biological mechanism related to *IKZF1* deletions and prognosis in ALL.

Our data do not support, however, the suggestion of Qazi and Uckun that in pediatric BCP-ALL *IKZF1* deletions occur in a minority of leukemic cells in an oligoclonal heterogeneous population of leukemic B-cell precursors. In our study,[1] having applied the low-sensitivity multiplex ligation-dependent probe amplification (MLPA) technique (which is not able to detect aberrations in minor cell populations), we should in fact have detected only *IKZF1* deletions in major cell subpopulations.[1] Although alternative sensitive tests could detect *IKZF1* subclonal deletions,[3] their prognostic significance should be evaluated.

On the other hand, whether *IKZF1* deletions occur in 'inactive' alleles, although fascinating, must be formally demonstrated in a context different from the canonical one for IG/TR loci,[4] as a new mechanism of escape from major damage, that, to our knowledge, has yet to be described in literature.

Certainly, the hypothesis that *IKZF1* deletion-associated adverse outcome would be a reflection of underlying genomic instability in aggressive leukemic clones, rather than lost or diminished *IKZF1* function caused by *IKZF1* haploinsufficiency, as originally proposed,[5,6] merits further investigation.

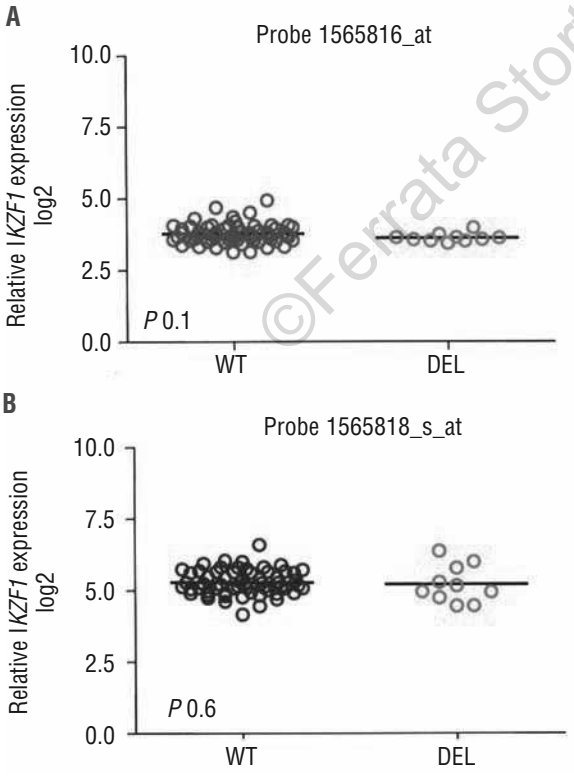

Figure 1. Gene expression values for *IKZF1* probes 1565816_at (A) and 1565818_s_at (B) in patients with (DEL) and without (WT) *IKZF1* deletions.

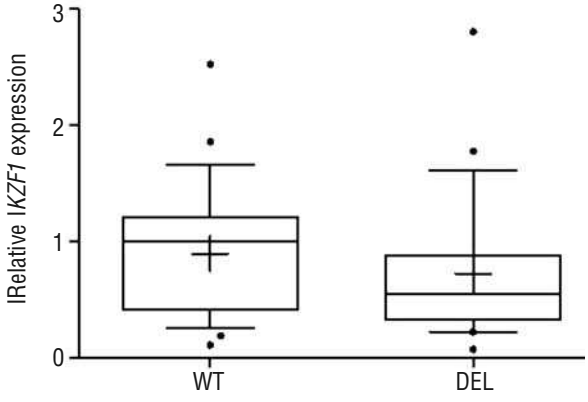

Figure 2. Gene expression values for *IKZF1* by RQ-PCR in patients with (DEL) and without (WT) *IKZF1* deletions. Boxes include 10-90 percentile, mean (internal line) and median (cross) are shown. Dots indicate outliers.

The prognostic significance of *IKZF1* deletions in our study[1] was, indeed, enhanced when additional copy number abnormalities (CNA) involving other genes were present. We specifically looked by MLPA 385 kit at *CDKN2A/B*, PAR region, *PAX5*, *ETV6*, *BTG1*, *RB1* and EBF1 deletions. In our series, out of 54 *IKZF1* deleted cases, 28 carried additional CNA. More precisely, 16 had at least one additional lesion (in 11 of 16 this was the *ETV6* deletion), 6 had 2 and 6 had 3 additional CNA. The incidence of additional CNA was the same in final Standard or Intermediate Risk groups. Out of the only 4 cases at High Risk, one had no CNA additional to *IKZF1* deletion. Nine were the relapses among the 28 *IKZF1* deleted cases with additional CNA *versus* only 3 out of 25 *IKZF1* deleted cases without additional CNA, pointing to a poor outcome when a major genetic instability was observed.[1]

Still, we are also puzzled by having observed no difference in outcome in haploinsufficient patients (with whole *IKZF1* gene deletion) *versus* cases carrying the dominant negative Δ4-7 deletion variant.[1] Interestingly, in Ph$^+$ ALL, which frequently carry *IKZF1* deletions, the haploinsufficient cases have an even worse outcome compared to cases carrying the Δ4-7 deletion variant (A van der Veer *et al*., 2013, *submitted manuscript*). This further observation indicates that either the suspected deleterious (post-transcriptional) effect of the dominant negative Δ4-7 deletion variant is not worse than losing one *IKZF1* copy, or that both aberrations are epiphenomena of genetic instability. It is also interesting to observe that *IKZF1* deletions and other CNA are over-represented in the so-called 'Ph-like' subgroup of BCP-ALL cases with gene expression signatures similar to Ph$^+$ ALL without the presence of the t(9;22) translocation.[6-8] Thus, it remains difficult to separate the contribution of single gene aberrations from a cumulative effect of several aberrations on the biology of leukemic cells, as reflected by a common gene expression signature.

In any case, if the hypothesis of *IKZF1* deletions in inactive alleles holds true, and/or assuming that the *IKZF1* deletion is only an epiphenomenon of the accumulation of CNA, it still remains to be demonstrated that other CNA occur in active alleles, and altogether (or specifically some of them) are responsible for the worse outcome as a manifestation of broader chromosomal instability. One interesting candidate to look at is the *CRLF2-P2RY8* fusion, which has been shown to have an independent worse outcome.[9] It would be very instructive to collect cases carrying both *IKZF1* deletions and *CRLF2-P2RY8* fusion and analyze the effect of their combination on outcome and evaluate whether this could be separated from additional CNA.

Chiara Palmi,[1] Tobia Lana,[2] Daniela Silvestri,[3] Angela Savino,[1] Geertruy Te Kronnie,[2] Valentino Conter,[4] Giuseppe Basso,[2] Andrea Biondi,[4] Maria Grazia Valsecchi,[3] and Giovanni Cazzaniga[1]

[1]Centro Ricerca Tettamanti, Clinica Pediatrica, Università di Milano Bicocca, Ospedale San Gerardo/Fondazione MBBM, Monza; [2]Laboratorio di Oncoematologia, Dipartimento di Pediatria, Università di Padova; [3]Centro di Biostatistica per l'Epidemiologia Clinica, Università di Milano Bicocca, Monza; and [4]Clinica Pediatrica, Università di Milano Bicocca, Ospedale San Gerardo/Fondazione MBBM, Monza, Italy.

Correspondence: abiondi.unimib@gmail.com
doi:10.3324/haematol.2013.099077

Key words: IKZF1 deletions, pediatric Ph- BCP-ALL, copy number abnormalities, prognosis.

Acknowledgments: this work was supported by grants from: Fondazione Tettamanti (Monza), Fondazione Città della Speranza (Padova), Associazione Italiana Ricerca sul Cancro (AIRC) (to GB, AB, MGV, GteK and GC), MIUR (to GB and AB), Fondazione Cariplo (to AB, GC and GteK) and CARIPARO project of excellence (to GteK). This work was (partly) funded by the European Commission (FP7) under the contract ENCCA (NoE-2011-261474).

Information on authorship, contributions, and financial & other disclosures was provided by the authors and is available with the online version of this article at www.haematologica.org.

References

1. Palmi C, Valsecchi MG, Longinotti G, Silvestri D, Carrino V, Conter V, et al. What is the relevance of Ikaros gene deletions as prognostic marker in pediatric Philadelphia negative B-cell precursor acute lymphoblastic leukemia? Haematologica. 2013;98(8):1226-31.
2. Asai D, Imamura T, Suenobu S, Saito A, Hasegawa D, Deguchi T, et al. IKZF1 deletion is associated with a poor outcome in pediatric B-cell precursor acute lymphoblastic leukemia in Japan. Cancer Med. 2013;2(3):412-9.
3. Caye A, Beldjord K, Mass-Malo K, Drunat S, Soulier J, Gandemer V, et al. Breakpoint-specific multiplex polymerase chain reaction allows the detection of IKZF1 intragenic deletions and minimal residual disease monitoring in B-cell precursor acute lymphoblastic leukemia. Haematologica. 2013;98(4):597-601.
4. Brady BL, Steinel NC, Bassing CH. Antigen receptor allelic exclusion: an update and reappraisal. J Immunol. 2010;185(7):3801-8.
5. Mullighan CG, Su X, Zhang J, Radtke I, Philips LAA, Miller CB, et al. Deletion of IKZF1 and Prognois in Aute Lymphoblastic Leukemia. N Engl J Med. 2009;360(5):470-80.
6. Mullighan CG, Miller CB, Radtke I, Phillips LA, Ma J, White D, et al. BCR-ABL1 lymphoblastic leukemia is characterized by the deletion of Ikaros. Nature. 2008;453(7191):110-4.
7. Den Boer ML, van Slegtenhorst M, De Menezes RX, Cheok MH, Buijs-Gladdines JG, Peters ST, et al. A subtype of childhood acute lymphoblastic leukaemia with poor treatment outcome: a genome-wide classification study. Lancet Oncol. 2009;10(2):125-34.
8. Harvey RC, Mullighan CG, Wang X, Dobbin KK, Davidson GS, Bedrick EJ, et al. Identification of novel cluster groups in pediatric high-risk B-precursor acute lymphoblastic leukemia with gene expression profiling: correlation with genome-wide DNA copy number alterations, clinical characteristics, and outcome. Blood. 2010;116(23):4874-84.
9. Palmi C, Vendramini E, Silvestri D, Longinotti G, Frison D, Cario G, et al. Poor prognosis for P2RY8-CRLF2 fusion but not for CRLF2 over-expression in children with intermediate risk B-cell precursor acute lymphoblastic leukemia. Leukemia. 2012;26(10):2245-53.

APPENDIX 3

Analyst

PAPER

View Article Online
View Journal

Cite this: DOI: 10.1039/c5an02377g

Sensing protein antigen and microvesicle analytes using high-capacity biopolymer nano-carriers†

Saroj Kumar,‡§[a] Gloria Milani,‡[b] Hideyo Takatsuki,‡[a] Tobia Lana,[b] Malin Persson,[a] Chiara Frasson,[b] Geertruy te Kronnie[b] and Alf Månsson*[a]

Received 17th November 2015,
Accepted 23rd November 2015

DOI: 10.1039/c5an02377g

www.rsc.org/analyst

Lab-on-a-chip systems with molecular motor driven transport of analytes attached to cytoskeletal filament shuttles (actin filaments, microtubules) circumvent challenges with nanoscale liquid transport. However, the filaments have limited cargo-carrying capacity and limitations either in transportation speed (microtubules) or control over motility direction (actin). To overcome these constraints we here report incorporation of covalently attached antibodies into self-propelled actin bundles (nanocarriers) formed by cross-linking antibody conjugated actin filaments *via* fascin, a natural actin-bundling protein. We demonstrate high maximum antigen binding activity and propulsion by surface adsorbed myosin motors. Analyte transport capacity is tested using both protein antigens and microvesicles, a novel class of diagnostic markers. Increased incubation concentration with protein antigen in the 0.1–100 nM range (1 min) reduces the fraction of motile bundles and their velocity but maximum transportation capacity of >1 antigen per nm of bundle length is feasible. At sub-nanomolar protein analyte concentration, motility is very well preserved opening for orders of magnitude improved limit of detection using motor driven concentration on nanoscale sensors. Microvesicle-complexing to monoclonal antibodies on the nanocarriers compromises motility but nanocarrier aggregation *via* microvesicles shows unique potential in label-free detection with the aggregates themselves as non-toxic reporter elements.

Introduction

Cheap, rapid and sensitive methods for diagnostics of disease using simple blood or urine samples aid strategies to overcome accelerating health care costs. In this context, there is growing interest to develop lab-on-a-chip devices[1–3] where a series of analyses are performed on a single chip. These devices are preferably integrated with nanoscale sensors for optimal sensitivity and multiplexing capabilities[4] *e.g.* to detect a panel of analytes/biomarkers (proteins, nucleic acid fragments, exosomes, microvesicles *etc.*). However, despite significant progress,[2] existing devices often use expensive and bulky accessory equipment[2,3] including pumps for driving liquid flow. Moreover, liquid flow does not overcome limitations associated with diffusion of biomarkers to nanoscale detectors.[4] Other potential problems include biosafety issues[5] *e.g.* related to the use of potentially toxic inorganic nanostructures as reporter elements signaling the presence of analyte molecules.

In order to circumvent the above problems, lab-on-a-chip systems with molecular motor driven transport have been proposed.[6–11] In some tested versions of such arrangements, recognition molecules, *e.g.* antibodies[12–14] or oligonucleotides[15,16] are attached to cytoskeletal filaments (actin filaments and microtubules) that are propelled by molecular motors for nanoseparation and concentration on a detector area.[8,17,18] Importantly, due to self-propelling features of the system (driven by turnover of adenosine-5′-triphosphate, ATP), these motor-propelled cytoskeletal shuttles[19] do not require external pumps. Furthermore, they capture biomarkers from a large solution volume and actively[7] transport them to the detector,[6,8,9] thereby overcoming diffusion limitations. In addition, the detection may be achieved in unique ways, *e.g.* by observations of co-localization and co-transportation of filaments and biomarkers[12,20–22] or by aggregation of the cytoskeletal filaments *via* analyte.[10,23] Due to the large number of fluorescent dye molecules that may be attached to each filament,

[a]*Department of Chemistry and Biomedical Sciences, Linnaeus University, SE-391 82 Kalmar, Sweden. E-mail: alf.mansson@lnu.se*
[b]*Department of Women's and Children's Health, University of Padova, 35128 Padova, Italy*

† Electronic supplementary information (ESI) available: Materials and methodological details including protein preparations, preparation of flow cells, antibody conjugation to actin, *in vitro* motility assays and formation and characterization of antibody-labeled fascin–actin bundles, CD45 expression: screening of cell lines and MVs isolation, MVs isolation and preservation in MOPS buffer, optimization of CFSE staining and extended MV shelf-life. Furthermore, ESI figures and movies. See DOI: 10.1039/c5an02377g

‡ These authors contributed equally to this work.

§ Present address: Department of Biotechnology, Delhi Technological University, Delhi-110042, India.

aggregates are readily detected without labeling with *e.g.* fluorescent, and potentially toxic, nanoparticles.

Both the actin and myosin II motor system (underlying muscle contraction) and the kinesin or dynein and microtubule systems (underlying intracellular transport) have been explored in work towards motor driven lab-on-a-chip devices (*cf.*;[12,20–22] reviewed in ref. 10 and 24) each with different advantages and challenges.[10] The actin filaments thus exhibit ten-fold higher speed with rapid transport to a detector site[10,18] whereas microtubule based transport may be more robust against cargo induced disturbances.[10] Furthermore, the higher flexural rigidity of microtubules facilitates guiding along microfabricated tracks[25] and enhances concentration on a detector.[18,26]

For both the microtubule- and actin-based system, antibodies have been covalently attached to single filaments but it would be desirable to increase the total number of active antibodies on the surface of each nanocarrier.[14] For optimized molecular motor driven lab-on-a-chip devices it is also of interest to combine the advantages of the microtubule and actin based systems. It has been suggested[27–29] that this should be possible using unipolar bundles of actin filaments formed by cross-linking *via* fascin, the protein that underlies actin-bundling in filopodia at the leading end of motile cells. The fascin–actin bundles exhibit high flexural rigidity similar to that of microtubules[28,30,31] but are propelled by myosin motors at similar high velocity as individual actin filaments. The bundles also have the capacity to carry cell-sized cargoes without disturbances in motility.[27] However, only streptavidin-biotin links have been tested for cargo attachment with biotin non-covalently attached to the actin filament *via* phalloidin.[27,29] This approach cannot form the basis for a practically useful device because the phalloidin-actin binding is reversible with a dissociation half-time of around 20 min.[32] It is, on the other hand, not clear whether covalent antibody-conjugated actin filaments[14] can be incorporated into bundles together with fascin. Furthermore, if this turns out to be possible it is not self-evident that such a construct maintains self-propulsion and antigen binding.

Here we first demonstrate successful incorporation of covalently antibody-conjugated actin filaments into fascin–actin bundles with well-preserved self-propulsion and an unprecedented maximum capacity to bind and transport protein antigens. The use of this novel nanocarrier allowed 10-fold improvement in the signal-to-noise ratio for fluorescence detection of protein antigens compared to single actin filaments. We also studied binding and transport of microvesicles (MVs), an emerging class of biomarkers in the form of lipid vesicles (100–1000 nm) that are pinched off from living cells in physiological and pathological conditions.[33] The MVs exhibit appreciable potential as biomarkers in cancer and other diseases.[34–42] Here, we found that MVs released by cells positive for CD45 antigen were captured by actin filaments and actin filament bundles functionalized with anti-CD45 monoclonal antibodies. Even if nanocarrier based transportation of the MVs was challenging, the capacity to capture the MVs opens for novel label-free sensing schemes based on aggregation of fluorescent actin filaments or fascin–actin bundles.[23]

Results and discussion

We report findings at the interface of biology, chemistry, materials science and clinical medicine. A key element is production of a novel self-propelled nanomaterial, a nanocarrier, where covalent conjugation of antibodies to actin filaments is combined with self-assembly of the filaments by specific biomolecular recognition using actin-binding proteins as cross-linkers. We evaluate the performance of this nanocarrier in capturing, transporting and detecting protein antigens as well as microvesicles, a novel class of clinically relevant biomarkers.

Assembly of nanocarrier and capture of protein antigen

Actin filaments were first covalently conjugated with antibodies, either polyclonal anti-rabbit IgG (a-rIgG) or monoclonal anti-CD45 (a-CD45), using hetero-bifunctional cross-linkers.[14,43–45] These antibody conjugated filaments formed bundles upon mixing with the actin-binding protein fascin[28,31] (Fig. 1). The success of this approach was somewhat surprising in view of appreciably larger molecular weight (150 kDa) of the antibodies than of fascin (~57 kDa) and also a shape (Y-shape) with expected larger effective space occupancy. However, the actin–fascin bundles with antibodies contained only 7.3 ± 2.2 filaments (mean ± 95% CI; N = 46 bundles), lowered ($p < 0.05$;

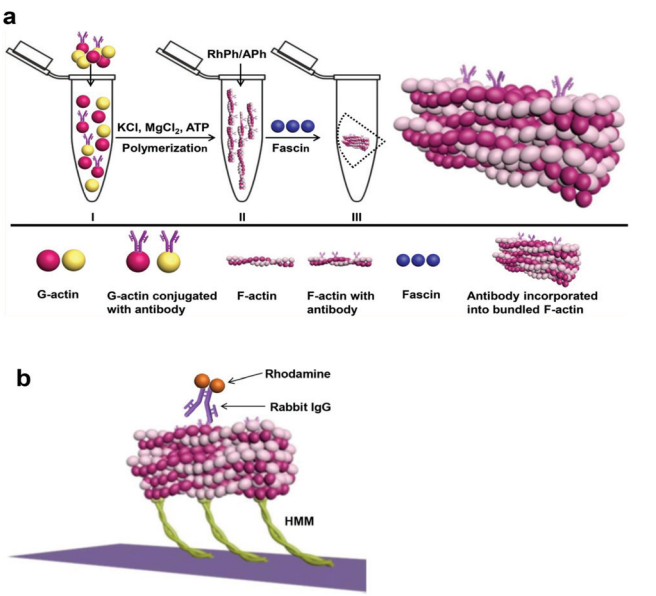

Fig. 1 Schematic illustration of the formation of fascin–actin bundles with antibodies and subsequent transportation of antigen (Rh-rIgG) captured by antibodies. (a) Bundle formation from antibody-conjugated G-actin monomers (I) *via* actin filaments (II) and finally, assembled bundles (III). (b) HMM driven transport of Rh-rIgG antigen captured by anti-rabbit IgG antibody.

t-test) to 4.1 ± 1.7 filaments (N = 15) approximately 5 min after ATP addition due to bundle disassembly (size distributions in Fig. S1†). Simultaneously, the bundle fraction was reduced from 15.3 and 14.6% to 7.6 and 10.6%, respectively, in two experiments, reducing the fraction of filaments incorporated into bundles from close to 60% to about 30%. The bundle size was less than without antibodies (~20).[28,31,46] However, antigen-binding to antibodies seemed to reduce the ATP-induced disassembly, possibly due to cross-linking of neighbouring filaments *via* antigen. For instance, the average observed bundle size 5 min after ATP-addition was 6.4 ± 2.2 (N = 30) in the presence of 1 nM rhodamine labeled rabbit IgG (Rh-rIgG).

Successful incorporation of a-rIgG conjugated actin filaments (also Alexa Fluor®-488 phalloidin (APh) labeled) into fascin–actin bundles was verified using fluorescence microscopy (Fig. 2a–d and S2†) after immobilizing bundles to a surface coated with heavy meromyosin (HMM) in the absence of ATP. For this purpose we used fluorescent rabbit IgG (Rh-rIgG) as antigen. Binding of Rh-rIgG to a-rIgG-actin was observed both for individual actin filaments and fascin–actin-bundles following 1 min of incubation (Fig. 2). The results imply effective incorporation of antibody-functionalized actin filaments into the bundles as well as effective antigen binding of these antibodies.

Evaluation on basis of Rh-rIgG fluorescence intensity (Fig. 2e), showed a concentration-dependent increase in the fraction of bundles (independent of size) and single filaments with observed Rh-rIgG labeling. The concentration dependence of the binding was also reflected in increased stoichiometric ratio of Rh-rIgG to actin.

The fraction of labeled fascin–actin bundles increased from 1–5% at 0.1 nM to 100% at 10 nM Rh-rIgG, following 1 min incubation (Fig. 2e). The results demonstrate appreciably improved detection of antigen binding to bundles compared to isolated filaments with limit of detection lowered from the range 1–10 nM to 0.1–1 nM. Here, the number of Rh labeled bundles and filaments were used as relevant signals. With about 30% or more of all filaments incorporated into bundles (see above) only limited additional improvement would be achieved by preventing bundle disassembly by further cross-linking (*e.g.* covalent or streptavidin-biotin based).

The degree of Rh-rIgG labeling was estimated for the most heavily Rh-rIgG labeled bundles by comparing the Rh and the APh intensity of the same bundles (see Experimental section). This analysis suggests a highly variable maximum Rh-rIgG/actin stoichiometric ratio of 0.14, 0.16 and 0.80 (at 10 nM Rh-rIgG), in three independent experiments.

HMM driven transportation of captured protein antigen

We next asked whether the velocity and fraction of motile HMM propelled filaments/bundles were affected either by antibody-labeling (anti-rabbit IgG) and/or by the subsequent binding of protein antigen (Rh-rIgG). Our results (Fig. 3 and Movies S1–S4†) show that the mean fraction of motile bundles and the mean sliding velocities decreased with increased Rh-rIgG concentration. Whereas most (>80%) fascin–actin bundles that were labeled with Rh-rIgG at 10 nM incubation concentration were non-motile, one bundle with >1200 Rh-rIgG bound per μm of its length (at 0.14 actin-Rh-rIgG ratio and with ~20 actin filaments) was propelled for more than 10 μm at a velocity of 2.4 μm s^{-1}. This was more than 50% of the velocity observed for bundles in the absence of antigen and clearly demonstrates that high degree of Rh-rIgG loading does not necessarily inhibit motility.

For large bundles the motility inhibition at high Rh-rIgG binding was partly due to the formation of cross-links between differently oriented parts of the bundles *via* antigens (*cf.* Fig. S3†). On the other hand, the motility of an appreciable fraction of single filaments, particularly small fragments was also inhibited. This is related to the observation that the amount of non-specifically adsorbed antigen outside filaments and bundles was clearly increased when the Rh-rIgG concen-

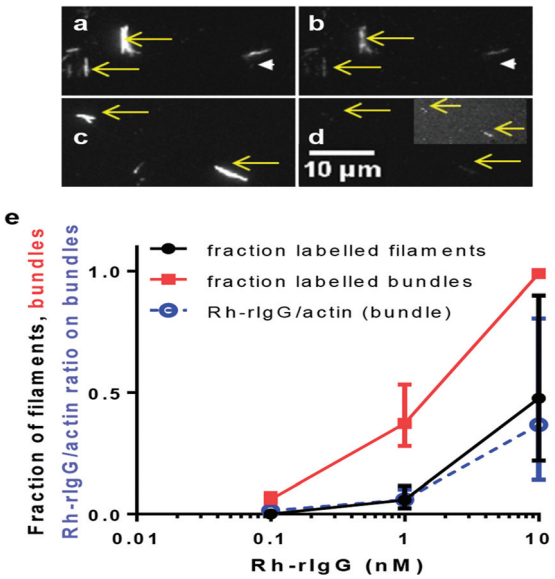

Fig. 2 Capture of Rh-rIgG antigen by APh labeled actin filaments and fascin–actin bundles. (a, c) APh labeling observed using a fluorescein isothiocyanate (FITC) filter set in *epi*-fluorescence microscope. (b) Same region as in (a) a few seconds later after switch to a tetramethyl rhodamine isothiocyanate (TRITC) filter set for observation of Rh-rIgG antigens (incubation with 10 nM for 1 min) captured by a-rIgG antibodies on filaments and bundles. (d) Same region as in (c) a few seconds later after switch to TRITC filter set for observation of Rh-rIgG antigens (incubation with 1 nM for 1 min) on bundles. Inset. After histogram stretching for maximum contrast and brightness. Full length arrows indicate bundles whereas arrow-heads indicate occasional single actin filaments. Similar exposure time and gain in (a) and (b) (exposure time 0.1 s) and in (c) and (d) (0.4 s). The filaments and bundles are bound to a trimethylchlorosilane (TMCS) derivatized surface coated with HMM in the absence of ATP. (e) The fraction of isolated actin filaments (circles, black) and fascin–actin bundles (squares, red) with Rh-rIgG labeling and the Rh-rIgG/actin stochiometric ratio for the 2–4 bundles with most extensive Rh-rIgG labeling (blue open circles). Incubation time, 1 min. Data from 3 independent experiments at each Rh-rIgG concentration. Error bars: range.

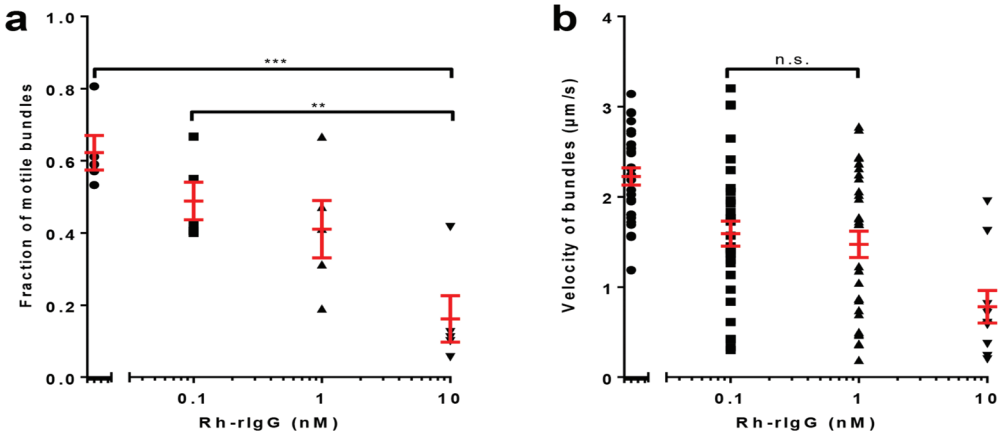

Fig. 3 Effect of increasing Rh-rIgG incubation concentration on motility quality of fascin-crosslinked bundles composed of anti-rabbit-IgG-conjugated actin filaments also labeled with APh. (a) The fraction of motile bundles. Individual data points (black) from five observed image frames at 3 different experimental occasions given with overall mean ± SEM (red). Significant difference between overall mean values was observed at 0 and 0.1 nM on the one hand and 10 nM on the other. ***, $p < 0.001$; **, $p < 0.01$. (b) Sliding velocity. Individual data points ($N = 10–31$ bundles: black) at each Rh-rIgG concentration from 3 different experimental occasions given with overall mean ± SEM (red). Statistically significant difference ($p < 0.05$) between mean values in all separate groups except in the case indicated by "n.s." Temperature, 21–23 °C. Statistical hypothesis testing was performed using one way analysis of variance (ANOVA) followed by Tukey's *post hoc* test for differences between separate groups.

tration increased within the range 1 to 100 nM (shown for 0, 1 and 10 nM Rh-rIgG in Fig. S4†).

The effect of Rh-rIgG binding on the fraction of motile bundles was small for incubation concentrations of 0.1–1 nM and motility was observed for several bundles carrying Rh-rIgG antigen after incubation at 0.1 nM (Fig. 4). The good motility under these conditions is in accordance with very low density of Rh-rIgG, both non-specifically adsorbed to the surface and specifically bound to antibodies on the bundles. However, small but statistically significant changes in mean velocity and increased variability in velocity (Fig. 3b) suggest disturbance of motility also at low Rh-rIgG concentrations (<1 nM). Nevertheless, we have demonstrated that actin–fascin-antibody bundles show appreciable potential to function as a novel nanocarrier under several conditions.

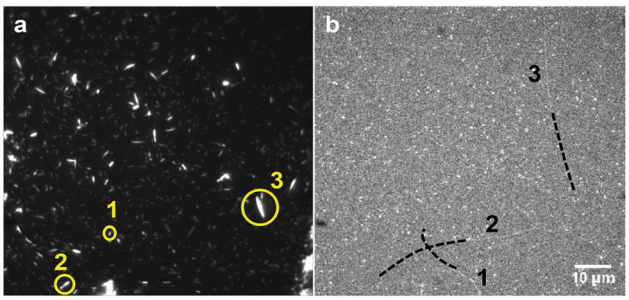

Fig. 4 Observation of motile fascin–actin bundles with captured Rh-rIgG antigen after 1 min incubation with 0.1 nM Rh-rIgG. (a) Snapshot (0.4 s) illustrating APh labeled actin filaments and fascin–actin bundles imaged using *epi*-fluorescence microscope and FITC filter set. Numbers and circles depict three bundles that are motile and that transport Rh-rIgG molecules as shown in (b). (b) ImageJ-derived *Z*-stack of same area as in (a) after shifting to TRITC filter set. This image shows the standard-deviation of the pixel intensities of 35 (0.4 s) image frames starting approximately 10 s after the snapshot in (a). The weak bright traces (1–3) indicate the motion of Rh-rIgG molecules during the 35 frame period. The dashed lines indicate the approximate paths of the Rh-rIgG-carrying bundles from the observations in (a).

Specific capture of CD45 positive microvesicles on actin filaments

Leukemic cell lines were screened in order to select a cell system positive for the CD45 cell surface antigen and for robust *in vitro* production of MVs with CD45 positivity similar to that of the cells. On this basis we selected the human T-cell leukemia cell line DND41 cells as positive control (CD45+) and an MG63 human osteosarcoma cell line as negative control (CD45−) (Fig. S5 and S6†). MVs were isolated from both cell lines and checked for CD45 presence by flow cytometry (Fig. S7 and S8†).

Because MV-capture has not previously been attempted using antibodies on single filaments, we first performed experiments using isolated actin filaments labeled with CD45 specific monoclonal antibodies. Experiments were performed using dilutions in the flow cell of 1/10–1/50 of standard MV preparations from cell lines giving less than 200 MVs per image frame after 5 min incubation. This includes non-specifically surface adsorbed MVs and MVs specifically captured by antibodies. The specific capturing by anti-CD45-conjugated actin filaments of CD45+ MVs, labeled with carboxyfluorescein diacetate succinimidyl ester (CFSE), was confirmed by fluorescence co-localization experiments. In these experiments (Fig. 5), CFSE labeled DND41 MVs were captured by anti-CD45-

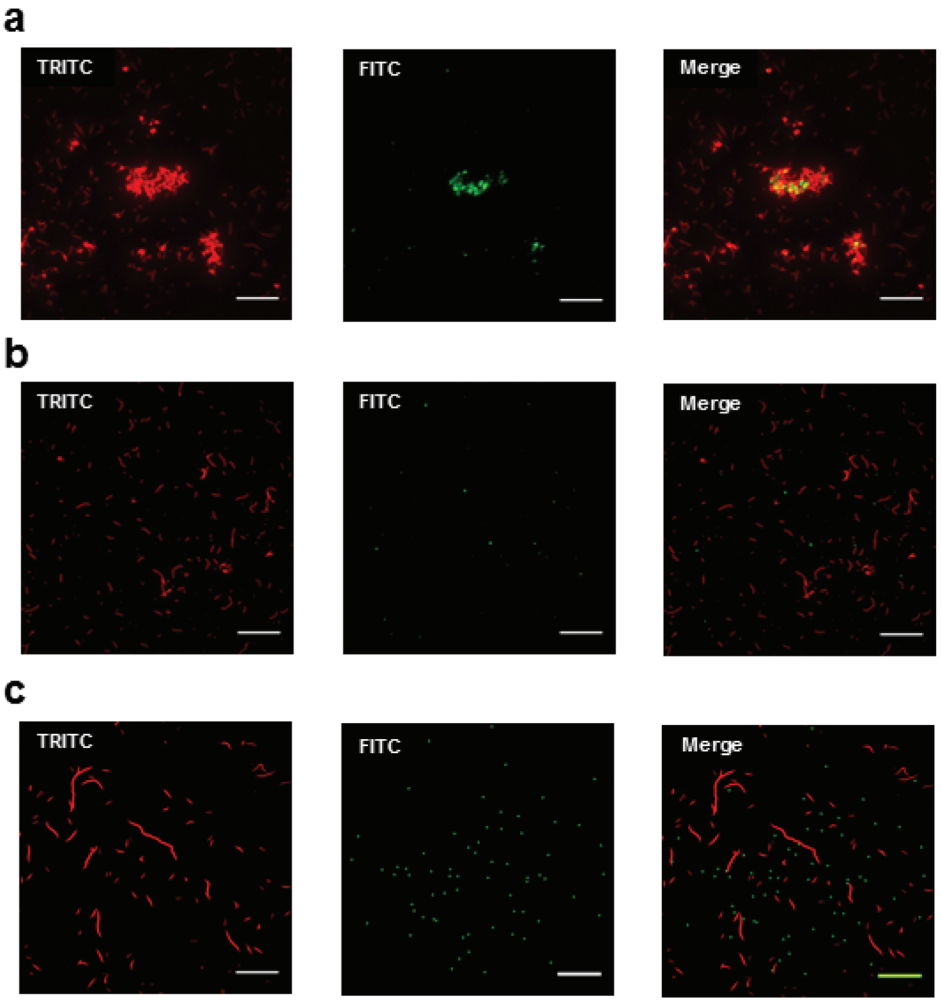

Fig. 5 Co-localization of antibody-conjugated or antibody-free actin filaments (RhPh labeled; TRITC panel, red) and CFSE labeled MVs (FITC panel, green). (a) CFSE labeled CD45+ MVs captured by anti-CD45 conjugated actin filaments. Co-localization (yellow) observed in merged panel. (b) MG63 MVs labeled with CFSE mixed with RhPh labeled and CD45 conjugated actin filaments. Note, no co-localization observed in merged panel. (c) RhPh labeled actin filaments without antibodies mixed with CFSE-labeled and CD45+ MVs. Note, no co-localization observed. Scale bar: 10 μm. Images in (c) subjected to smoothing and brightness adjustment by histogram stretching to reveal weak MV-CFSE fluorescence. The labelling, "FITC" and "TRITC" refer to fluorescence filter used.

actin filaments in solution and then transferred to a HMM coated surface. *Epi*-fluorescence microscopy using both FITC and TRITC filter sets then clearly revealed CD45+ MV co-localization with a-CD45-actin filaments (Fig. 5a). This suggests extensive cross-linking of actin filaments with the formation of large aggregates.

To assess the specificity of the binding of CD45 positive MVs to anti-CD45-actin filaments, two different analyses were performed. First, no co-localization was observed between anti-CD45-actin filaments and CD45 negative MVs, isolated from MG63 cells (Fig. 5b). As a second negative control, CD45 positive MVs were incubated with tetramethylrhodamine isothiocyanate-phalloidin (RhPh) labeled actin filaments (without antibody) in solution. Neither in this case was any non-specific binding of CD45 positive MVs to actin filaments detected (Fig. 5c).

Capture and transportation of MVs by anti-CD45-fascin–actin bundles

Anti-CD45 monoclonal antibodies were next incorporated into fascin–actin bundles as described above for a-rIgG. We tested whether these antibodies could capture CD45+ MVs and whether the MVs could be transported by HMM. For this purpose, the HMM coated flow cells were first incubated with fascin-anti-CD45-RhPh actin filament nanocarriers and then with MVs labeled with CFSE. After MgATP addition, the sliding of the nanocarrier was observed (Fig. 6 and Movies S5, S6†) using TRITC filter (RhPh labeled) while the possible transportation of MVs bound to carrier was visualized using FITC filter (CFSE labeling). First, in 3 independent experiments (30–39 bundles in each) we found that 27 ± 5.4% (mean ± SEM) of all bundles were associated with at least one CFSE labeled MV.

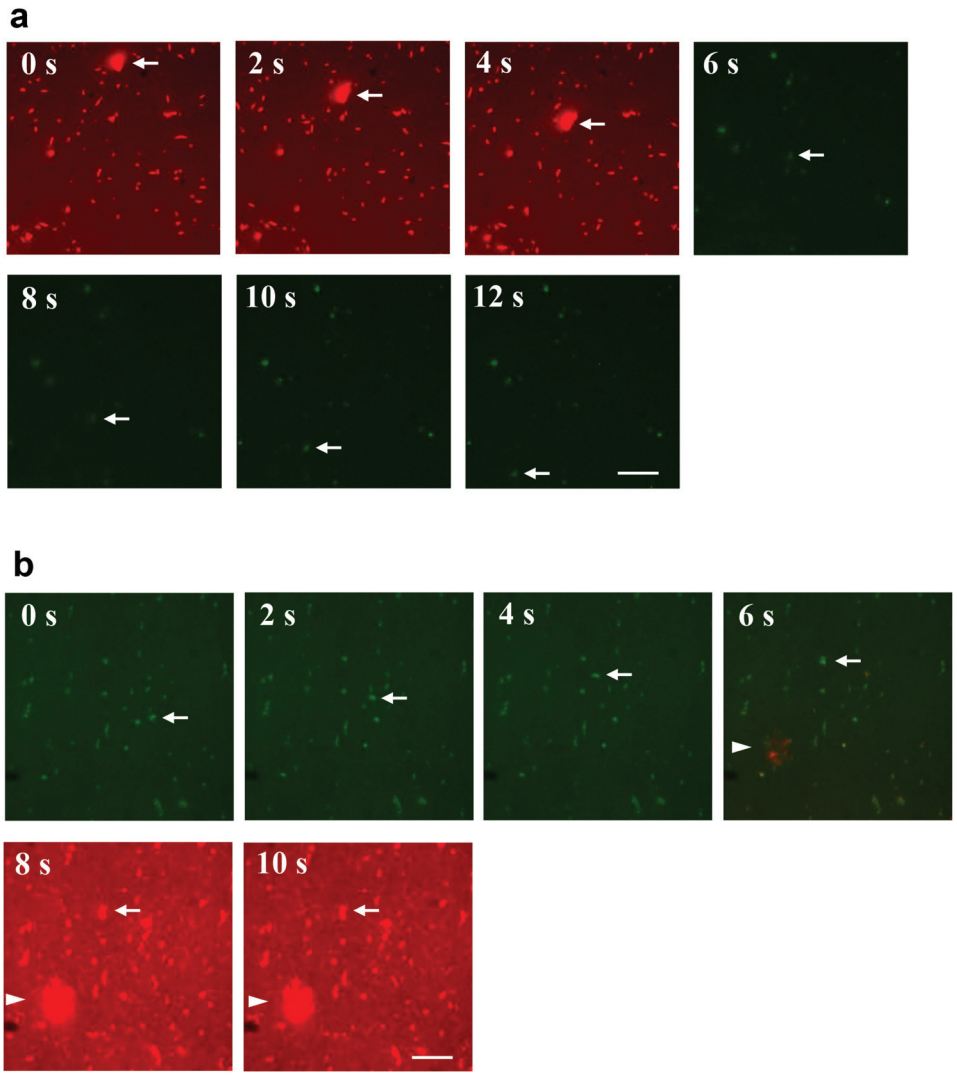

Fig. 6 Image sequences showing HMM propelled microvesicles and aggregation of fascin–actin bundles conjugated by CD45 antibody in the *in vitro* motility assay. (a) Unidirectional movement of bundle (red) carrying microvesicle (green). (b) Small and large aggregates of stationary bundles (red) formed by microvesicles (green) during transport. Bundles (red) and microvesicles (green) were visualized under TRITC and FITC filters, respectively. Switch between filters between 4 and 6 s and 6 and 8 s in A and B, respectively. Arrows and arrowheads denote individual bundles with MVs and stationary bundle-MV aggregates, respectively. Scale bar: 10 μm.

The fraction of motile nanocarriers with or without captured MVs were, in these experiments, 0.23 ± 0.09 (mean ± SEM) when a MV was bound to the bundle and 0.28 ± 0.02 otherwise. The velocity (μm s^{-1}) of anti-CD45 antibody labeled nanocarriers with and without captured MVs was 3.13 ± 0.28 and 3.28 ± 0.11. Thus, both velocity and the fraction of motile carriers were similar in these experiments whether microvesicles were observed to bind to the bundles or not.

However, the fraction of motile nanocarriers was reduced following incubation with MVs (compared to >60% motile fraction without MVs). This suggests that motility inhibition is partly due to the exposure to the MV-containing solution and not due to MV binding *per se*. However, cross-linking of bundles *via* microvesicles, with formation of aggregates, also contributes to motility inhibition, at least after some time of sliding (Fig. 6b).

Key findings and relation to previous results

A central finding is the effective incorporation of antibody-conjugated actin filaments into fascin–actin bundles to form a novel complex biopolymer nanocarrier. This carrier exhibited maintained fast actomyosin driven transportation and an unprecedented maximum capacity to transport protein antigens.[14,22] A second key finding is the observation, for the first time, of the MV capture by monoclonal antibodies on filaments and bundles and aggregation of these filaments/bundles *via* the MVs. Particularly, the aggregation in solution is the first experimental verification of a recently patented idea

for biosensing[23] and our results demonstrate the potential of this approach in detection of the emerging class of vesicular biomarkers.[33]

The HMM driven velocity of bundles that carried protein antigen was reduced by increased incubation concentration but the effects on motility were minimal after 1 min incubation at concentrations of 1 nM or less. The statistically significant effects on velocity and fraction of motile filaments seen in the 1–10 nM range could be useful as a basis for biosensing applications.[47] On the other hand, the minimal effects on motility at sub-nM concentration are also important by enabling use of the nanocarrier in rapid nanoseparation and concentrator nanodevices.[8,18] At higher Rh-rIgG binding the fraction of motile nanocarriers was reduced as well as the sliding velocity but transport was occasionally maintained for an analyte/G-actin stochiometric ratio up to almost 20%. This is similar to what has been observed for single actin filaments.[14] However, importantly, with the bundles it corresponds to as much as one analyte molecule every 1 nm (about 250 fluorophores per diffraction limited spot of 250 nm with bundle diameter <100 nm). This can be compared to only 1 per about 20 nm for single actin filaments and microtubules.[22] That is, the bundles provide 20-fold increased maximal binding and transportation capacity per unit length. This explains that all bundles had bound fluorescent analyte after 1 min incubation with protein antigen at 10 nM concentration and that the limit of detection was improved one order of magnitude compared to single filaments (see also[14]).

Our results suggest that the average antigen binding capacity of the antibodies on nanocarries is at least as good as for antibodies on isolated single filaments despite expected complications due to inaccessibility to the bundle interior (see above). This may be due to more effective two-dimensional diffusional search on the bundle surface compared to a filament surface,[48] or to preferential location of antibodies on the outside surface of the bundles.

Binding and transport of MVs has not been attempted previously whether microtubules, actin filaments or actin bundles have been used as shuttles. On the other hand, lipid vesicles of simple composition and with attachment to biotinylated single actin filaments *via* streptavidin, appreciably compromised motility of isolated filaments[27,49] but not of fascin–actin bundles.[27] The latter finding is in contrast to the rather poor transportation of MVs observed here, probably reflecting the complexity of our cell-derived system compared to lipid vesicles.

Mechanism of motility inhibition with increased analyte concentration

Fascin cross-links actin filaments in a parallel arrangement, with the same polarity of all filaments, *i.e.* with all rapidly polymerizing plus ends of individual filaments in the same direction.[28,31,46] This arrangement is the basis for the effective transportation[28,31] of fascin–actin bundles by myosin motor fragments in the *in vitro* motility assay. Due to the large size of antibodies compared to fascin one would expect a disturbance in the ordered arrangement. Because the largest HMM-transported bundles contained 24 filaments, several filaments must, in this case, be in the bundle interior. With an inter-filament distance of ~8 nm[50] determined by the size of the fascin cross-links there would be little room for antibodies (dimensions $14 \times 8 \times 4$ nm^3).[51] This implies disturbances of the parallel arrangement of the actin filaments which in that case may have detrimental effects on motile function. Alternatively, antibodies attached to actin filaments are mainly on the bundle surface (see above). The fact that bundle integrity was well maintained with antibody conjugation is consistent with the second alternative. This alternative is also consistent with well-maintained motility[49] in the absence of antigen capture and for occasional large motile bundles. The idea also fits with considerations that the energetic penalty of bundle formation would be lowest with the covalently attached antibodies pointing outwards. We therefore conclude that antibody induced disturbances in internal bundle structure has negligible effect on motility quality.

Instead we considered the possibility that a large fraction of the antibodies and bound antigen on the outside of the bundles inhibits actin–HMM interactions. Fluorescence data, cannot distinguish between fluorophores in the interior of bundles and on their surface. This suggests that the stoichiometric ratio between analyte molecules (preferably on the bundle surface) and actin subunits (distributed uniformly over the bundle cross-section) is higher on the bundle surface than overall (*i.e.* >0.15). Therefore, the antibodies and their bound protein antigens most likely block an appreciable fraction of the actin monomers from HMM binding. Whereas this may be a factor behind motility inhibition at high Rh-rIgG loading of the bundles, we found no mandatory motility inhibition under these conditions of maximum labeling. This accords with recent findings[49] where streptavidin was linked to 1/5 of the actin monomers on biotinylated actin filaments without reduction in sliding velocity.

One may then ask why the fraction of motile nanocarriers and their velocity was reduced with increased analyte concentration. After discarding the above suggestions we attribute this finding to two mechanisms. First, several bundles and filaments become cross-linked to each other *via* Rh-rIgG molecules due to polyclonal a-rIgG antibodies on the bundles/filaments (Fig. 5). Unlike the isolated fascin–actin bundles, these higher order structures do not have all actin filaments oriented in parallel and with their fast-growing plus end in one direction. Clearly, since the actin polarity determines the sliding direction with myosin II walking towards the plus end of actin filaments, such non-polar aggregates will inhibit motility. Second, motility may also be inhibited if antibodies on filaments and bundles cross-link to analytes non-specifically bound to HMM or to the underlying motility assay surface. Antibodies on the surface of the fascin–actin bundles that are oriented downwards towards the HMM layer will not be readily reached by diffusion during the incubation period. Upon addition of ATP and gliding to other areas they may therefore bind surface adsorbed analyte molecules, causing inhibition

of motility in analogy to what is seen with so called loaded motility assays.[52] That the density of surface adsorbed analyte molecules is increased at high analyte incubation concentration was apparent from fluorescence micrographs (Fig. S4†).

Cross-linking of different bundles *via* antigen was observed to even higher degree in attempts to transport microvesicles. However, also other factors may contribute to poor motility in this case such as the lipid composition of the microvesicles. The fact that the negatively charged actin filaments with anti-CD45 antibodies formed cross-links with CD45-positive but not with CD45-negative microvesicles is consistent with evidence[53] that the microvesicles predominantly express negatively charged phospholipids on their surface. This finding is of importance for detection schemes that rely on cytoskeletal filament aggregation[23] *via* antibodies on the filaments/bundles and antigen on MV surfaces. If the MVs instead had exhibited positive surface charge, non-specific aggregation *via* negatively charged actin filaments would be expected.[54] On the other hand, for detection schemes relying on transportation,[6,8,17,18] the negative surface charge may be detrimental by binding of MVs to the positively charged actin binding region of myosin.[54] The fact that transportation of MVs could be observed occasionally may be explained by MV attachment to the bundle in a way that prevents contact with the myosin coated surface or that the particular MV has different surface properties than the majority of the MV. A related factor that needs to be considered is the isoelectric point (pI) of the IgG antibodies that may vary between 5 and 9.[55] We did not measure pI but lack of effect of antibody conjugation on myosin driven motility and actin–myosin binding, which depend strongly on electrostatic interactions,[56] suggest that antibody conjugation does not substantially modify the electrostatic properties of actin filaments/bundles. A final factor that may be operational in explaining motility inhibition after addition of MVs is rupture of MVs to release proteins from their interior. This is consistent with the inhibition of motility also of those bundles that were not observed to have bound MVs and with recent findings of motility inhibition upon addition of cytosolic protein components to motility assays.[21]

With regard to detection by filament aggregation, it is important to exclude presence of aggregates or aggregate-like structures *e.g.* by incomplete resuspension of MV pellets during the enrichment phase. However, this risk was considered and minimized and we did not observe any aggregates immediately after resuspension. One may also consider the risk of fusion of several small vesicles, mimicking aggregate formation, as previously shown for phosphatidylserine containing liposomes.[57] However, we did not include Ca^{2+} in the buffer which was important in mediating fusion in the previous studies. Furthermore, importantly, we did not observe aggregate-like assemblies of MVs in the absence of actin filaments/bundles with specific anti-CD45 antibodies (Fig. 5). Nevertheless, in a future device it will be important to rule out any form of non-specific aggregation or membrane fusion effects. Therefore, proper negative controls (as in Fig. 5) need to be integrated with the system at all times. Furthermore, conditions will be optimized to prevent aggregation and membrane fusion (*e.g.* low Mg^{2+} and Ca^{2+} concentrations).

Towards practical diagnostics applications

A range of detection principles that take advantage of specific properties of cytoskeletal filaments and of motor driven nanoseparation and concentration to detector areas have been suggested for use in diagnostics applications.[6,8,10,12,16–18,23,26,58–60] Out of these principles, filament or bundle aggregation *via* analytes,[23] such as observed here with MVs, has however, not been observed to any useful degree previously. The large aggregates formed between filaments and MVs in solution or between bundles and MVs on the motility assay surface, signal the presence of analyte (MVs) without the need to fluorescence-label these. Effective detection of the aggregates in solution will be feasible by pelleting using a simple table-top centrifuge followed by observation of fluorescence attributed to the large number of fluorophores on the actin filaments. This procedure is facilitated by novel methods[53] for isolation and effective pre-concentration of microvesicles.

In contrast to the MV data, our results with protein antigen show that the use of fascin–actin-antibody nanocarriers will enhance motor driven nanoseparation/concentration procedures due to appreciably improved antigen binding capacity compared to single filaments and maintained high actomyosin velocity at low antigen labeling. The data in Fig. 2 show about ten-fold improvement in sensitivity by switching from filaments to bundles. Further, optimizations to achieve picomolar to femtomolar sensitivity for protein antigens will require a range of routine tests. However, it is obvious that a ten-fold increase of the incubation time would increase sensitivity about ten-fold by increased antigen binding to the bundles. A further ten-, to hundred-fold improvement in detection limit would be achieved using motor-driven nanoseparation and concentration methods.[8,18] This may be further improved using enhanced fluorescence detection approaches[20,60–62] and elimination of background fluorescence as well as magnetic pre-separation steps.[63]

Conclusions

We have demonstrated production of high-capacity nanocarriers in the form of fascin–actin bundles covalently conjugated with antibodies. The nanocarrier shows unprecedented maximum antigen carrying capacity for protein antigens and combines advantages of actin-, and microtubule based systems, *e.g.* the speed is similar to that of myosin propelled actin filaments whereas the flexural rigidity is similar to that of microtubules. In addition to the expected usefulness in nanoseparation and concentration devices for high-sensitivity detection of protein antigens we have also demonstrated the usefulness for specific detection of antigen presenting MVs by aggregation *via* these vesicles. In this scheme, the fluorescence

labeled filaments/bundles contain thousands of APh dye molecules thereby also serving as bright reporter elements, substituting potentially toxic inorganic nanoparticles.

Experimental section

Protein preparations and *in vitro* motility assays

Actin filaments and heavy meromyosin (HMM) proteolytically derived from myosin II from fast rabbit skeletal muscle were prepared as described previously.[14,64,65] All experiments using animal material were performed in accordance with national and EU-legislation and were approved by the Regional Ethical Committee for Animal experiments (reference # 96-11), Linköping, Sweden. The actin filaments were labeled by using APh or RhPh (both from Molecular Probes Invitrogen, Eugene, OR). *In vitro* motility assays with actin filaments propelled by HMM (room temperature: 21–23 °C) were performed as described recently. Briefly, flow cells, with trimethylchlorosilane (TMCS) derivatized coverslips as HMM binding substrate,[14] were incubated with HMM (120 μg ml^{-1}), followed by blocking with bovine serum albumin (BSA) before adding fluorescent actin filaments and ATP-containing assay solution.[14,64] The latter contained 1 mM MgATP and had an ionic strength of 60 mM. After the standard incubation for an *in vitro* motility assay, we added antigen, either Rh-rIgG for 1 min or DND41 MVs or MG63 MVs for 5 min.

Antibodies conjugated to F-actin and formation of fascin : actin bundles

F-actin was conjugated with a-rIgG (Rockland Immunochemicals, Gilbertsville, USA) or a-CD45 monoclonal antibody (Universal Biologicals LTD, Cambridge, UK) using heterobifunctional cross-linkers[14] followed by assembly into fascin–actin bundles. In brief, non-conjugated or antibody-conjugated F-actin (0.25 mg mL^{-1}; 6 μM on monomer basis) with fluorescent phalloidin (RhPh or APh) in labeling buffer (10 mM 3-morpholinopropane-1-sulfonic acid (MOPS), 60 mM KCl, 2 mM $MgCl_2$, 0.1 mM K_2-ethylene glycol tetraacetic acid (EGTA), 3 mM NaN_3) was gently mixed with His-tagged fascin (Novus Biologicals, Novus Europe, UK) in 20 mM Tris-HCl buffer (including 100 mM NaCl, 2 mM dithiothreitol (DTT) and 20% glycerol), followed by overnight incubation at 4 °C. The procedure is schematically illustrated in Fig. 1. The solutions contained actin and fascin in molar ratios of 1 : 1 and 1 : 2 for F-actin-a-rIgG and F-actin-a-CD45, respectively. This is expected[28] to produce fascin–actin bundles containing actin and fascin at 4 : 1 and 2 : 1 molar ratios. The bundles were stored on ice before use in experiments and protein concentrations were measured by Bradford assay.

Analysis of antibody incorporation and protein antigen-binding to filaments and bundles

The degree of incorporation of actin filaments conjugated with a-rIgG into fascin–actin bundles was evaluated by detection of Rh-rIgG binding. Here, the fluorescence intensity due to Rh-rIgG reflects the number of a-rIgG molecules with antigen binding capacity. For these analyses, the flow cells were pre-incubated as for a standard *in vitro* motility assay before addition of, fascin-a-rIgG-actin bundles (60 nM; labeled with APh). Image sequences were recorded using an EMCCD camera as described above and fluorescence intensity per rhodamine molecule was estimated from the fluorescence intensity per actin filament length assuming 362 fluorescent phalloidins per 1 μm of the actin filament. The number of fluorescent antigens per bundle and the antibody/actin subunit ratio were then calculated from the corrected (Fig. S9†) ratio of the background subtracted Rh-rIgG and APh fluorescence intensities. In this process bleed-through effects due to APh fluoresence in the TRITC filter-set, were too small to be of significance when analyzing week Rh-fluorescence.

Cell culture and screening of cell lines for CD45 expression

Human leukemic cell lines were purchased from DSMZ German Collection of Microorganisms and Cell Cultures (Braunschweig, Germany) while the MG63 osteosarcoma cell line was purchased from ATCC (Manassas, VA, USA). B leukemic cell lines SEM and RS(4;11) and T leukemic cell lines P12 ICHIKAWA, TALL1, CEM, MOLT3 and DND41 were cultured in RPMI 1640 (GIBCO, Invitrogen Life Technologies, Carlsbad, CA, USA) with 10% fetal calf serum (FCS), L-glutamine (2 mM; GIBCO), penicillin (100 U ml^{-1}; GIBCO) and streptomycin (100 μg ml^{-1}; GIBCO), and maintained at 37 °C in a humidified atmosphere with 5% CO_2. MG63 cells were maintained in DMEM 1× (GIBCO) supplemented with 10% FCS, L-glutamine (2 mM; GIBCO), penicillin (100 U ml^{-1}; GIBCO) and streptomycin (100 μg ml^{-1}; GIBCO), at 37 °C in a humidified atmosphere with 5% CO_2. In order to detect cells with CD45 expression, we stained cell pellets with anti-human CD45 monoclonal antibody (Beckman Coulter, Inc., Miami, FL) and CD45 expression was detected by flow cytometry (Fig. S5 and S6†).

MVs isolation from cell lines

For MVs isolation, culture medium was centrifuged twice at 2500 g for 15 minutes to remove cells and bigger bodies. Cell-free media was filtered by means of a 1.2 μm size cut-off filter, followed by centrifugation at 18000 g for 1 h at 4 °C. Importantly the latter step leaves all vesicles smaller than 0.1 μm (such as exosomes) in the supernatant. This means (considering the previous filtering step) that MVs with a diameter between 0.1 and 1.2 μm were recovered as pellet. The latter was carefully re-suspended in PBS (1×, pH 7.4; GIBCO).

MVs staining and detection by flow cytometry and fluorescence microscopy

To detect MVs by flow cytometry (FACS ARIA III, Becton Dickinson, Franklin Lakes, NJ), MVs were stained using the cytoplasmic dye CFSE (1 μM; CellTrace™ CFSE Cell Proliferation Kit, Molecular Probes, Invitrogen, Eugene, OR). The CFSE is retained in MVs for long time due to covalent coupling with intravesicular molecules. In order to check for the presence of CD45, MVs were also stained with anti-human CD45 monoclonal antibody

(Beckman Coulter, Inc.) following the manufacturer's instructions and then detected by FACS (Fig. S7 and S8†).

For motility assays, CFSE+ MVs were suspended in MOPS buffer (buffer A; *cf.* Fig. S10†). For fluorescence microscopy based detection of MVs on the HMM coated surface, CFSE staining was optimized, increasing the CFSE incubation concentration to 10 μM to better discriminate MVs from background (Fig. S11†). Another centrifugation step and CFSE+ MVs resuspension in PBS 1× was also added after the staining. Once isolated, CFSE+ MVs were stored in PBS 1× at 4 °C for up to 2 weeks before use (Fig. S12†).

The number of MVs present in a microscope image (84 × 84 μm^2) was obtained using an inverted fluorescence microscope (Eclipse TE300, Nikon, Tokyo, Japan) equipped with a Nikon 100× objective (NA 1.4 and a CCD camera (C9100-12, Hamamatsu, Hamamatsu City, Japan).

Analysis of MV-binding to filaments and bundles in solution

For studies of MV binding to actin filaments and fascin–actin bundles, the following mixtures were prepared: (i) DND 41-MVs (10 μl) mixed with a-CD45 actin filaments (6.25 μl) (ii) MG63-MVs (10 μl) mixed with a-CD45-actin filaments (6.25 μl) and (iii) DND 41-MVs (10 μl) mixed with actin filaments without antibodies (6.25 μl). Subsequently 108 μl of buffer D (buffer A with 1 mM DTT) was added followed by incubation for 15 min at 21–23 °C. Flow cells (see above), for observation of the mixtures, were pre-incubated as for a standard *in vitro* motility assay until the step before addition of fluorescent actin filaments. At this point we instead incubated with one of the mixtures i–iii for 3 min, followed by wash with buffer D, and addition of r60 solution (buffer A with 10 mM DTT, 35 mM KCl, ionic strength 60 mM) supplied with an anti-bleach system (final activity concentrations of 3 mg mL^{-1} glucose, 20 U mL^{-1} glucose oxidase and 870 U mL^{-1} catalase). The co-localization between actin filaments and MVs was observed using *epi*-fluorescence microscopy with TRITC and FITC filter sets (details in ESI;† exemplified in Fig. 5 below).

Data analysis

Velocities of single F-actin or fascin–actin bundles were measured using a tracking program developed in a Matlab environment (The MathWorks Inc, Natick, MA).[66] Linear and non-linear curve fittings were performed using Graphpad Prim software (version 6.0, Graphpad software, CA). Image J and Fiji software (Rasband, W.S., ImageJ, U. S. National Institutes of Health, Bethesda, Maryland, USA, http://imagej.nih.gov/ij/, 1997–2012.) were used for analyses of brightness as well as for thresholding and superimposition of images.

Conflict of interest

Alf Månsson is a co-founder, co-owner and CEO of the start-up company ActoSense Biotech AB (Kalmar, Sweden) aiming to develop diagnostic devices based on the aggregation of cytoskeletal elements, particularly actin filaments, in solution. Moreover, A. Månsson holds two Swedish patents as well as one US and one European patent in this field.

Acknowledgements

This work was funded by The European commission (FP7) under the contract MONAD (NMP4-SL-2009-228971), The Carl Trygger Foundation, The Swedish Research Council (Project 621-2010-5146), The Faculty of Natural Sciences and Engineering and the Faculty of Health and Life Sciences at Linnaeus University. S. K. thanks SERB-DST, Govt. of India for the award of Fast Track Young Scientist. We thank Prof. Kazuhiro Kohama, Gunma University, Japan for suggestions and discussions about fascin–actin bundle experiments. Finally, we would like to thank Camilla Mohlin at Linnaeus University, Kalmar for help with cell culturing.

Notes and references

1 D. A. Giljohann and C. A. Mirkin, *Nature*, 2009, **462**, 461–464.
2 G. M. Whitesides, *Nature*, 2006, **442**, 368–373.
3 J. V. Jokerst, J. W. Jacobson, B. D. Bhagwandin, P. N. Floriano, N. Christodoulides and J. T. McDevitt, *Anal. Chem.*, 2010, **82**, 1571–1579.
4 P. E. Sheehan and L. J. Whitman, *Nano Lett.*, 2005, **5**, 803–807.
5 S. T. Yang, Y. Liu, Y. W. Wang and A. Cao, *Small*, 2013, **9**, 1635–1653.
6 T. Fischer, A. Agarwal and H. Hess, *Nat. Nanotechnol.*, 2009, **4**, 162–166.
7 P. Katira and H. Hess, *Nano Lett.*, 2010, **10**, 567–572.
8 C. T. Lin, M. T. Kao, K. Kurabayashi and E. Meyhofer, *Nano Lett.*, 2008, **8**, 1041–1046.
9 Y. M. Huang, M. Uppalapati, W. O. Hancock and T. N. Jackson, *Biomed. Microdevices*, 2007, **9**, 175–184.
10 T. Korten, A. Månsson and S. Diez, *Curr. Opin. Biotechnol.*, 2010, **21**, 477–488.
11 D. Steuerwald, S. M. Fruh, R. Griss, R. D. Lovchik and V. Vogel, *Lab Chip*, 2014, **14**, 3729–3738.
12 S. Ramachandran, K. H. Ernst, G. D. Bachand, V. Vogel and H. Hess, *Small*, 2006, **2**, 330–334.
13 C. M. Soto, B. D. Martin, K. E. Sapsford, A. S. Blum and B. R. Ratna, *Anal. Chem.*, 2008, **80**, 5433–5440.
14 S. Kumar, L. ten Siethoff, M. Persson, M. Lard, G. te Kronnie, H. Linke and A. Månsson, *PLoS One*, 2012, **7**, e46298.
15 S. Diez, C. Reuther, C. Dinu, R. Seidel, M. Mertig, W. Pompe and J. Howard, *Nano Lett.*, 2003, **3**, 1251–1254.
16 S. Hiyama, R. Gojo, T. Shima, S. Takeuchi and K. Sutoh, *Nano Lett.*, 2009, **9**, 2407–2413.
17 P. Katira and H. Hess, *Nano Lett.*, 2010, **10**, 567–572.

18 M. Lard, L. Ten Siethoff, S. Kumar, M. Persson, G. Te Kronnie, H. Linke and A. Månsson, *Biosens. Bioelectron.*, 2013, **48**, 145–152.
19 H. Hess, J. Clemmens, D. Qin, J. Howard and V. Vogel, *Nano Lett.*, 2001, **1**, 235–239.
20 A. Månsson, M. Sundberg, M. Balaz, R. Bunk, I. A. Nicholls, P. Omling, S. Tågerud and L. Montelius, *Biochem. Biophys. Res. Commun.*, 2004, **314**, 529–534.
21 S. Korten, N. Albet-Torres, F. Paderi, L. Ten Siethoff, S. Diez, T. Korten, G. Te Kronnie and A. Månsson, *Lab Chip*, 2013, **13**, 866–876.
22 C. M. Soto, B. D. Martin, K. E. Sapsford, A. S. Blum and B. R. Ratna, *Anal. Chem.*, 2008, **80**, 5433–5440.
23 A. Månsson and S. Tågerud, *US patent*, US 8,658,381, 2014.
24 A. Agarwal and H. Hess, *Prog. Polym. Sci.*, 2010, **35**, 252–277.
25 T. Nitta, A. Tanahashi, Y. Obara, M. Hirano, M. Razumova, M. Regnier and H. Hess, *Nano Lett.*, 2008, **8**, 2305–2309.
26 T. Nitta and H. Hess, *Cell. Mol. Bioeng.*, 2012, **6**, 109–115.
27 H. Takatsuki, H. Tanaka, K. M. Rice, M. B. Kolli, S. K. Nalabotu, K. Kohama, P. Famouri and E. R. Blough, *Nanotechnology*, 2011, **22**, 245101.
28 H. Takatsuki, E. Bengtsson and A. Månsson, *Biochim. Biophys. Acta*, 2014, **1840**, 1933–1942.
29 H. Takatsuki, K. M. Rice, S. Asano, B. S. Day, M. Hino, K. Oiwa, R. Ishikawa, Y. Hiratsuka, T. Q. Uyeda, K. Kohama and E. R. Blough, *Small*, 2010, **6**, 452–457.
30 M. M. Claessens, M. Bathe, E. Frey and A. R. Bausch, *Nat. Mater.*, 2006, **5**, 748–753.
31 R. Ishikawa, T. Sakamoto, T. Ando, S. Higashi-Fujime and K. Kohama, *J. Neurochem.*, 2003, **87**, 676–685.
32 E. M. DelaCruz and T. D. Pollard, *Biochemistry*, 1996, **35**, 14054–14061.
33 G. Raposo and W. Stoorvogel, *J. Cell Biol.*, 2013, **200**, 373–383.
34 G. Turturici, R. Tinnirello, G. Sconzo and F. Geraci, *Am. J. Physiol.: Cell Physiol.*, 2014, **306**, C621–C633.
35 Y. J. Yoon, O. Y. Kim and Y. S. Gho, *BMB Rep.*, 2014, **47**, 531–539.
36 Y. Lee, S. El Andaloussi and M. J. Wood, *Hum. Mol. Genet.*, 2012, **21**, R125–R134.
37 C. Tetta, E. Ghigo, L. Silengo, M. C. Deregibus and G. Camussi, *Endocrine*, 2013, **44**, 11–19.
38 J. Ratajczak, K. Miekus, M. Kucia, J. Zhang, R. Reca, P. Dvorak and M. Z. Ratajczak, *Leukemia*, 2006, **20**, 847–856.
39 A. L. Revenfeld, R. Baek, M. H. Nielsen, A. Stensballe, K. Varming and M. Jorgensen, *Clin. Ther.*, 2014, **36**, 830–846.
40 Y. Sun and J. Liu, *Clin. Ther.*, 2014, **36**, 863–872.
41 V. R. Martins, M. S. Dias and P. Hainaut, *Curr. Opin. Oncol.*, 2013, **25**, 66–75.
42 V. R. Minciacchi, M. R. Freeman and D. Di Vizio, *Semin. Cell Dev. Biol.*, 2015, **40**, 41–51.
43 A. Grotzky, Y. Manaka, T. Kojima and P. Walde, *Biomacromolecules*, 2011, **12**, 134–144.
44 G. Iyer, F. Pinaud, J. Xu, Y. Ebenstein, J. Li, J. Chang, M. Dahan and S. Weiss, *Bioconjugate Chem.*, 2011, **22**, 1006–1011.
45 J. Y. Byeon, F. T. Limpoco and R. C. Bailey, *Langmuir*, 2010, **26**, 15430–15435.
46 M. M. Claessens, C. Semmrich, L. Ramos and A. R. Bausch, *Proc. Natl. Acad. Sci. U. S. A.*, 2008, **105**, 8819–8822.
47 T. Korten and S. Diez, *Lab Chip*, 2008, **8**, 1441–1447.
48 H. C. Berg and E. M. Purcell, *Biophys. J.*, 1977, **20**, 193–219.
49 M. Persson, M. Gullberg, C. Tolf, A. M. Lindberg, A. Månsson and A. Kocer, *PLoS One*, 2013, **8**, e55931.
50 S. Jansen, A. Collins, C. S. Yang, G. Rebowski, T. Svitkina and R. Dominguez, *J. Biol. Chem.*, 2011, **286**, 30087–30096.
51 V. R. Sarma, E. W. Silverto, D. R. Davies and W. D. Terry, *J. Biol. Chem.*, 1971, **246**, 3753.
52 W. Bing, A. Knott and S. B. Marston, *Biochem. J.*, 2000, **350**, 693–699.
53 Z. Brownlee, K. D. Lynn, P. E. Thorpe and A. J. Schroit, *J. Immunol. Methods*, 2014, **407**, 120–126.
54 N. Albet-Torres, A. Gunnarsson, M. Persson, M. Balaz, F. Hook and A. Månsson, *Soft Matter*, 2010, **6**, 3211–3219.
55 S. Takahashi, N. Wada, K. Harada and M. Nagata, *Kidney Int.*, 2004, **66**, 1556–1560.
56 M. A. Geeves, R. Fedorov and D. J. Manstein, *Cell. Mol. Life Sci.*, 2005, **62**, 1462–1477.
57 S. T. Sun, C. C. Hsang, E. P. Day and J. T. Ho, *Biochim. Biophys. Acta*, 1979, **557**, 45–52.
58 T. Kim, L. J. Cheng, M. T. Kao, E. F. Hasselbrink, L. Guo and E. Meyhofer, *Lab Chip*, 2009, **9**, 1282–1285.
59 M. G. van den Heuvel, M. P. de Graaff and C. Dekker, *Science*, 2006, **312**, 910–914.
60 L. Ten Siethoff, M. Lard, J. Generosi, H. S. Andersson, H. Linke and A. Månsson, *Nano Lett.*, 2014, **14**, 737–742.
61 M. Lard, L. Ten Siethoff, A. Månsson and H. Linke, *Sci. Rep.*, 2013, **3**, 1092.
62 D. Axelrod, *Methods Enzymol.*, 2003, **361**, 1–33.
63 S. Kumar, L. ten Siethoff, M. Persson, N. Albet-Torres and A. Månsson, *J. Nanobiotechnol.*, 2013, 11.
64 S. J. Kron, Y. Y. Toyoshima, T. Q. Uyeda and J. A. Spudich, *Methods Enzymol.*, 1991, **196**, 399–416.
65 J. D. Pardee and J. A. Spudich, *Methods Cell Biol.*, 1982, **24**, 271–289.
66 A. Månsson and S. Tagerud, *Anal. Biochem.*, 2003, **314**, 281–293.